SWITCHING PROPERTIES OF ELECTROTHERMAL DEVICES

Thesis for the Degree of Ph. D.
MICHIGAN STATE UNIVERSITY
Dipankar Nagchoudhuri
1973

This is to certify that the

thesis entitled

SWITCHING PROPERTIES OF

ELECTROTHERMAL DEVICES

presented by

Dipankar Nagchoudhuri

has been accepted towards fulfillment
of the requirements for

Ph. D. degree in E.E.

Major professor

Date

O-7639

SWIT

Electro
duction in band
bulk devices fa
trolled negati
tional switchi
been reported
order of hund

The p
tion of the
computer-bas
of the ETD;
ier mobilit
a set of th
equations.
from thermo
In effect,
temperatur
the sum of
thermal di
generaliz

ABSTRACT

SWITCHING PROPERTIES OF ELECTROTHERMAL DEVICES

By

Dipankar Nagchoudhuri

Electrothermal semiconductor materials undergo a drastic reduction in band gap above a critical temperature, T_{cr}. Two-terminal, bulk devices fabricated from these materials can exhibit current-controlled negative resistance I-V characteristics and high-speed bidirectional switching. Switching times of the order of nanoseconds have been reported, though associated with large storage times, often of the order of hundreds of microseconds.

The primary purpose of this dissertation is to study the initiation of the switching process in electrothermal devices (ETD's). A computer-based model is developed incorporating the salient features of the ETD; e.g., the abrupt narrowing of the band gap and rise in carrier mobility at the critical temperature T_{cr}. The model consists of a set of three coupled, nonlinear, second-order, partial differential equations. The first of these, the Temperature Equation, is arrived at from thermodynamical considerations of energy balance within the ETD. In effect, the heat energy per unit time associated with the rate of temperature rise at any point in the interior of the ETD is equated to the sum of the net electrical power dissipated and the heat input by the thermal diffusion process. The second, the Continuity Equation, is a generalized form of the continuity of charge equation, which states that

the sum of the r

element and the

carrier current

of three compone

presence of an e

the mobile charg

the temperature

Poisson's Equati

field to be cons

The elec

termined by plac

circuit containi

and a switch S.

shaped, the two

are assumed to b

four surfaces ar

thermal and elec

To facil

is quantized int

finite difference

obtaining 1331 e

time interval.

tions. The Tempe

using Douglas' I

dimensions. The

using Successive

predictor-correct

G 87797

the sum of the rate of increase of charge in any differential volume element and the divergence of the carrier current is zero. Here, the carrier current is assumed to be due to electrons only and comprises of three components, namely, a conduction current component due to the presence of an electric field, and two diffusion components, one due to the mobile charge carrier concentration gradients and the other due to the temperature gradients within the ETD. The third equation is the Poisson's Equation obtained from Gauss' Law by assuming the electric field to be conservative within the ETD.

The electrical boundary conditions for these equations are determined by placing the sample between two electrodes in an electrical circuit containing an ideal voltage source V_{app}, a source resistor R_s, and a switch S. The sample geometry chosen is a rectangular parallelepiped, the two opposite surfaces being in contact with electrodes which are assumed to be ideal heat sinks and electrical conductors. The other four surfaces are in contact with air, which is assumed to be an ideal thermal and electrical insulator.

To facilitate the numerical solution of the equation, the sample is quantized into 10 x 10 x 10 identical rectangular parallelepipeds, and finite dirrerence equations were developed for each volume element, thus obtaining 1331 equations for each partial differential equation for each time interval. Different algorithms are used to solve each set of equations. The Temperature Equation, which is parabolicin form, is solved using Douglas' Implicit Alternating Direction (IAD) method in three space dimensions. The Continuity Equation and the Poisson's Equation are solved using Successive Over Relaxation (SOR) methods. In addition, an overall predictor-corrector loop is employed to achieve simultaneity.

Three r

$_{?}O_2$ as the prot

biassing circui

ED, and by pho

thermal charact

parallelism to

analysis of the

also compare we

storage times o

is shown to be t

tudinally in bot

field, as shown

The model also p

experimentally i

flux in the inte

photoswitching u

Three methods of inducing switching in the ETD are studied using VO_2 as the prototype material--by Joule heating due to the external biassing circuit, by the simulation of a defect within the bulk of the ETD, and by photoswitching. The results of the simulations establish the thermal character of the preswitching region as evidenced by the close parallelism to the results obtained from simplified one-dimensional analysis of the Temperature Equation. The results of the simulations also compare well with the experimental I-V curves and the switching and storage times observed in VO_2 devices. The mechanism of the switching is shown to be the propagation of the narrowing of the band gap longitudinally in both directions in a line parallel to the applied electric field, as shown by the electric field data obtained from the simulations. The model also provides information regarding the profiles of various experimentally inaccessible bulk variables like power density and heat flux in the interior of the ETD. Finally, the possibility of inducing photoswitching under suitable bias conditions is predicted by the model.

SWI

in

Department

SWITCHING PROPERTIES OF ELECTROTHERMAL DEVICES

By

Dipankar Nagchoudhuri

A THESIS

Submitted to
Michigan State University
in partial fulfillment of the requirements
for the degree of

DOCTOR OF PHILOSOPHY

Department of Electrical Engineering and Systems Science

1973

A co

and encourag

few names, h

exceptional

mittee, notal

active and co

and Wellso fo

team of compu

Finally, I wi

typed up the

press my sinc

ACKNOWLEDGEMENTS

A complete list of all those who contributed in time, effort, and encouragement would resemble, I'm sure, a telephone directory. A few names, however, cannot escape mention: Dr. P. D. Fisher, for his exceptional support and guidance and, of course, members of my committee, notably Drs. Giacolletto, Ho, Nyquist, and Sinna for their very active and considerate co-operation. I also wish to mention Drs. Frame and Wellso for their invaluable help at very crucial times, and the team of computer consultants for '72-73 for their extraordinary patience. Finally, I wish to express my gratitude to the corps of friends who typed up the initial rough draft. To all of these people I wish to express my sincere thanks.

TABLE OF CONTENTS

Appendix

LIST OF APPENDICES

Table

LIST OF TABLES

Figure

LIST OF FIGURES

In the m

devices was disc

among workers in

plagued initiall

these devices ex

stance, the swit

resistance to lo

though large del

perties were th

manufacturing, a

Since in

associated with

these devices w

devices" or sim

served in some

Thanks to resea

O-F-O model)(11

progress was ma

rials to be ana

with convention

electrothermal

like CdS[17] , G

CHAPTER I

INTRODUCTION

In the mid 1960's, a new class of bulk semiconductor switching devices was discovered, arousing considerable curiosity and excitement among workers in the area of solid state electronics[7]. Though plagued initially with problems of repeatability and reliability[1,2], these devices exhibited many desirable properties[3,4,5,6,7]. For instance, the switching process was fast; switching times from the high-resistance to low-resistance state were on the order of nanoseconds even though large delay times were always present[4]. Other significant properties were the memory and hysteresis effects, their relative ease of manufacturing, and their immunity to radiation damage[8].

Since investigations indicated that electrical switching was associated with the thermal characteristics of the device material[9,10], these devices will be referred to here generically as "electrothermal devices" or simply ETD's. Initially, this switching phenomena was observed in some amorphous transition metal oxides and chalcogenide glasses. Thanks to researchers like Cohen, Fritzsche, and Ovshinsky (founders of the C-F-O model)[11,12], Sir Neville Mott[13,14,15], and Gubanov[16], rapid progress was made in formulating a transport theory for amorphous materials to be analysed using many of the well-established techniques used with conventional crystalline semiconductors. More recently, however, electrothermal switching has also been observed in crystalline materials like CdS[17], GaAs[18,19], and Te[20].

1.1. Overview

Characteristically, in ETD materials, the band gap narrows dramatically above a critical temperature, T_{cr}. In this dissertation, a computer-based model is developed for simulating the transport and terminal characteristics of such semiconductors. The model is tested against experimental data and then used to predict a photo-switching phenomenon. The first few chapters are devoted to model development. The earlier sections of this first chapter enumerate some of the properties observed in electrothermal switches. Subsequently, theoretical formulations of some of the major workers in the field are discussed in order to establish the need to develop a new model. In Chapter 2, the model itself is constructed. The various electrical and thermal properties are described in light of the assumptions and idealizations of the model. In Chapter 3, the model is mathematically formulated. Applying the fundamental laws of electrodynamics and thermodynamics, a set of equations is obtained which describe the electrical and thermal transport properties of the material under certain specified conditions. In Chapter 4, each differential equation is re-expressed as a set of difference equations, and then the total coupled system of equations is discussed.

Chapter 5 deals with investigations of the switching phenomena. Results of various experiments are presented. These experiments were used to test the model against existing experimental data, as well as to predict some as yet unobserved phenomena. An analysis and discussion of these results are also presented in Chapter 5. In Chapter 6, some conclusions are drawn on the basis of the results obtained, and suggestions are made for further model development, simulations, and laboratory experiments.

1.2. Electrotherm

Until abou

charge carrier mot

reasonably slow ar

parameters show a

teristic critical

treated as step fu

be primarily respo

In the sections in

of some important

1.2.1. Temperatur

For most s

perature, as expre

$E_g(T) = E$

In electrothermal

certain transitio

Specific material

Band Ga

Material
VO_2
VO
Ti_2O_3
V_2O_3

1.2. Electrothermal Device Parameters

Until about a decade ago, semiconductor parameters like band gap, charge carrier mobility, and carrier conductivity were presumed to be reasonably slow and continuous functions of temperature. However, ETD parameters show a very strong temperature dependence near the characteristic critical temperature; in fact, some of these parameters can be treated as step functions of temperature. This behavior is thought to be primarily responsible for the switching effects observed in ETD's[28]. In the sections immediately following, observed temperature dependences of some important ETD parameters are noted.

1.2.1. Temperature Dependence of the Band Gap

For most semiconductors, the band gap reduces slowly with temperature, as expressed by the following equation:

$$E_g(T) = E_g(0) - \beta T \tag{1.2.1}$$

In electrothermal switches, however, the band gap reduces abruptly at a certain transition temperature, T_{cr}, where T_{cr} is characteristic of the specific material, as illustrated in Table 1.1.

Table 1.1

Band Gap Data for Various Electrothermal Materials

Material	Critical Temp. (K)	E_g $T < T_{cr}$ (V)	E_g $T \geq T_{cr}$ (V)
VO_2	341	0.45	0.045
VO	126	0.14	0.10
Ti_2O_3	450	0.04	Metallic
V_2O_3	150	0.12	0.07

As might be expected, there is often evidence of a structural change at the critical temperature[22,27]; for instance, VO changes from an orthorhombic structure below the transition temperature, 126 K, to a rock salt structure above it; VO_2 changes from a monoclinic to a rutile structure at the transition temperature, 340 K.

1.2.2. Conductivity-vs-Temperature Characteristics

If the proper range of temperatures is chosen, the electrical conductivity is also a strong function of temperature for most semiconductors. This is because the conductivity is related to the mobile carrier density and carrier mobility[21], both of which are temperature dependent parameters, the relation being:

$$\sigma = ne\mu_n + pe\mu_p \qquad (1.2.2)$$

where σ = conductivity of the semiconductor,

n = density of mobile electrons,

p = density of mobile holes,

e = charge on an electron (magnitude only),

n = electron mobility which is defined as the carrier drift velocity per unit applied electric field, and

p = hole mobility.

In electrothermal devices, the conductivity-temperature dependence is much stronger than in other semiconductors. For instance, in Futaki's "Critical Temperature Resister"[33], it increased by as much as three orders of magnitude at the critical temperature. Some typical conductivity-versus-temperature curves are shown in Figs. 1.1a and 1.1b.

From the Eq. (1.2.2), it is apparent that a sharp increase in conductivity is possible if the mobile carrier concentration increases abruptly. In a doped, partially-ionized semiconductor, the mobile carrier

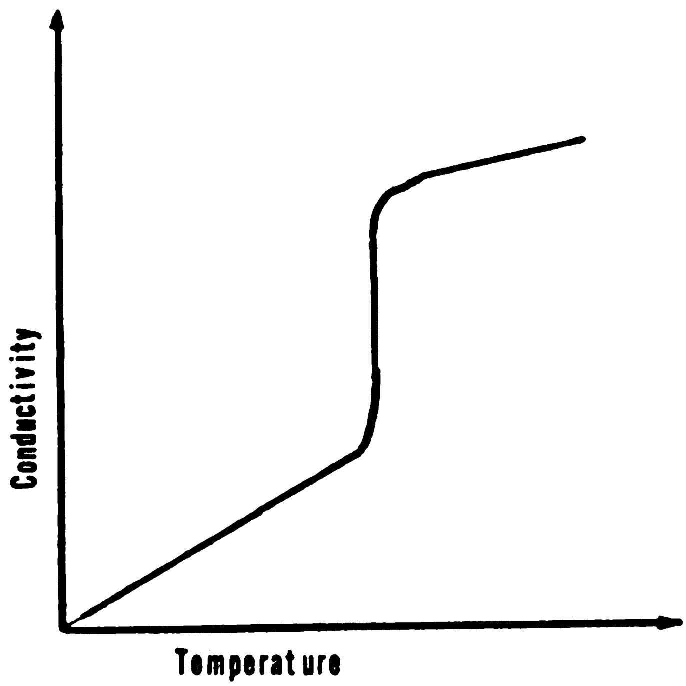

Figure 1.1a

A Typical Conductivity-vs-Temperature
Characteristic Observed in ETD's

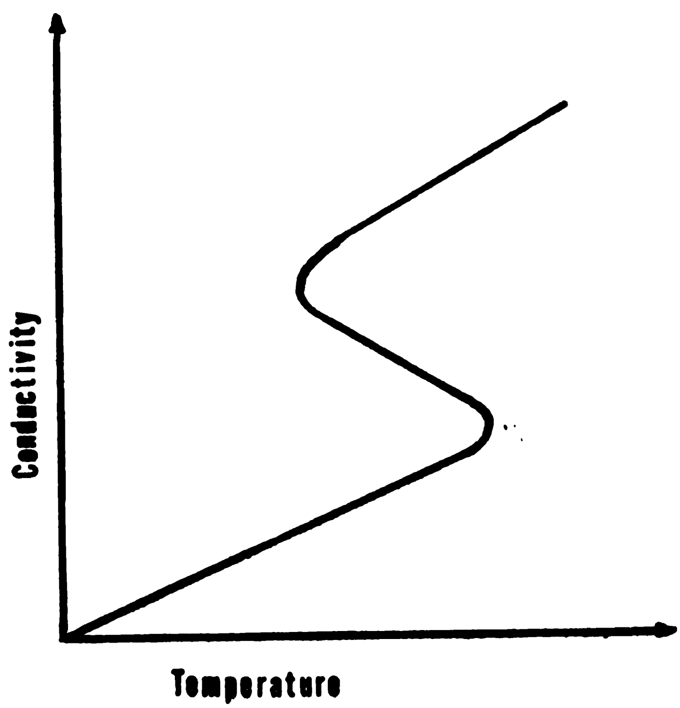

Figure 1.1b

Typical S-shaped Conductivity-vs-Temperature
Characteristic of ETD's

density is primarily determined by the ionized donor density. The ionized donor density is determined in part by the activation energy E_a of the ionizing impurity level of the semiconductor, the activation energy E_a for a donor impurity being the energy difference between the donor level and the conduction band edge[6].

$$\sigma(T) \sim A_o \exp(-E_a(T)/kT) \qquad (1.2.3)$$

where A_o is a material constant,

k is Boltzmanns constant,

T is the temperature, and

E_a is the activation energy.

The conductivity can also change abruptly due to a sudden jump in carrier mobility. Many ETD's, in fact, do exhibit such jumps. These "mobility gaps" are an integral part of the C-F-O model[11] referred to earlier, and are often associated with a structural transformation of the electrothermal material[22,27]. A local structural change often introduces an increase in the free carrier concentration in the immediate vicinity. The screening effect on the neighbor lattice centers increases; in other words, the effective local binding potential reduces, increasing the mobility of more electrons. The effect spreads rapidly through the material causing an abrupt increase in mobility[13].

Some ETD's also show hysteresis in their conductivity-temperature plots as shown in Fig. 1.2. This feature is utilized in memory devices[28,29]. The energy associated with the area of the hysteresis loop is believed to be related to the energy[27,28] involved in the structural change, that is, the latent heat of transformation.

1.3. Switching in Electrothermals

The large change in conductivity is primarily responsible for the negative resistance region in the static I-V curves of ETD's. The

Hyst

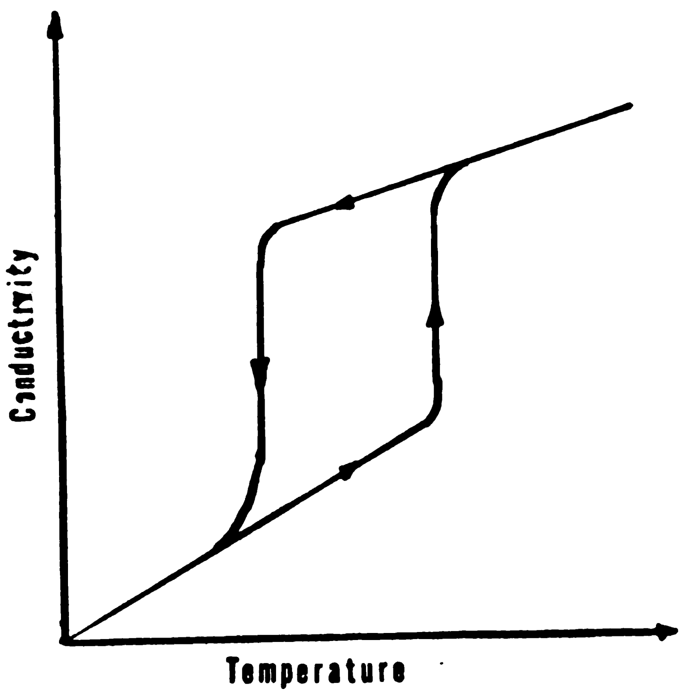

Figure 1.2

Hysteresis in Conductivity-vs-Temperature
Characteristic of ETD's

I-V characteristics of ETD's differ markedly from junction switches in a couple of respects. Junction diode[21] switches are directional; current is allowed in one direction and opposed in the other. On the other hand, electrothermal switches are bidirectional; the switching is essentially a level-sensing and not a direction-sensing mechanism. As soon as a certain temperature level is reached within the device, switching will take place regardless of the direction of current in the external electrical circuit.

Also, the electrothermal switches are current-controlled, negative-resistance devices. In contrast, typical negative-resistance semiconductor devices[21] like the Gunn diode and the tunnel diode exhibit voltage-controlled negative resistances. The difference is illustrated in Figs. 1.3 and 1.4. Because of its shape, the I-V characteristics of the ETD are also called S-curves[5].

1.4. Principal ETD Switching Models

The S-curves are believed to be caused by "filament" formation, which have been actually observed in some electrothermal devices[43]. The "filament" is a thin, highly localized, conductive region extending throughout the length of the material. In filamentary switching, the "off" resistance is determined by the bulk conductivity of the material. In the "on" state, the filament has already formed. The "on" resistance is largely determined by the conductivity of the filament. From purely thermodynamic considerations, Ridley[30] demonstrated that filament formation was possible in a current-controlled negative differential resistance device. The actual mechanism of filament formation was not dealt with. In a later chapter, an equation for energy balance will be derived in close parallelism to Ridley's development.

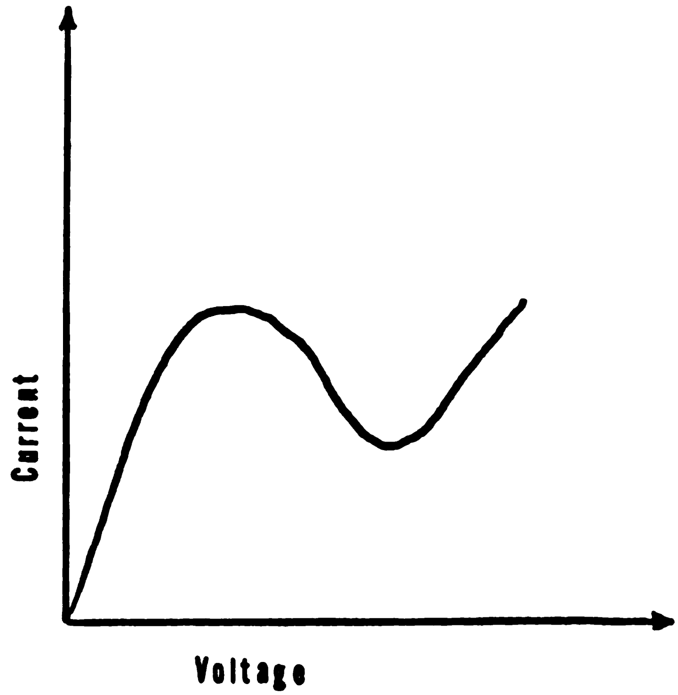

Figure 1.3

Voltage Controlled Negative Resistance Device
I-V Characteristics

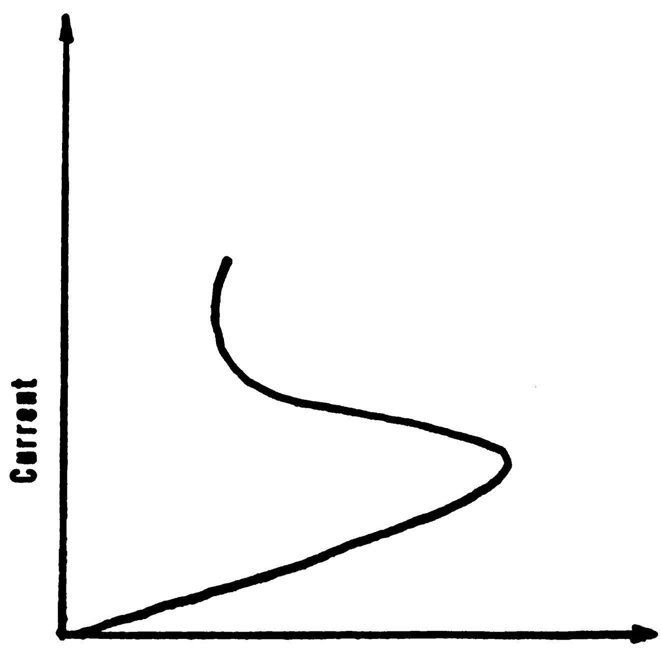

Figure 1.4

Current Controlled Negative Resistance Device
I-V Characteristics

A specific equation for the system energy balance was first determined by Boer and Dohler[31]; subsequently, Berglund[34], Fritzsche[12], Ovshinsky[10], and others have contributed significantly to its development. In their development, the net electrical energy input at any point is balanced by the temperature rise and the net thermal energy flowing out from the point. The equation forms a sound basis for explaining many of the features observed in electrothermal devices. A computer simulation on the basis of this equation was performed by Warren[35].

The addition of the continuity equation to the model was another step forward towards the understanding of these devices. Using the steady state continuity equation

$$\nabla . \overline{J} = 0 \qquad (1.4.1.)$$

and the appropriate energy balance equation, Kaplan[36], and others were able to obtain the steady-state curves of the devices with reasonable accuracy.

1.5. The Need for a New Model

Despite these numerous modeling efforts, many deficiencies existed. Most importantly, all the models previously developed were essentially static in nature. The only time constant involved was in the energy equation. This thermal time constant is of the order of a few hundred microseconds and cannot explain the nanosecond switching observed.

Also, several significant features of the electrothermal switches have not been accounted for in models to date. For instance, the "mobility gap" and the reduction of the "band gap" don't play any part in the formulation of the models. Instead, a change in conductivity, which might include mobility in addition to other bulk parameters, is used as a lumped parameter, explicitly dependent on the temperature.

Previously developed models do not take into account the diffusion of charge carriers due to the high thermal and carrier concentration gradients that would be inevitably set up when a thermal filament is formed. Secondarily, carrier diffusion would cause extremely high local electric fields to be set up. These effects have been completely neglected in previous models.

The present model accounts for the dynamic behavior of the ETD's by incorporating many pertinent features neglected to date by other workers. Both the "mobility gap" and the reduction of the "band gap" have been incorporated, and conductivity is treated as a function of both the mobile carrier density and the carrier mobility. Also, diffusion effects are included by using a more generalized form of the continuity equation.

CHAPTER II

THE MODEL

A dynamic model suitable for observing the high-speed switching phenomenon is developed here. Due to the complexity of the phenomenon, various simplifying assumptions are made. Each of these assumptions is either immediately or later justified. Care has been taken to retain all of the significant characteristic features of the ETD. An isotropic, nondegenerate, homogeneous, uniformly doped "n" type electrothermal semiconductor is considered, the sample being initially in equilibrium at the ambient temperature T_{amb}. Being "n" type, it has a net donor concentration of N_d atoms/m^3, not all of which are ionized at room temperature.

2.1. The Band Structure

For simplicity, consider the semiconductor to be a direct band gap semiconductor possessing a single parabolic valence band and a single parabolic conduction band. Further, the semiconductor is assumed to be nondegenerate in the entire temperature range of operation; in other words, though the Fermi-Dirac statistics are applicable, the Boltzmann distribution can be used as a reasonable approximation[21].

In a nondegenerate semiconductor, the Fermi level E_f lies within the band gap, and, since the material is "n" type, E_f lies in the upper half of the band gap. Since it is assumed that the material is only partially ionized at the room temperature, the Fermi level E_f would lie approximately half way between the donor level E_d and the conduction band edge E_c[13]. The energy level diagram under these conditions is shown in Fig. 2.1a, where E_i is the intrinsic energy level.

In an ETD, the band gap E_g reduces sharply when the critical temperature T_{cr} is reached. As discussed in Appendix G, the activation energy E_a will also reduce correspondingly. Thus, the form of the energy level diagram of Fig. 2.1a remains the same after the transition temperature T_{cr}. Since the energy gap E_g and the activation energy E_a change so dramatically at the critical temperature T_{cr}, the continuous change with temperature is negligable in comparison. So, the activation energy E_a is simulated by a step function with respect to temperature, the step occurring at T_{cr}. Below and above T_{cr}, it is a constant. (See Fig. 2.1b.)

2.2. Donors, Electrons, and the Net Charge Density

As stated earlier, the donors are assumed to be only partially ionized below the transition temperature. The donor atoms ionize thermally, creating one free electron per atom. It is assumed also that thermal ionization of the donors is the only significant process existing within the material which can create mobile charge carriers. If Boltzmann statistics are applicable and if E_a is the thermal energy associated with ionization, then the net density of ionized donors at any point in the material is given by:

$$n_d^+(\bar{r},t) = N_d \exp\left[-E_a(T)/2kT(\bar{r},t)\right] \qquad (2.2.1)$$

where N_d is the uniform donor density, $n_d^+(\bar{r},t)$ is the ionized donor density, k is the Boltzmann's constant, and $T(\bar{r},t)$ is the temperature. This equation is developed in some detail in Appendix G. Since $E_a(T)$ is a step function of temperature only (refer Fig. 2.1b), and N_b is a scalar constant for the material, n_d^+ is an explicit function of temperature, as shown in Fig. 2.2.

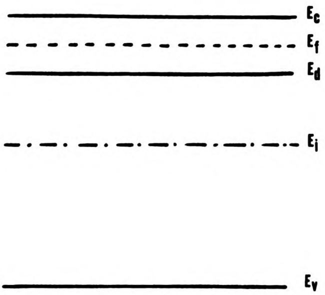

Figure 2.1a

Energy Level Diagram at the Ambient Temperature of the Model ETD

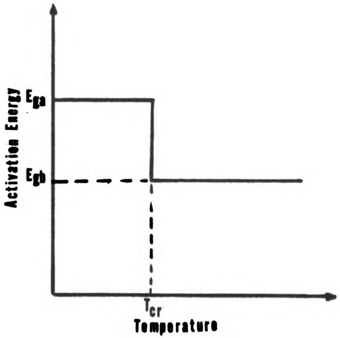

Figure 2.1b

Activation Energy Plotted as a Function of Temperature of the Model ETD

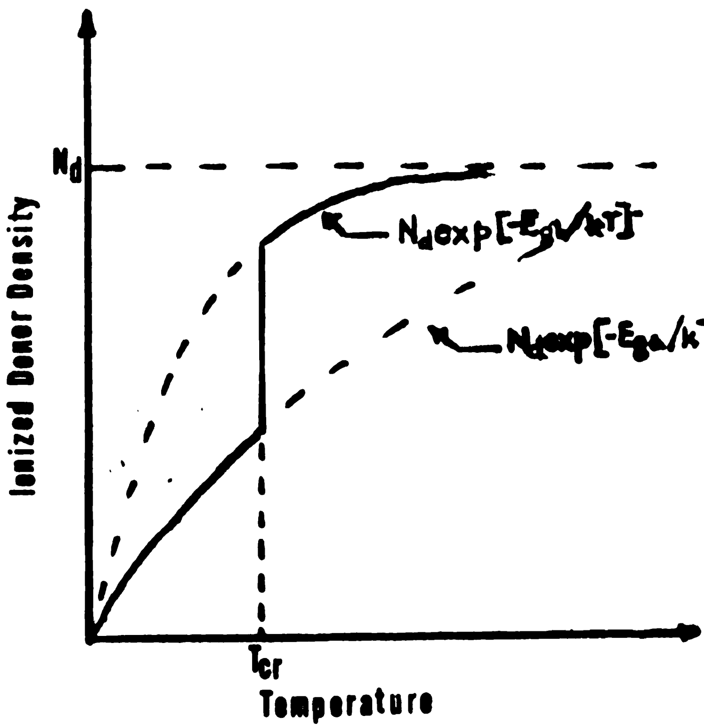

Figure 2.2

Ionized Donor Density-vs-Temperature Characteristic of Model ETD

Like the donor atoms, the donor ions are stationary, but each ion carries a charge of +e. The ionized donors are assumed to be the only positive charges within the material; i.e., the density of holes and other positive charge carriers are negligible. Therefore, the total positive charge q^+ at any point within the material is:

$$q^+(\bar{r},t) = en_d^+(\bar{r},t) \tag{2.2.2}$$

Similarly, mobile electrons are assumed to be the only significant negative mobile charge present. The total negative charge, q^-, at any point is, therefore,

$$q^-(\bar{r},t) = -en(\bar{r},t) \tag{2,2,3}$$

where n is the free electron concentration. Thus the net charge density ρ at any point $(\bar{r},t)$ is:

$$\rho(\bar{r},t) = q^+(\bar{r},t) + q^-(\bar{r},t) = en_d^+(\bar{r},t) - en(\bar{r},t) \tag{2.2.4}$$

The net charge density if not necessarily zero everywhere within the material, because of temperature gradients and possible diffusion effects, as will be discussed in a later section. The Eqs. (2.2.1)-(2.2.4) are thus assumed to be valid for the entire operating temperature range.

Again, since mobile electrons are created only by donor ionization on a one-to-one basis, the rate of generation of electrons and donor ions are equal:

$$\frac{dn(\bar{r},t)}{dt} = \frac{dn_d^+(\bar{r},t)}{dt} \tag{2.2.5}$$

So the net charge creation rate is zero everywhere as follows:

Using (2.2.4),

$$\frac{d\rho(\bar{r},t)}{dt} = \frac{d}{dt}(q^+(\bar{r},t) + q^-(\bar{r},t))$$

Applying (2.2.2) and (2.2.3) to the above,

$$\frac{d\rho(\bar{r},t)}{dt} = e\frac{dn_d^+(\bar{r},t)}{dt} - e\frac{dn(\bar{r},t)}{dt} = 0 \tag{2.2.6}$$

But, due to drift and diffusion of electrons, $\frac{\partial \rho}{\partial t}(\bar{r},t)$ will not be zero everywhere. Instead, the equation of charge continuity applies. (See Appendix H.)

$$\frac{d\rho}{dt}(\bar{r},t) = \frac{\partial \rho}{\partial t}(\bar{r},t) + \nabla.\bar{J}(\bar{r},t)$$

Using (2.2.6) this reduces to

$$\frac{\partial \rho}{\partial t}(\bar{r},t) + \nabla.\bar{J}(\bar{r},t) = 0 \tag{2.2.7}$$

where $\bar{J}(\bar{r},t)$ in the above two equations is the net electron current density.

The time of ionization is assumed to be "instantaneous"; this is a reasonable assumption since this is an atomic process and involves times of the order of 10^{-15} sec.[37].

2.3. Carrier Mobility and Conductivity

Since the material contains only one type of mobile carrier, namely electrons, the carrier mobility refers only to the mobility of the mobile electrons. Also, the mobility is a scalar, since the material is isotropic; and it is a function of temperature, since "mobility gaps" exist in such materials. But, the mobility change at T_{cr} is so drastic that the mobility, like the activation energy, can be taken to be a step function of temperature as depicted in Fig. 2.3. Note that this choice is made to simplify the mathematics of the problem; any given mobility profile could have been chosen in Fig. 2.3.

The mobility change is assumed to be an explicit function of temperature only. For instance, if the temperature of the material everywhere is less than its critical temperature T_{cr}, the mobility is scalar constant having a value μ_a; if the temperature everywhere is above T_{cr}, the mobility is a constant of value μ_b.

Since only n-type carriers are involved and no minority p-carriers are present, the conductivity relation of Eq. (1.2.2) reduces to

$$\sigma(\bar{r},t) = n(\bar{r},t)e\mu(T) \tag{2.3.1}$$

The conductivity is thus not a function of temperature only; however, a fair approximation can be obtained from the following consideration: Though $n(\bar{r},t)$ is not an explicit function of temperature, $n_d^+(\bar{r},t)$ is. Also, at any point $(\bar{r},t)$, n_d^+ and n cannot be very radically different; a large difference in the two would imply a large local charge separation. This would result in tremendously large electric fields being set up tending to reduce the separation. Thus, for many points within the material, the conductivity-versus-temperature plot can be obtained by using

$$\sigma(T) \sim n_d^+(T)e\mu(T) \tag{2.3.2}$$

The product of Figs. 2.2 and 2.3 yields Fig. 2.4 which bears a close resemblance to Futaki's experimental curve (Fig. 1.1a) where σ_1, the asymptote to the first section of the curve is $N_d e\mu_a$ and σ_2, the asymptote to the second section is $N_d e\mu_b$.

For purposes of the model, however, Eq. (2.3.1) is utilized; otherwise, the effects of the large local electric fields would not be observed.

2.4. Electric Fields and Potential

The electric field $\bar{E}$ within a material is defined as the force in newtons exerted on a unit charge (coulombs). In rationalized m.k.s. units, which is used consistently throughout, $\bar{E}$ is expressed in volts/m. There are two factors that can contribute to the existence of the electric field $\bar{E}$. Firstly, it could be due to the application of an external applied field and secondly, to the creation of local fields by internal charge separation.

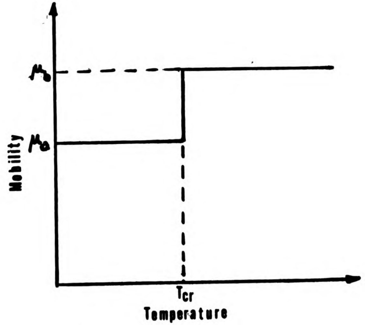

Figure 2.3

Temperature Dependence of Mobility
in Model ETD

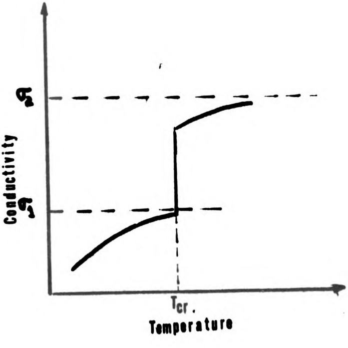

Figure 2.4

Approximate Conductivity-vs-Temperature
Characteristic of Model ETD

In the present model, two kinds of charged particles are present, namely electrons and singly ionized donor atoms. Although the donor ions are stationary, a net local charge separation may occur due to the movement of the mobile electrons. Gauss's Law states:

$$\nabla \cdot \bar{E}(\bar{r},t) = \rho(\bar{r},t)/\epsilon \qquad (2.4.1)$$

where ρ is the net charge distribution as defined earlier and ϵ is the permittivity. The only assumption in the above equation is that is a scalar constant. Since the ETD has already been assumed isotropic, the preceding statements imply that is assumed independent of temperature.

In addition to the above, an electric field can also result due to a rate of change of magnetic flux in the material. Maxwell's second equation expresses the above statement of Faraday's Law mathematically:

$$\nabla \times \bar{E}(\bar{r},t) = -\frac{\partial \bar{B}(\bar{r},t)}{\partial t} \qquad (2.4.2)$$

The rate of change of magnetic fields is associated[38] with inductive effects; it is large if:

1. the frequency of operation is large.
2. the magnetic permeability $\bar{\mu}$ of the material is large.
3. the current through the material is large and rapidly varying.
4. the path length of the current through the device is long and strongly coupled to itself, as in a coil.
5. it is coupled strongly to external magnetic fields in its neighborhood.

In the system discussed in the next chapter, the dimensions are kept small and the geometry simple. The electrothermal material is nonmagnetic and often disordered; so the relative permeability $\bar{\mu}_r$ is approximately unity. Also, there are no strong externally applied magnetic fields in proximity to the device. Even the external circuit is chosen such that the current is limited by an external resistor. Here the magnetic field effects are neglected and Eq. (2.4.2) can be rewritten as

$$\nabla \times \overline{E}(\overline{r},t) = 0 \qquad (2.4.3)$$

The validity of this assumption is discussed further in Chapter 6.

From the principles of vector calculus, it is known that if the curl of a vector field is zero, then the vector field is conservative and can be expressed as the gradient of a scalar potential function. The potential function corresponding to the electric field is called the electric potential V. Hence:

$$\overline{E}(\overline{r},t) = -\nabla V(\overline{r},t) \qquad (2.4.4)$$

Combining the above equation with Gauss' Law, Eq. (2.4.1), Poisson's equation is obtained:

$$\nabla . \nabla V(\overline{r},t) = -\rho(\overline{r},t)/\epsilon \qquad (2.4.5)$$

2.5. Electrical Current Mechanisms

The electrical current mechanisms in a semiconductor can be subdivided into two broad classes: mechanisms which involve a physical transport of mobile charge carriers and those which do not. In the latter category is the capacitative or displacement current.

The displacement current density $\overline{J}_{disp}(\overline{r},t)$ at any point is obtained from the following relation:

$$\overline{J}_{disp}(\overline{r},t) = \frac{\partial \overline{E}(\overline{r},t)}{\partial t} \qquad (2.5.1)$$

It is related to the rate of change of electric field and will be large when the electric field varies rapidly, as may happen when switching takes place.

The mechanisms which can result in an actual transport of the mobile charges, i.e., electrons, are drift and diffusion. The presence of an electric field causes drift. This drift or conduction current density $\bar{J}_{cond}$ is given by:

$$\bar{J}_{cond}(\bar{r},t) = \sigma(\bar{r},t)\bar{E}(\bar{r},t) \qquad (2.5.2)$$

where $\sigma(\bar{r},t)$ is the conductivity and $\bar{E}$ is the net electric field.

Electron diffusion is produced by two methods: due to thermal diffusion caused by temperature gradients in the material and due to concentration diffusion caused by a non-uniform distribution of free electrons in the electrothermal semiconductor. The expression for the total diffusion current $\bar{J}_{diff}$ is:

$$\bar{J}_{diff}(\bar{r},t) = \alpha\nabla T(\bar{r},t) + eD\nabla n(\bar{r},t) \qquad (2.5.3)$$

and so

$$\bar{J}(\bar{r},t) = \alpha\nabla T(\bar{r},t) + eD\nabla n(\bar{r},t) + \sigma(\bar{r},t)\bar{E} \qquad (2.5.4)$$

The above expression can be more rigorously obtained by a direct consideration of the distribution function (Appendix A1). α and D are proportionality factors. In Appendix A2, α and D are evaluated, assuming Maxwell-Boltzmann statistics closely approximate the actual non-equilibrium carrier distribution function. Hence $\bar{J}_{diff}(\bar{r},t)$ becomes

$$\bar{J}_{diff}(\bar{r},t) = (k/e)\mu(T)[n(\bar{r},t)\nabla T(\bar{r},t) + T(\bar{r},t)\nabla n(\bar{r},t)]$$

which can be rewritten as:

$$\bar{J}_{diff}(\bar{r},t) = (k/e)\mu(T)\nabla[n(\bar{r},t)T(\bar{r},t)] \qquad (2.5.5)$$

where the symbols have the same meanings as already defined.

The total current density $\bar{J}(\bar{r},t)$, comprising the drift and diffusion components, is obtained by combining Eqs. (2.5.2) and (2.5.5):

$$\bar{J}(\bar{r},t) = \sigma(\bar{r},t)\bar{E} + k\mu(T)\nabla[n(\bar{r},t)T(\bar{r},t)] \qquad (2.5.6)$$

Substituting for σ, the conductivity, and $\bar{E}$, the electric field, by previously obtained Eqs. (2.4.4) and (2.3.1), the above can be expressed in terms of scalar variables only:

$$\bar{J}(\bar{r},t) = -n(\bar{r},t)e\mu(T)\nabla V + k\mu(T)\nabla[n(\bar{r},t)T(\bar{r},t)] \qquad (2.5.7)$$

$$= \mu(T)\left\{k\nabla\left[n(\bar{r},t)T(\bar{r},t)\right] - en(\bar{r},t)\nabla V(\bar{r},t)\right\} \quad (2.5.8)$$

In summary, the model assumes that carrier current is attributable to electron motion only, which is made up of diffusion and conduction components:

$$\bar{J} = \bar{J}_{cond} + \bar{J}_{diff} \quad (2.5.9)$$

the conduction component being due to the electrical potential gradients in the material

$$\bar{J}_{cond} = -n(\bar{r},t)e\mu(T)\nabla V \quad (2.5.10)$$

and the diffusion resulting from both thermal and concentration gradients

$$\bar{J}_{diff} = \mu k\nabla(nT) \quad (2.5.11)$$

A third component, the displacement current, is also present, which is contained in the $\frac{\partial\rho}{\partial t}$ term of the continuity equation:

$$\frac{\partial\rho}{\partial t} + \nabla.\bar{J} = 0$$

or

$$\frac{\partial\rho}{\partial t} + \nabla.\bar{J}_{cond} + \nabla.\bar{J}_{diff} = 0 \quad (2.5.12)$$

2.6. Thermal Properties: Heat Content and Heat Transfer

Since the particle transport in the material involved the motion of the electrons only, the mechanisms were predominantly electrical. The thermal parameters play an important role, too, primarily when dealing with the energy transport in the material. The two important thermal parameters for this system are the heat capacity c and the thermal conductivity k_{th}.

The heat capacity c is defined as the amount of heat energy input (joules) required to raise unit volume of the solid ($1m^3$) through 1 K. It is expressed in units of joules/(m^3 - K). The increase in heat content increases the lattice vibrational energy as well as the energy of random motion of the mobile carriers--the conduction electrons. But the latter is generally negligible compared to the former unless the lattice vibrational energy is very small: e.g., when the temperature approaches 0 K. At room temperature, the electron contribution can be safely neglected. The vibrational heat capacity is usually a weak function of temperature. Over the limited temperature range used in the model, it can be assumed to be independent of temperature. Also, the model assumes material isotropy and allows only temperature related inhomogeneities. Observe that the specific heat has about the same numerical value for most solids; it is very weakly dependent on the structure. Thus, if a new structure is achieved beyond T_{cr}, the specific heat can be assumed to remain the same. So, the heat capacity of the solid will also remain unaltered provided no change takes place in the overall volume of the solid. This is in fact assumed to be the case in the model under discussion. This assumption is discussed further in the next section. Therefore, if the temperature of the system at any point increases by an amount T, the corresponding increase in internal energy u is

$$\Delta u = c\Delta T \tag{2.6.1}$$

Of the three heat transfer mechanisms--radiation, convection, and thermal conduction--only thermal conduction is significant here. Radiation heat transfer is proportional to the fourth power of the difference in temperatures between the two bodies exchanging heat (Stefan's Law)[39]. It is insignificant if large temperature differences do not exist between the sample and a neighboring body; in other words, it is negligible if there are no heat sources in the vicinity. Convection implies fluid motion; in a solid sample, there are no convection currents.

In thermal conduction, the thermal flux density is related to the temperature gradient by Fourier's Law[39]

$$\bar{J}_q = -k_{th}\nabla T \qquad (2.6.2)$$

k_{th} is the thermal conductivity of the material and is expressed in units of watts/(m - K). Like σ and ϵ, it is, in general, a tensor. However, in the model, it is assumed to be a scalar constant. Since the ETD has already been assumed isotropic, the preceding statement implies that k_{th} is assumed to be independent of temperature.

2.7. Entropy and Energy Transfer

All material variables can be conveniently divided into two classes[39,46]. The first class, called extensive variables, depend on the mass of the material, typical examples being volume V, internal energy U, number of carriers N or P, total charges Q, etc. On the other hand, intensive variables do not depend on the mass of the material. Typical examples are temperature T, chemical potential K, pressure p, and electrical potential V. Similar classifications exist in other fields of study; extensive variables are closely related to "flux" used in physics and engineering or the "through" variables of systems science, whereas intensive variables resemble the "potential" or "across" variable. A frequently used extensive variable in thermodynamics is "entropy". It is a measure of the order of the system, and, for a totally closed system, it always increases with time. For ideal, perfectly reversible processes, the entropy for the system remains constant.

Each extensive variable in the system is linked to a specific intensive variable; for instance, the entropy S is usually linked to the temperature T, the electrical potential V with Charge Q, etc. To describe a system of variables completely, a complete set of extensive variables is required, together with the set of corresponding intensive variables.

The total internal energy U of the electrothermal sample is a function of all other relevant extensive variables S, V, N, P, Q.

$$U = U(S,\ V,\ N,\ P,\ Q) \qquad (2.7.1)$$

Taking the total time derivative of the above equation

$$\frac{dU}{dt} = \left.\frac{\partial U}{\partial S}\right|_{V,\ N,\ P,\ Q} \frac{dS}{dt} + \left.\frac{\partial U}{\partial V}\right|_{S,\ N,\ P,\ Q} \frac{dV}{dt} + \left.\frac{\partial U}{\partial N}\right|_{S,\ V,\ P,\ Q} \frac{dN}{dt}$$

$$+ \left.\frac{\partial U}{\partial P}\right|_{S,\ V,\ N,\ Q} \frac{dP}{dt} + \left.\frac{\partial U}{\partial Q}\right|_{S,\ V,\ N,\ P} \frac{dQ}{dt} \qquad (2.7.2)$$

The partials in the above expression correspond to the associated intensive variables as follows:

$$\frac{\partial U}{\partial S}/V,\ N,\ P,\ Q = T \quad \text{(the temperature)} \qquad (2.7.3a)$$

$$\frac{\partial U}{\partial V}/S,\ N,\ P,\ Q = p \quad \text{(the pressure)} \qquad (2.7.3b)$$

$$\frac{\partial U}{\partial N}/S,\ N,\ P,\ Q = K_n \quad \text{(chemical potential for electrons)} \qquad (2.7.3c)$$

$$\frac{\partial U}{\partial P}/S,\ V,\ P,\ Q = K_p \quad \text{(chemical potential for + charges)} \qquad (2.7.3d)$$

$$\frac{\partial U}{\partial Q}/S,\ V,\ N,\ Q = V \quad \text{(electrical potential)} \qquad (2.7.3e)$$

Eq. (2.7.2) can therefore be rewritten as:

$$\frac{dU}{dt} = T\frac{ds}{dt} + p\frac{dV}{dt} + K_n\frac{dN}{dt} + K_p\frac{dN^{+}_{d}}{dt} + V\frac{dQ}{dt} \qquad (2.7.4)$$

The above equation has the general form:

$$\frac{dU}{dt} = \sum_i p_i \frac{dq_i}{dt},$$

where q_i is a general extensive or flux variable of the system and p_i is the general intensive variable, or the potential responsible for the flux q_i.

In view of the various assumptions made, Eq. (2.7.4) can be simplified considerably. The second term is disregarded since the volume of the system i

ical work done

work is being d

$$\frac{dV}{dt} = 0$$

Also, the only

electrons. Thu

$$V \frac{dQ}{dt} =$$

Using t

by the volume of

$$\frac{du}{dt} = T \frac{d}{d}$$

where u, s, n, n

electrons, and n

sample.

The energ

tion is also negl

parent in a later

Eq. (2.7.

The overall rate

the various energ

a measure of the

upon as a loss te

zero. The term K

due to the chem

the creation and

tion diffusion.

ionized donors.

of the system is assumed to remain constant. The term $\frac{dV}{dt}$ is the mechanical work done by or on the system; the model assumes that no mechanical work is being done.

$$\frac{dV}{dt} = 0 \tag{2.7.5}$$

Also, the only kind of mobile charge carriers present in the system are electrons. Thus, the term $V \frac{dQ}{dt}$ can be rewritten as:

$$V \frac{dQ}{dt} = -eV \frac{dN}{dt} \tag{2.7.6}$$

Using the above simplifying assumption and dividing the Eq. (2.7.4) by the volume of the system V, it becomes:

$$\frac{du}{dt} = T \frac{dS}{dt} + K_n \frac{dn}{dt} + K_p \frac{dn_d^+}{dt} - eV \frac{dn}{dt} \tag{2.7.7}$$

where u, s, n, n_d^+ refer to the internal energy, entropy, number of free electrons, and number of ionized positive charges per unit volume of the sample.

The energy associated with the chemical reaction causing ionization is also neglected. The implications of this statement will be apparent in a later chapter.

Eq. (2.7.7) is an expression of the energy balance of the system. The overall rate of change of internal energy $\frac{du}{dt}$ is equal to the sum of the various energy components of the system. The first term, $T \frac{ds}{dt}$, is a measure of the increase of disorder in the system; it can be looked upon as a loss term. In an idealized, reversible system, this term is zero. The term $K_n \frac{dn}{dt}$ is the energy associated with the mobile electrons n due to the chemical potential K_n. It is thus the energy involved in the creation and transport of mobile electrons by thermal and concentration diffusion. $K_p \frac{dn_d^+}{dt}$ is the energy associated with the creation of the ionized donors. Lastly, the term $-eV \frac{dn}{dt}$ is the energy associated with

the transport of electrons due to the presence of the electrical potential V. In other words, it accounts for the drifting of conduction electrons due to the electric field $\overline{E}$. Each of these energies contribute to the overall rate of increase of internal energy of the ETD.

CHAPTER III

MATHEMATICAL FORMULATIONS OF THE MODEL

The previous chapter dealt with the various properties of the electrothermal material and how they were affected by the idealizations and assumptions of the model. In this chapter, a specific geometry is chosen, and the sample is placed in an electrical circuit, comprising a battery B, a resistor R_s, and a switch S. Using the material properties discussed in Chapter 2, a set of equations describing the overall system is obtained, together with the necessary initial and boundary conditions.

3.1. Sample Geometry

Experimenters have commonly used three kinds of geometries in studying the electrothermal switching device(41), namely: a) The Bead or Pellet Configuration; b) The Planar Structure; c) The Sandwich Configuration. The three types are illustrated in Figs. 3.1, 3.2, and 3.3 respectively.

Electrothermal switching was perhaps first observed in sintered metal-oxide complexes(33). The sintering was done under pressure using two half-ellipsoidal molds, with the electrodes laid as rods across the middle and protruding at either end. The resultant beads, however, had one major practical disadvantage--they had poor thermal contact with the heat sink, which, of course, was the electrode itself. Moreover, the mathematical analysis of such ellipsoidal structures is quite complex.

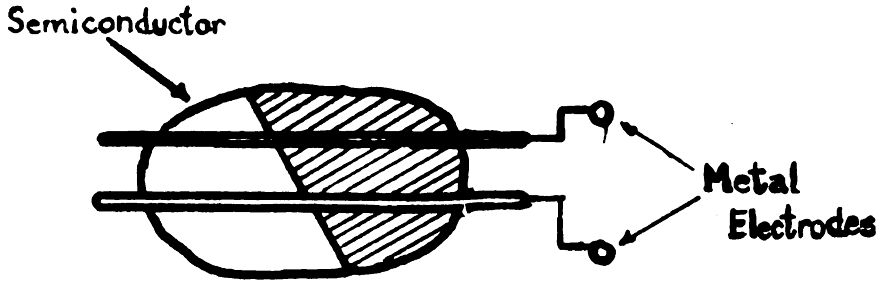

Figure 3.1

The Bead Geometry

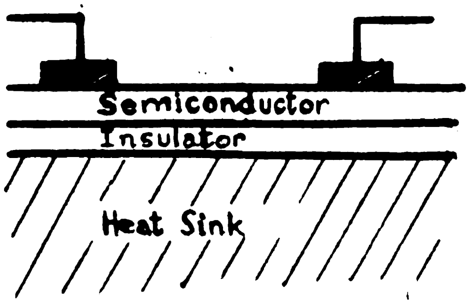

Figure 3.2

The Planar Geometry

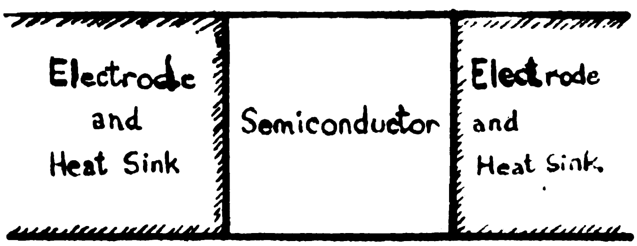

Figure 3.3

The Sandwich Structure

The planar geometry, obtained by thin-film deposition techniques and used by Berglund[34], Duchene[40], and numerous other workers[41,42,43,34], proved experimentally far more satisfactory, particularly because of the large contact area with the heat sink. But the structure was asymmetric, and so, the analytic solution of such a geometry was not very simple.

The sandwich structure is the simplest to analyze, especially if a simple geometrical shape, like a cube, cylinder, or rectangular parallelepiped, is selected as the semiconductor geometry. It also possesses the advantages of the sandwich structure in that there is good thermal contact with the heat sink. The advantages of the various geometries have been discussed at some length by Yu[41]. Nevertheless, the underlying principles governing the operation of the ETD remain the same regardless of the geometry chosen.

For purposes of this model, the material geometry is selected to be a rectangular parallelepiped with a square cross section. For mathematical analysis, a Cartesian co-ordinate system is chosen with the origin at one corner of the sample,* such that the y and z -axes lie almost along the edges forming the square face, and the x-axis lies along the other edge. Thus, the sample is located entirely in the positive octant of the co-ordinate system. (See Fig. 3.4.)

The semiconductor is assumed to have the dimensions of L_x,** L_y, and L_z along the x, y, and z -axes respectively. Since the material is assumed to have a square cross section: $L_y = L_z$. As pointed out earlier, this choice of a square cross section has been

---

*Actually, the origin is chosen to lie a distance within the sample where $\delta > 0$ and $\delta \lll L_x$. This is convenient because of the boundary conditions.

**More accurately, $L_x + 2\delta$ where $\delta \lll L_x$. This is discussed in detail when discussing the boundary conditions at the semi-electrode interface in Section 3.5.

made merely for mathematical convenience; the model would work equally well even if $L_y \neq L_z$.

3.2. The External Electrical Circuit Configuration

The external circuit, connected between nodes 1 and 2 of the sample (refer Fig. 3.4), comprises of the following:

a) an ideal d-c voltage source of V_{app},

b) a series resistor R_s, assumed to be independent of temperature and the current through it,

c) an ideal single pole single throw switch S which is initially off and which is turned on at some time t = 0, and

d) two highly conducting electrodes at nodes 1 and 2 between which the sample is connected and which is turned on at some time t = 0. Also, the electrodes make ideal ohmic contacts with the sample at each node. Thus, there is no voltage drop either at the electrode or at the interface of the electrode and the ETD.

The circuit diagram is shown in Fig. 3.5. Node 2 is grounded, and node 1 is the live terminal of the ETD.

In addition, the following assumptions are made regarding the system: (a) The electrodes are assumed to be ideal heat sinks. (b) Air, which surrounds the ETD on four sides, is assumed to be an ideal thermal insulator and dielectric. (c) Initially, before the switch S is turned on, the ETD is in equilibrium. Let the equilibrium temperature be T_{amb}. (d) In comparison to the various circuit parameters, cable capacitances and lead inductances are assumed negligible. (e) The switch S is turned on at time t = 0: i.e., all times t are measured with reference to the instant the switch is turned on. (f) In this model, the various variables

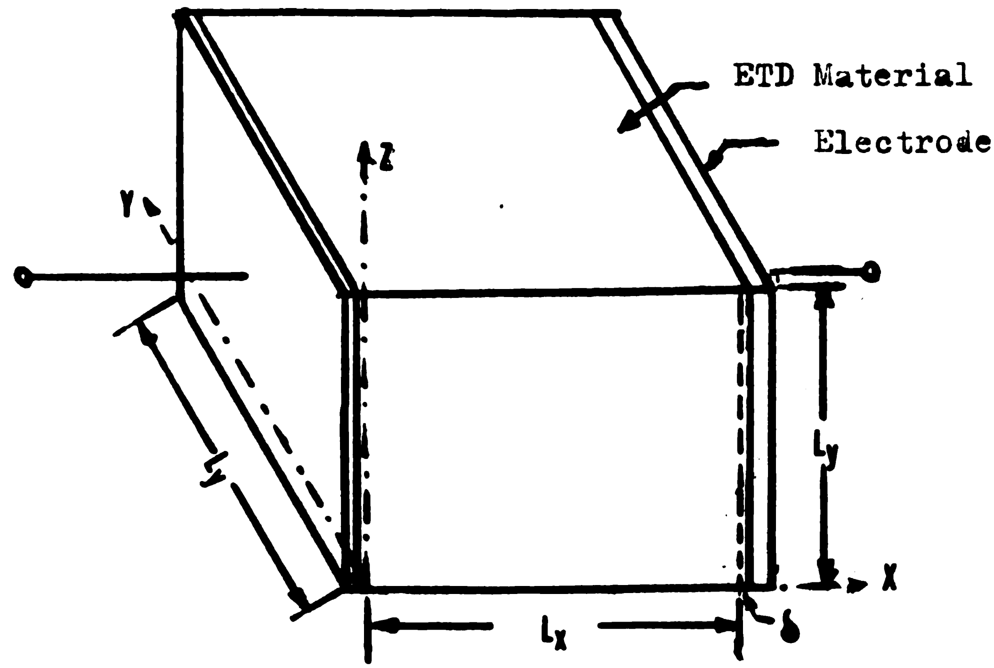

Figure 3.4

Sample Geometry of the Model ETD

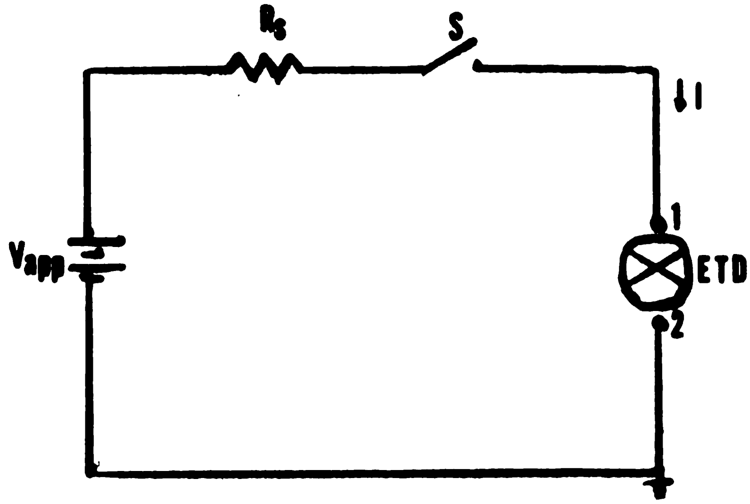

Figure 3.5

Circuit Diagram of the External Electrical
Circuit Used in the Simulations

associated with the sample are evaluated at different times, starting from a time Δt_0 after the switch S is turned on. The time Δt_0 is chosen large enough such that the initial transients due to the switching impulse have died down. But, Δt_0 is chosen small compared to the thermal time constant τ_a. (This time constant is discussed in more detail in Section 3.4.) (g) The ETD is assumed to be electrically neutral at all points in the sample before t = 0. In other words,

$$n(\bar{r},0) = n_d^+(\bar{r},0) = N_d \exp[-E_a/kT_{amb}] \qquad (3.2.1)$$

$$\delta(\bar{r},0) = 0 \qquad (3.2.2)$$

3.3. The Static D-C Characteristics

When the switch S is turned on at t = 0, the entire system is in thermal equilibrium, and the semiconductor is uniformly at the ambient temperature T_{amb}. If σ_0 is the conductivity of the sample at the ambient temperature, then its d-c resistance R_0 at this time is given by

$$R_0 = \frac{L_x}{\sigma_0 L_y^2}, \qquad (3.3.1)$$

where all surface effects are assumed to be negligible.

Consider the ETD at a time Δt_0 . Δt_0 is a time large enough such that the initial switching transients due to turning on the switch S have died out. However, Δt_0 is much smaller than the thermal time constant τ_a associated with the ETD.* At this time, the direct current I_0^+ at node 1 is given by:

$$I_0^+ = V_{app}/(R_s + R_0) \qquad (3.3.2)$$

If R_s is chosen to be a fraction $f(f \leq \infty)$ of R_0 such that: $R_s < fR_0$ ohms, then the current I_0^+ can be rewritten as:

$$I_0^+ = V_{app}/R_0(1 + f) \qquad (3.3.3)$$

---

*This is discussed further in Sections 3.4 and 3.5.

Substituting the expression for R_0 from Eq. (3.2.1), the current measured at node 1 at $t = 0^+$ is

$$I_0^+ = \frac{V_{app}\sigma_0 L_y^2}{L_x} \cdot \frac{1}{1+f} \text{ A} \tag{3.3.4}$$

The voltage appearing across the sample at $t = 0^+$ is, therefore, $V_0^+ = R_0 I_0^+$.

Substituting Eq. (3.2.3) in the above equation:

$$V_0^+ = \frac{V_{app}}{1+f} \tag{3.3.5}$$

Because the conductivity of the semiconducting sample is finite, power is dissipated due to the current in the semiconductor. The dissipated power is converted to heat; therefore, the temperature of the sample will rise. Increased temperature implies increased ionization, and so the conductivity will also increase. The conduction current will increase with time until a final steady state is reached. Hence, the voltage V_0^+ and current I_0^+ are the static maximum terminal voltage and minimum terminal current at node 1 of the sample respectively and so are designated hereon as V_{max} and I_{min}.

To obtain the limits of maximum static current I_{max} and minimum static voltage V_{min}, it is assumed that the semiconductor is completely and uniformly ionized at some temperature T . Since the material is uniformly ionized, no thermal or concentration gradients exist, and the only component of current in the sample is conduction current. The conductivity of the sample at this time is (using Eq. 2.3.1)

$$\sigma_{max} = N_d e \mu_b \tag{3.3.6}$$

Note that in the above expression, the electron concentration is taken to be the donor concentration. This is because the model has only one mechanism for creation of electrons, namely donor ionization. Consequently, at any instant, the total number of ionized donors exactly equal the number of mobile electrons. Hence,

$$\sigma_{max}/\sigma_0 = \frac{N_d e \mu_b}{N_d \exp(-E_{ga}/kT_{amb}) e \mu_a} \quad (3.3.7)$$

If the mobility gap ratio is represented by μ_r:

$$\frac{\sigma_{max}}{\sigma_0} = \mu_r \exp(E_{ga}/kT_{amb}) \quad (3.3.8)$$

Hence: $\sigma_{max} = \sigma_0 \mu_r \exp(E_{ga}/kT_{amb})$

and so:

$$R_{min} = \frac{L_x}{\sigma_{max} L_y^2} = \frac{R_0}{\mu_r \exp(E_{ga}/kT_{amb})} \quad (3.3.9)$$

Thus, the maximum external circuit current I_{max} is:

$$I_{max} = V_{app}/(R_s + R_{min}) = \frac{V_{app}}{R_0\left[f + \frac{1}{\mu_r}\exp(-E_{ga}/kT_{amb})\right]} \quad (3.3.10)$$

Similarly, V_{min} is given by:

$$V_{min} = I_{max} R_{min} = \frac{V_{app}}{R_0\left[f + \frac{1}{\mu_r}\exp(\frac{-E_{ga}}{kT_{amb}})\right]} \times \frac{R_0}{\mu_r \exp(\frac{E_{ga}}{kT_{amb}})}$$

$$= \frac{V_{app}}{\left[1 + f\mu_r \exp(E_{ga}/kT_{amb})\right]} \quad (3.3.11)$$

Summarizing and using the symbol I_0 to represent current V_{app}/R_0: i.e., $I_0 = V_{app}/R_0$, the maximum limits of the static voltage and current that are allowed by the external circuit configuration are

$$V_{max} = \frac{V_{app}}{1 + f}, \quad (3.3.12)$$

$$V_{min} = \frac{V_{app}}{1 + f\mu_r \exp(E_{ga}/kT)}, \quad (3.3.13)$$

$$I_{min} = \frac{I_0}{1 + f}, \text{ and} \quad (3.3.14)$$

$$I_{max} = \frac{I_0 \mu_r \exp(E_{ga}/kT)}{1 + f\mu_r \exp(E_{ga}/kT)} \quad (3.3.15)$$

The above expressions are the limits of the static terminal currents and voltages. As will be discussed further in the coming section, these can be used as tests indicative of the stability of the results obtained; if the terminal variables were to lie outside the range defined, the ETD would be in an oscillatory state or even a physically unrealizable situation.

3.4. Energy Storage Mechanisms and Time Constants of the ETD

In spite of the apparent simplicity of the circuit, its dynamic behavior involves more than just two resistances in series. This is because of the various energy storage mechanisms present in the system, each of which can be associated with a distinct time constant.

First, there is the thermal time constant, τ_a, due to the energy storage associated with the heat capacity of the ETD. If c is the heat capacity, k_{th} the thermal conductivity and L_x^2 the cross-sectional area of a uniform cube of the material, then τ_a is given by

$$\tau_a = \frac{cL_x^2}{k_{th}} \tag{3.4.1}$$

For the ETD sample chosen, the time constant associated with unit cube of the material is computed below.

The relevant material parameters are

$k_{th} = 6.0\ W/(m - K)$

$c = 3.3 \times 10^5\ J/(m^3 - K)$

$L_x = 10^{-4}\ m$

$\tau_a = 550\mu s$

This time constant plays a significant role in the energy balance equation which is discussed in detail in a later section. Since k_{th} and c have been assumed constant, this time constant τ_a is a constant characteristic of the ETD in this model.

A second time constant τ_a is associated with the thermal and concentration diffusion of the conduction electrons, and is related to the mobility of the electrons.

$$\tau_b = \frac{L_x^2}{\mu(T)kT} \tag{3.4.2}$$

Unlike τ_a, τ_b is a function of temperature and so is not a constant for the material. The value of τ_b is evaluated at two characteristic temperatures T_{amb} and T_{cr} for easy reference:

a) $T_{amb} = 300$ K

$\mu_a = 4.3 \times 10^{-6}$ $m^2/V - s$

$\tau_{b_1} = 90.8$ ms

b) $T_{cr} = 341$ K

$\mu_b = 4.3 \times 10^{-5}$ $m^2/V - s$

$\tau_{b_2} = 7.88$ ms

This time constant is an important factor in the continuity equation that is developed in Section 3.8.

A third important time constant is that associated with the permittivity ϵ of the ETD giving rise to bulk capacitance effects. There again the time constant τ_c

$$\tau_c = \frac{\epsilon}{\sigma(\bar{r},t)} \tag{3.4.3}$$

is not a constant for the material. Since is a function of the free electron density n and mobility μ, τ_c is a fairly complex function of $(\bar{r},t)$.

Good estimates of τ_c can be obtained by using the approximations discussed in Chapter 2.

$$\sigma \sim n_d^+(T)e\mu(T) \qquad \text{(from 2.3.2)}$$

Thus for the two characteristic temperatures, the approximate values of τ_c are:

a) $T = 300$ K

$\epsilon = 4.425 \times 10^{-11}$ F/m

$\sigma_0 = 800$ mhos/m

$\tau_{c_1} = .055$ ps

b) $T = 341$ K

$\sigma_2 = 6.15 \times 10^{4}$ mhos/m

$\tau_{c_2} = 0.00717$ ps

In addition to these three, there are other time constants which have been neglected in the model. For instance, the time constants due to lead inductances and capacitances have been neglected in the formulation of the external circuit equation; and so has the inductive time constant due to the time rate of change of magnetic field in the material.

The limiting values of the terminal current and voltage can be assumed to be the maximum limits, even when the dynamic characteristics of this model ETD are studied. Thus, the relationships (3.3.12) - (3.3.15) for the limiting terminal current and voltages hold for the entire time spans of observation; they are used to test that the overall solution obtained at any t is a physically realizable one.

The time constants obtained in this section are summarized in Table 3.1.

Table 3.1

τ_a	-	550 ms
τ_{b_1}	-	90.8 ms
τ_{b_2}	-	7.88 ms
τ_{c_1}	-	0.055 ps
τ_{c_2}	-	0.00717 ps

3.5. The Thermal Boundary Conditions

Looking back on to the circuit diagram of Fig. 3.5, observe that the rectangular semiconducting block, i.e., the ETD is in contact with perfectly conducting electrodes at two of its surfaces $x = -\delta$ and $x = L_x + \delta$, and with air, which is assumed to be a perfect insulator, on the other four surfaces. In the above statement, the terms "conducting" and "insulator" refer to both thermal and electrical conduction. Because the electrodes are ideal heat sinks, the temperature at each of these electrodes will remain at the ambient temperature T_{amb} for all time. Thus, for all time t,

$$T(-\delta, y, z, t) = T_{amb} \tag{3.5.1}$$

$$T(L_x + \delta, y, z, t) = T_{amb} \tag{3.5.2}$$

Since $\delta \ll L_x$, the temperature at a distance inside the material can be expected to be not significantly different from the temperature at the electrode interface at all times t. Thus

$$T(0, y, z, t) = T_{amb} \tag{3.5.3}$$

$$T(L_x, y, z, t) = T_{amb} \tag{3.5.4}$$

Since the surfaces $y = 0$, $y = L_y$, $z = 0$, and $z = L_z$ are assumed to be in contact with a perfect insulator, there is no heat flowing out of these surfaces[39]; the normal component of the heat flux density is therefore zero everywhere on these surfaces:

$$Jq_y = 0 \text{ at } y = 0 \text{ and at } y = L_y \tag{3.5.5}$$

$$Jq_z = 0 \text{ at } z = 0 \text{ and at } z = L_z \tag{3.5.6}$$

Hence, applying Fourier's Law (Eq. 2.6.2)

$$k_{th}\frac{\partial T}{\partial y} = 0 \text{ at } y = 0 \text{ and at } y = L_y$$

$$k_{th}\frac{\partial T}{\partial z} = 0 \text{ at } z = 0 \text{ and at } z = L_z$$

Thermal conductivity being a finite non-zero scalar constant, the boundary conditions become:

$$\frac{\partial T}{\partial y}(x,\ 0,\ z,\ t) = 0, \tag{3.5.7}$$

$$\frac{\partial T}{\partial y}(x,\ L_y,\ z,\ t) = 0, \tag{3.5.8}$$

$$\frac{\partial T}{\partial z}(x,\ y,\ 0,\ t) = 0, \text{ and} \tag{3.5.9}$$

$$\frac{\partial T}{\partial z}(x,\ y,\ L_z,\ t) = 0. \tag{3.5.10}$$

3.6. The Electric Potential at the Electrode-Semiconductor Interface

Consider the ETD at a time Δt_0 after switch S has been turned on. Recall that time Δt_0 is large enough such that the initial transients due to closing the switch have died down; yet, it is small compared to the thermal time constant $_a$ discussed in the previous section. Δt_0 is the first observation time; for the model, this has been taken to be 10 μs.

Since this time is small compared to the thermal time constant, the resistance of the ETD is assumed to be not significantly different from R_0, where R_0 has been defined as the ETD resistance when it is uniformly at the ambient temperature T_{amb}. Hence, the voltage at node 1 at t_0 is given by Eq. (3.3.5). Hence,

$$V_1(\Delta t_0) = V_0^+ = V_{app}/(1 + f) \tag{3.6.1}$$

Also, since node 2 is grounded,

$$V_2(\Delta t_0) = V_2(t) = 0 \tag{3.6.2}$$

Again, since the electrodes are highly conducting and make ohmic contacts with the ETD at the interfaces, the potential at each point on a face in contact with an electrode will have the node voltage corresponding to the electrode. Hence:

$$V(-\delta,\ y,\ z,\ \Delta t_0) = V_1(\Delta t_0) \tag{3.6.3}$$

$$V(L_x + \delta,\ y,\ z,\ \Delta t_0) = 0 \tag{3.6.4}$$

Obviously, the above is true not only for $t = \Delta t_0$, but for all values of t.

$$V(-\delta,\ y,\ z,\ t) = V_1(t) \tag{3.6.5}$$

$$V(L_x + \delta,\ y,\ z,\ t) = 0 \tag{3.6.6}$$

The distance δ has been chosen such that it is smaller than the grid spacing,* but larger than the Debye length associated with the sample. The Debye length for the semiconductor λ_D is obtained from the relation [48] (3.6.7).

$${}_D = \sqrt{\frac{kT}{4\pi ne^2}} \tag{3.6.7}$$

For the present simulation, the minimum grid spacing x and the Debye length λ_D are compared below.

${}_D = 3.334 \times 10^{-6}$ m at T = 300 K

$x = 1 \times 10^{-5}$ m

A value of δ of 5×10^{-6} m is therefore appropriate. Since δ is much smaller than the space dimensions, i.e., $\delta \ll L_x$, L_y the potential at points near either electrode within a δ-neighborhood of the electrode interface can be assumed to be equal to the voltage at the electrode. Consequently, the Eqs. (3.6.6) and (3.6.7) for any time become

$$V(0,\ y,\ z,\ t) = V_1(t) \tag{3.6.8}$$

$$V(L_x,\ y,\ z,\ t) = 0 \tag{3.6.9}$$

Specifically, at Δt_0, the relations become (using Eq. (3.6.1)):

$$V(0,\ y,\ z,\ \Delta t_0) = V_{app}/(1 + f) \tag{3.6.10}$$

$$V(L_x,\ y,\ z,\ \Delta t_0) = 0 \tag{3.6.11}$$

---

*The grid structure is discussed in Chapter 4.

$V_1(t)$ for all other times $t > \Delta t_0$ is evaluated in a subsequent section.

Because of the power dissipation in the ETD due to the electrical current, the temperature of the ETD will rise. However, this temperature rise will not be uniform due to the thermal boundary conditions of the ETD.

3.7. Net Charge Density at the Electrode-Semiconductor Interface

Once the switch S is turned on, a surface charge of $-\sigma_s$ and $+\sigma_s$ is built up at the semiconductor surfaces $x = -\delta$ and $x = L_x + \delta$, the magnitude of which is determined by the bulk capacitance of the ETD. If ϵ is the permittivity of the semiconductor, σ_s at Δt_0 is given by

$$\sigma_s = \frac{\epsilon L_y^2}{L_x} V_1(\Delta t) \text{ coulombs} \tag{3.7.1}$$

However, at a distance δ within the semiconductor from an electrode, there is no surface charge density, since δ has been assumed to be much larger than the Debye length. The volume charge density ρ at such a point can be obtained from a consideration of Gauss' Law:

$\rho = \epsilon \nabla . \bar{E}$

Consider the semiconductor at the instant Δt_0 where

$t_0 \ll \tau_a$, the thermal time constant

$t_0 \gg \tau_c$, the time constant

associated with the turning-on of the switch. Writing the continuity equation at this time:

$$\frac{\partial \rho}{\partial t} + \nabla . [\sigma \bar{E}] = 0 \tag{3.7.2}$$

which after a little algebraic manipulation and applying Gauss' Law, yields

$$\frac{\partial \rho}{\partial t} = \frac{\sigma \rho}{\epsilon} + \bar{E} . \nabla \sigma = 0 \tag{3.7.3}$$

Now $\bar{E}.\nabla\sigma = \frac{\partial\sigma}{\partial x} E_x + \frac{\partial\sigma}{\partial y} E_y + \frac{\partial\sigma}{\partial z} E_z$ where E_x, E_y, and E_z are the electric field components along x, y, and z directions respectively. But, near the metal electrodes, the tangential components of the E-fields must be zero, because the tangential component of the E-field must be continuous across a boundary, and, in a metal, there can be no electric fields. Hence, E_y and E_z are zero and so, Eq. (3.7.3) becomes

$$\frac{\partial\rho}{\partial t} + \sigma\frac{\rho}{\epsilon} + \frac{\partial\sigma}{\partial x} E_x = 0 \tag{3.7.4}$$

Hence, at the boundaries, can be obtained by assuming E_x to be a constant with respect to t. The solution for ρ is approximately,

$$\rho = \rho_0 + Be^{-\frac{\sigma}{e}t}$$

Thus, for all $t >> \epsilon/\sigma$, $\rho = \rho_0$ at $x = 0$ and $x = L_x$. For this model, it is assumed that the above statement is true for all times $t > \Delta t_0$. It may be noted that this is not strictly true, since, in the above argument, the material was assumed to be homogeneous. Hence,

$$\rho(0, y, z, t) = \rho_0 \tag{3.7.5}$$

$$\rho(L_x, y, z, t) = \rho_0 \tag{3.7.6}$$

3.8. Boundary Conditions at the Air-Semiconductor Interfaces

Consider now the conditions existing at the four surfaces of the semiconductor exposed to air, for instance, at the plane y = 0. At this boundary, E_x in air is non-zero since the tangential component of the electric field is continuous across the boundary. This is the "fringing" field. The normal component E_y is responsible for the normal conduction current,

$$J_{\text{cond } y} = \sigma E_y$$

Since air is assumed to be a perfect insulator, there cannot be any conduction currents if surface charge effects are neglected. Within the semiconductor, σ, the electrical conductivity is non-zero; hence, E_y

at the surface $y = 0$ is zero. This is similarly true for all four surfaces $y = 0$, $y = L_y$, $z = 0$, and $z = L_y$. Using the relation $\bar{E} = -\nabla V$ developed in Chapter 2, the boundary conditions can be written mathematically as:

$$\frac{\partial V}{\partial y}(x, 0, z, t) = 0,$$

$$\frac{\partial V}{\partial y}(x, L_y, z, t) = 0,$$

$$\frac{\partial V}{\partial z}(x, y, 0, t) = 0, \text{ and}$$

$$\frac{\partial V}{\partial z}(x, y, L_z, t) = 0.$$

The volume charge density is related to the electric field by Gauss' Law $\rho = \epsilon \nabla \cdot \bar{E}$.

The tangential components E_x and E_z are continuous across the interface $y = 0$, and also, there is no conduction current across the interface. Constructing a pillbox of infinitesimally small thickness Δ, it can be shown that

$$\nabla \cdot \bar{E} \text{ at } y = 0.$$

Hence, by Gauss' Law

$$\rho(x, 0, z, t) = 0.$$

Similarly,

$$\rho(x, L_y, z, t) = 0,$$

$$\rho(x, y, 0, t) = 0, \text{ and}$$

$$\rho(x, y, L_y, t) = 0.$$

3.9. The External Circuit Equations

So far the terminal voltage $V_1(t)$ has only been evaluated at the first observation time Δt_0 (refer to Eq. (3.6.1)). The terminal voltage $V_1(t)$ and the terminal current $i(t)$ measured at node 1 are functions of time and are related to each other by Kirchhoff's Voltage Law:

$$V_1(t) = V_{app} - i(t) \cdot R_s \tag{3.9.1}$$

This is the load line equation.

Obviously, this terminal current is equal to the total current at x = 0. The current at x = 0 is comprised of three components:

a) Conduction Current,

b) Diffusion Current, and

c) Displacement Current.

The conduction current density in the x = 0 plane is:

$$J_{cond}(0, y, z, t) = -\sigma(0, y, z, t)\nabla V(0, y, z, t) \tag{3.9.2}$$

However, at x = 0, the temperature T remains the same for all t and, also no significant charge separation takes place here.* Hence,

$$\sigma(0, y, z, t) = n(0, y, z, t)e\mu(T_{amb}) \approx n_d^+(T_{amb})e\mu(T_{amb}) = \sigma_0$$

Thus, the Eq. (3.9.2) reduces to

$$J_{cond}(0, y, z, t) = -\sigma_0 \cdot \nabla V(0, y, z, t) \tag{3.9.3}$$

The diffusion current density at x = 0 is given by (refer Sec. 2.5):

$$\bar{J}_{diff}(0, y, z, t) = \mu(T)k\nabla(n(0, y, z, t).T(0, y, z, t))$$

Since the temperature at x = 0 is T_{amb} for all T, $\mu(T)$ is μ_a and so

$$\bar{J}_{diff}(0, y, z, t) = \mu_a k\nabla(n(0, y, z, t).T(0, y, z, t)) \tag{3.9.4}$$

The displacement current density $\bar{J}_{diff}$ is given by

$$\bar{J}_{diff}(0, y, z, t) = \epsilon\frac{\partial E}{\partial t}(0, y, z, t) \tag{3.9.5}$$

In Sec. 3.8, it was assumed E_x did not change with time.* Hence

$$\bar{J}_{diff}(0, y, z, t) = 0 \tag{3.9.6}$$

The total current density $\bar{J}_T$ at x = 0 is therefore:

$$\bar{J}_T(0, y, z, t) = -\sigma_0\nabla V(0, y, z, t) + \mu_a k\ (n(0, y, z,t) .T(0, y, z, t)) \tag{3.9.7}$$

---

*Surface charge effects are neglected in this model.

The total current can be obtained by integrating the above expression (3.9.7) over the face of the semiconductor at the x = 0 plane

$$i(t) = \int_{\text{surface of semi}} \bar{J} \cdot d\bar{s}. \qquad (3.9.8)$$

Resolving the carrier current density $\bar{J}$ into three components, J_x J_y, and J_z, along the three axes

$$\bar{J} = J_x\hat{x} + J_y\hat{y} + J_z\hat{z}.$$

Also,

$$d\bar{s} = ydy \times zdz = xdydz.$$

Hence,

$$\bar{J} \cdot d\bar{s} = J_x dydz.$$

Thus, the total current i(t) is given by

$$i(t) = \int_0^{L_y}\int_0^{L_z} J_x(0, y, z, t)dydz. \qquad (3.9.9)$$

$$i(t) = \int_0^{L_y}\int_0^{L_z} (\mu(T)k[\nabla(nT)]_x - \frac{\partial V}{\partial x})dydz. \qquad (3.9.10)$$

The above is obtained by substituting Eq. 2.5.8) in the Eq. (3.9.1). The subscripts (x, y, z, t) have been omitted for the sake of brevity.

Substituting this expression back into the load line Eq. (3.9.1)

$$V_1(t) = V_{app} - R_s \cdot \int_0^{L_y}\int_0^{L_x} \mu_a k \frac{\partial(nT)}{\partial x} - \frac{\partial V}{\partial x}) \cdot dydz \qquad (3.9.11)^*$$

In subsequent sections, equations for the voltage V and temperature T will be obtained.

3.10. The Continuity of Charge

The charge continuity equation was obtained for the ETD in Eq. (2.2.7).

---

*Note that $\mu(T)$ can be treated as a constant in the above expression, since the semiconductor surface, being in contact with an ideally thermally conducting electrode, is assumed earlier.

$$\frac{\partial \rho}{\partial t} + \nabla . \bar{J} = 0 \tag{3.10.1}$$

Where $\bar{J}$ is the current density, the current density $\bar{J}$ is given by Eq. (2.5.10):

$$\bar{J} = \sigma \bar{E} + k\mu(T)\nabla(nT) . \tag{3.10.2}$$

Substituting Eq. (2.4.4) and Eq. (2.3.1) in Eq. (3.10.2)

$$\bar{J} = k\mu(T)[\nabla(nT) - ne\nabla V] \tag{3.10.3}$$

Computing the divergence of the above expression:

$$\nabla . \bar{J} = k\mu(T)[\nabla^2(nT) - ne\nabla^2 V - e\nabla n . \nabla V] + k \nabla\mu . [\nabla(nT) - ne\nabla V] \tag{3.10.4}$$

where $T = T(\bar{r},t)$.

Also, recall that $\nabla^2 V = -\rho/\epsilon$ (Eq. 2.4.5). Substituting this into Eq. (3.10.4) yields

$$\nabla . \bar{J} = k\mu(T)[\nabla^2(nT) + ne\,\rho/\epsilon - e\nabla n . \nabla V] + [k\nabla\mu . \nabla(nT) - kne \nabla V . \nabla\mu] \tag{3.10.5}$$

Also, recall that in Eq. (2.2.4)

$$\rho = en_d^+(T) - en.$$

Rearranging terms in the above yields

$$en = en_d^+(T) - \rho \tag{3.10.6}$$

Substituting for n in Eq. (3.10.5) and working the algebra (see Appendix C), a parabolic partial differential equation for the volume charge density is obtained as shown below:

$$\frac{1}{\mu(T)}\frac{\partial\rho}{\partial t} + \nabla^2\rho . \left(\frac{-kT}{e}\right) + \nabla\rho . \left(\nabla V - \frac{2k}{e}\nabla T - \frac{kT}{e}\ln\mu\right) + \rho\left[-\frac{k}{e}\nabla^2 T + \frac{en_d^+}{\epsilon} - \frac{\rho}{\epsilon} + \ln\mu . \nabla\left(V - \frac{kT}{e}\right)\right] + 1\left[\mu k\nabla^2(n_d^+T) - e\mu n_d^+\nabla V + \ln\mu(-en_d^+\nabla V + k\nabla(n_d^+T))\right] = 0 \tag{3.10.7}$$

The differential equation obtained requires six boundary conditions on each face and an initial condition to be completely solvable, all of which have been arrived at in the previous sections.

3.11. The Poisson Equation

Once the net charge density ρ is known at every point in the semiconductor, the electrical potential V(x, y, z) within the semiconductor can be directly evaluated by using Poisson's Eq. (2.4.5).

$$\nabla \cdot \nabla V(x, y, z) = -\rho(x, y, z)/\epsilon \qquad (3.11.1)$$

Since $\rho(x, y, z)$ has been completely evaluated at each time step in the previous section, the above elliptic partial differential equation is solvable provided a complete set of six boundary conditions are known.

Two of the boundary conditions have been obtained by considering the external circuit in Sec. 3.3. The other four boundary conditions were arrived at when discussing the air-semiconductor interface in Sec. 3.8.

3.12. The Temperature Equation

The equation for the temperature at any point in the sample is obtained by considering the energy balance within the sample. Rewriting the Eq. (2.7.7) yields

$$\underset{(a)}{\frac{Tds}{dt}} = \underset{(b)}{\frac{du}{dt}} + \underset{(c)}{K_n\frac{dn}{dt}} + \underset{(d)}{K_p\frac{dp}{dt}} - \underset{(e)}{eV\frac{dn}{dt}} \qquad (3.12.1)$$

Each term of the above expression is considered in turn below:

(a) $\frac{Tds}{dt}$ -- This represents the rate of creation of entropy in the system. Since the system has been idealized, such that no less terms have been included, this term is zero.

(b) $\frac{du}{dt}$ -- Since u, the internal energy per unit volume, is a function of space and time, it can be expressed as: (see Appendix H)

$$\frac{du}{dt} = \underset{(f)}{\frac{\partial u(\bar{r},t)}{\partial t}} + \underset{(g)}{\nabla \cdot \bar{J}_u(\bar{r},t)} \qquad (3.12.2)$$

Considering each of the terms separately, $\frac{\partial u}{\partial t}$ represents the explicit rate of change of internal energy per unit volume at each point in the system. This must correspond to the explicit energy increase due to the rise in temperature of the material. Hence:

$$\frac{\partial u(\bar{r},t)}{\partial t} = c\,\frac{\partial T}{\partial t} \tag{3.12.3}$$

$\bar{J}_u$ represents the energy flux crossing a unit cross-sectional area in the material per sec and is expressed as $J/m^2 - S$). The energy flux in the semiconductor is composed of electrical and thermal, all other forms of energy flow having been assumed absent in the model.

$$\bar{J}_u = J_{\bar{q}} + \bar{J}_{elec} \tag{3.12.4}$$

where $J_{\bar{q}}$ and $\bar{J}_{elec}$ are the thermal and electrical energy per unit area per second, respectively.

Taking the divergence of both sides,

$$\nabla\cdot\bar{J}_u = \underset{(h)}{\nabla\cdot\bar{J}_{\bar{q}}} + \underset{(j)}{\nabla\cdot\bar{J}_{elec}} \tag{3.12.5}$$

Recalling Fourier's Law as stated in Eq. (2.6.2), (h) reduces to

$$\nabla\cdot\bar{J}_{\bar{q}} = -k_{th}\nabla^2 T \tag{3.12.6}$$

Again, the electrical energy flux density, $\bar{J}_{elec}$, is given by

$$\bar{J}_{elec} = \bar{J}_{cond}V \tag{3.12.7}$$

Computing the divergence of the above:

$$\nabla\cdot\bar{J}_{elec} = \bar{J}_{cond}\cdot\nabla V + V\nabla\cdot\bar{J}_{cond} \tag{3.12.8}$$

and substituting Eqs. (2.4.4) and (2.5.6) yields

$$\nabla\cdot\bar{J}_{elec} = -\bar{E}\cdot\bar{E} + V\nabla\cdot\bar{J}_{cond} \tag{3.12.9}$$

Substituting Eqs. (3.12.9) and (3.12.6) back into Eq. (3.12.5)

$$\nabla\cdot\bar{J}_u = -k_{th}\nabla^2 T - \sigma\bar{E}\cdot\bar{E} + V\nabla\cdot\bar{J}_{cond} \tag{3.12.10}$$

Substituting back Eqs. (3.12.3) and (3.12.10) for terms (f) and (g), the term (b) becomes:

$$\frac{du}{dt} = c\,\frac{\partial T}{\partial t} - k_{th}\nabla^2 T - \quad \overline{E} \cdot \overline{E} + V\,\nabla \cdot \overline{J}_{cond} \tag{3.12.11}$$

Thus Eq. (3.2.1) with terms (a) and (b) evaluated now becomes:

$$\underbrace{c\,\frac{\partial T}{\partial t} - k_{th}\nabla^2 T - \quad \overline{E} \cdot \overline{E}}_{(b)} + \underbrace{V\,\nabla \cdot \overline{J}_{cond}}_{(k)} + \underbrace{K_p\,\frac{dn_d^+}{dt}}_{(c)} + \underbrace{K_n\,\frac{dn}{dt}}_{(d)}$$

$$\underbrace{-\; eV\,\frac{dn}{dt}}_{(e)} \underbrace{= 0}_{(a)} \tag{3.12.12}$$

Consider now the last four terms in the expression (k), (c), (d), and (e). The term (d) represents the energy associated with the creation of electrons at any point in the sample due to the chemical potential K_n, which is responsible for thermal and concentration diffusion in the semiconductor. Using the now familiar technique outlined in Appendix H and remembering that the electron (particle) has a charge of -e,

$$\text{(d)}\quad K_n\,\frac{dn}{dt} = K_n\left(\frac{\partial n}{\partial t} - \frac{1}{e}\,\nabla \cdot \overline{J}_{diff}\right) \tag{3.12.13}$$

Similarly, expanding the term (e)

$$\text{(e)}\quad -eV\,\frac{dn}{dt} = -eV\left(\frac{\partial n}{\partial t} - \frac{1}{e}\,\nabla \cdot \overline{J}\right) \tag{3.12.14}$$

Combining Eq. (3.12.13 and (3.12.14) with (k), we obtain:

$$K_n\left(\frac{\partial n}{\partial t} - \frac{1}{e}\,\nabla \cdot \overline{J}_{diff}\right) + V\,\nabla \cdot \overline{J}_{cond} - eV\,\frac{\partial n}{\partial t} + V\,\nabla \cdot \overline{J}$$

$$= (k) + (d) + (e) \tag{3.12.15}$$

Recalling that the current density $\overline{J}$ due to electron motion is the sum of diffusion and conduction components,

$$\overline{J} = \overline{J}_{cond} + \overline{J}_{diff} \tag{2.5.14}$$

Eq. (3.12.15) reduces, after a little algebraic manipulation, to

$$(K_n - eV)\frac{dn}{dt} = (k) + (d) + (e)$$

But, $(K_n - eV)$ corresponds to the net electrochemical potential acting on the electrons. Hence, combining this with term (c):

$$(c) + (d) + (e) + (k) = \tilde{\mu}\frac{dn}{dt} + K_p\frac{dn_d^+}{dt} \qquad (3.12.16)$$

Moreover, recall that the net creation rate of donor ions and electrons is everywhere equal in the model. Hence using Eq. (2.2.5):

$$(c) + (d) + (e) + (k) = (\tilde{\mu} + K_p)\frac{dn}{dt}$$

$\tilde{\mu}$ and K_p are opposite in sign, and the expression gives the net energy involved in the ionization process. In the present model, this energy of ionization is neglected. The equation for temperature can therefore be written as

$$c\frac{\partial T}{\partial t} = k_{th}\nabla^2 T + \sigma\bar{E} \cdot \bar{E} \qquad (3.12.17)$$

This equation is identical in form to the equations used by Berglund and other investigators(31,34,36). However, the approach used here closely parallels Ridley's thermodynamic argument, thus demonstrating the consistency between the two.

3.13. Summary

In this chapter, three partial differential equations have been obtained, together with the necessary boundary conditions for T, the temperature, V, the potential, and ρ, the charge density. Since all other variables E_g, n_d^+, n, μ, $\bar{E}$, σ, $\bar{J}_{cond}$, $\bar{J}_{diff}$ can be expressed in terms of these three, the system is completely known if these three equations are solved. The numerical solution of these three partial differential equations by computer simulation forms the subject of the next chapter.

For easy reference, the relevant equations together with their boundary conditions are recapitualated below:

a) Voltage:

$$\nabla^2 V(x, y, z, t) = -\rho(x, y, z, t)/\epsilon$$

Boundary Conditions:

$$\frac{\partial V}{\partial y}(x, 0, z, t) = 0; \ \frac{\partial V}{\partial y}(x, L_y, z, t) = 0$$

$$\frac{\partial V}{\partial z}(x, y, 0, t) = 0; \ \frac{\partial V}{\partial z}(x, y, L_z, t) = 0$$

$$V(0, y, z, t) = V_1(t); \ V(L_x, y, z, t) = 0$$

Also,

$$V_1(t) = V_{app} - R_s \int_0^{L_y}\int_0^{L_z} (ak \frac{\partial(nT)}{\partial x} - \sigma_0 \frac{\partial V}{\partial x}) dy dz$$

At $t = \Delta t_0$,

$$V_1(\Delta t_0) = V_0^+ = \frac{V_{app}}{1 + f}$$

b) Charge:

$$\rho(\Delta t_0) = 0$$

$$\frac{1}{\mu(T)}\frac{\partial \rho}{\partial t} + \nabla^2 \rho \cdot (\frac{-kT}{e}) + \nabla\rho \cdot (\nabla V - \frac{2k}{e}\nabla T - \frac{kT}{e}\nabla \ln\mu)$$

$$+ \rho \cdot (\frac{-k}{e}\nabla^2 T + \frac{en_d^+}{\epsilon} - \frac{\rho}{\epsilon} + \nabla\ln\mu \cdot \nabla(V - \frac{kT}{e}))$$

$$+ (k\nabla^2(n_d^+ T) - e\nabla n_d^+ \nabla V + \nabla\ln\mu(-en_d^+\nabla V + k\nabla(n_d^+ T)))$$

Boundary Conditions:

$$\rho(0, y, z, t) = \rho_0; \ \rho(L_x, y, z, t) = \rho_0$$

$$\rho(x, 0, z, t) = 0; \ \rho(x, L_y, z, t) = 0$$

$$\rho(x, y, 0, t) = 0; \ \rho(x, y, L_z, t) = 0$$

c) Temperature:

$$c\frac{\partial T}{\partial t} = k_{th}\nabla^2 T + \sigma \overline{E} \cdot \overline{E}$$

Boundary Conditions:

$$T(0, y, z, t) = T_{amb};\ T(L_x, y, z, t) = T_{amb}$$

$$\frac{\partial T}{y}(x, 0, z, t) = 0;\ \frac{\partial T}{y}(x, L_y, z, t) = 0$$

$$\frac{\partial T}{\partial z}(x, y, 0, t) = 0;\ \frac{\partial T}{\partial z}(x, y, L_y, t) = 0$$

CHAPTER IV

A NUMERICAL APPROACH TO THE SOLUTION OF PARTIAL DIFFERENTIAL EQUATIONS

In the previous chapter, we developed a set of three partial differential equations, each associated with a complete set of boundary conditions. For convenience, these equations are listed again below; the subscripts (x, y, z, t) have been omitted for brevity:

a) $\nabla^2 V + \rho/\epsilon = 0$

b) $$\frac{1}{\mu(T)}\frac{\partial\rho}{\partial t} + \nabla^2\rho\left(\frac{-kT}{e}\right) + \nabla\rho\cdot\left(\nabla\phi - \nabla\frac{2kT}{e} - \frac{kT}{e}\nabla\ln\mu(T)\right)$$
$$+ \rho\left(\frac{-k}{e}\nabla^2 T + \frac{en_d^+(T)}{\epsilon} - \frac{\rho}{\epsilon} + \nabla\ln\mu(T)\cdot\nabla\left(\phi - \frac{kT}{e}\right)\right)$$
$$+ 1\left(k\nabla^2(n_d^+T) - e\nabla n_d^+(T)\nabla\phi + \nabla\ln\mu\cdot\left(k\nabla(n_d^+T) - en_d^+\nabla\phi\right)\right)$$
$$= 0 \qquad (4.0.2)$$

c) $$c\frac{\partial T}{\partial t} = k_{th}\nabla^2 T + \sigma\nabla V\cdot\nabla V \qquad (4.0.3)$$

The three dependent variables used to describe the system are V, the electric potential; ρ, the charge density; and T, the temperature at any point in the semiconducting material. If V, ρ, and T are known for all points (x, y, z) in the semiconductor at all times t, the system is completely described. In the three equations, the only other variables are n_d^+ and μ. However, both of these depend explicitly on temperature T, which is separately evaluated in Eq. (c). For easy reference, the expression for (T) and n_d^+ are recalled below:

$$\mu(T) = \mu_a \text{ -- } T < T_{cr} \qquad \text{[See Fig. 2.2]}$$
$$= \mu_b \text{ -- } T \geq T_{cr} \qquad (4.0.4)$$

$$n_d^+(T) = N_d \exp(-E_{ga}/2kT) \text{ -- } T < T_{cr} \qquad \text{[See Fig. 2.2]}$$

$$= N_d \exp(-E_{gb}/2kT) \text{ -- } T \geq T_{cr} \qquad (4.0.5)$$

The set of Eqs. (a), (b), and (c) are nonlinear and coupled, and hence are too complex to handle in a closed form analytically. An approach to numerically solving these equations is presented in the remainder of the chapter.

4.1. The Formation of Finite Difference Equations

The finite difference technique is perhaps the most convenient and frequently-used method to solve a partial differential equation (PDE) together with its associated initial and boundary conditions. In this method, a network of grid points is first established throughout the region of interest occupied by the independent variables. In this case, the independent variables are x, y, z, and t; and the region occupied by the spatial operators is the sample space which has dimensions of L_x, L_y, and L_z in the x, y, and z directions respectively. Next, the partial derivatives of the original PDE are approximated by suitable finite-difference expressions involving x, y, and z. The finite difference expressions are obtained by using Taylor's series expansions of the function. The only types of spatial partial derivatives that occur in our mathematical formulations are the gradient, divergence, and Laplacian operators. Thus, in Cartesian co-ordinates, no mixed partial derivatives of the form $\frac{\partial^2 f}{\partial x \partial y}$ are involved. The finite are involved. The finite difference expressions for these partial dederivatives are developed in Appendix B.

There are two major types of errors associated with this technique, namely the discretization error and the round-off error.

The discretization error, e, is the departure of the finite difference approximation from the solution of the PDE at any grid point; i.e., if f_1 be the solution of the PDE and f_2 the solution of the algebraic equation, then

$$e = \frac{f_1 - f_2}{f_1}$$

The discretization error plays an important role in the selection of the grid as discussed in the next section.

Also, the computational procedure is assumed to be capable of an exact representation of the solution of the finite difference equation. As only a finite number of digits can be retained by the computer, round-off error is introduced. Round-off error is minimized if

a) the number of arithmetic operations at any given location is minimized,

b) the numbers on which the operations are performed, as well as the result obtained, are of the same order of magnitude, and

c) all variables are of the order of unity.

The first criterion depends largely on the algorithm used in the solution as well as the grid size involved.

The useful technique to reduce errors of the types (b) and (c) is by "normalization". Here, the dependent variable is transformed by suitable additive and scaling factors to a dimensionless quantity lying between zero and one. For instance, consider the temperature equation

$$c \frac{\partial T}{\partial t} - k_{th} \nabla^2 T = P$$

obtained in the last chapter. In this model, we are interested primarily in the preswitching region, where the temperatures within the material would lie between the temperature T_{amb} and T_{cr}. Consider therefore the transformation

$$u = \frac{T - T_{amb}}{T_{cr} - T_{amb}} \qquad (4.1.1)$$

Here u is a dimensionless variable lying between zero and one. Using this transformation, the temperature equation becomes:

$$c\frac{\partial u}{\partial t} - k_{th}\nabla^2 T = \frac{P}{T_{cr} - T_{amb}} \qquad (4.1.2)$$

Note that this transformation is useful only in the preswitching region. Once switching takes place, the temperatures in the filament region can be expected to be much larger than the critical temperature T_{cr}.

The other transformations used are as follows:

$$\Delta x = \frac{L_x}{10}\hat{x};\ \Delta y = \frac{L_y}{10}\hat{y};\ \Delta z = \frac{L_z}{10}\hat{z};$$

$$V = V_{app}\phi;\ \varsigma = \frac{\epsilon V_{app}}{L_x^2}\chi;\ T = (T_{cr} - T_{amb})\,\theta, \qquad (4.1.2)$$

where , , and θ are the normalized dimensionless dependent variables corresponding to V, , and T and x, y, and z are unit vectors in the x, y, and z directions respectively. The transformed equations thus obtained from (a), (b), and (c) are

(a) $\mathrm{Dav}_{\hat{x}}\phi + \mathrm{Dav}_{\hat{y}}\phi + \mathrm{Dav}_{\hat{z}}\phi - \gamma_D\phi + \chi = 0,$

(b) $\frac{\partial\chi}{\partial t} + [F_b' \cdot \underline{\nabla} \cdot \eta\nabla(\xi\theta) - F_d''\underline{\nabla} \cdot \eta\nabla(\chi\theta) - F_a'\underline{\nabla} \cdot \eta\xi\nabla\phi$

$+ F_c'\underline{\nabla} \cdot (\eta\chi\nabla\phi] = 0,$ and

(c) $\frac{\partial\theta}{\partial t} - \frac{1}{\lambda_T}[\mathrm{Dav}_{\hat{x}}\theta + \mathrm{Dav}_{\hat{y}}\theta + \mathrm{Dav}_{\hat{z}}\theta - \gamma_D \cdot \theta] = P F_d',$

where

$$\mathrm{Dav}_{\hat{x}}f = f(x + \Delta x, y, z) + f(x - \Delta x, y, z)$$

$$\mathrm{Dav}_{\hat{y}}f = \gamma[f(x, y + \Delta y, z) + f(x, y - \Delta y, z)]$$

$$\mathrm{Dav}_{\hat{z}}f = \gamma[f(x, y, z + \Delta z) + f(x, y, z - \Delta z)]$$

$$\mathrm{Del}_{\hat{x}}f = \frac{f(x + \Delta x, y, z) - f(x - \Delta x, y, z)}{2}$$

$$Del_y f = \sqrt{\Upsilon}\,\frac{f(x, y + \Delta y, z) - f(x, y - \Delta y, z)}{2},$$

$$Del_z f = \sqrt{\Upsilon}\,\frac{f(x, y, z + \Delta z) - f(x, y, z - \Delta z)}{2},$$

$$\Upsilon_D = 2 + 4\Upsilon,$$

$$\lambda_T = \frac{c}{k_{th}},$$

$$\xi = \frac{n_d^+(T)}{N_d \exp(E_{gb}/T_{cr}) - N_d \exp(E_{ga}/T_{amb})}$$

$$\Psi = \frac{n(T)}{N_d \exp(E_{gb}/T_{cr}) - N_d \exp(E_{ga}/T_{amb})},$$

$$= \Psi * n * \left[(Del_x\phi)^2 + (Del_y\phi)^2 + (Del_z\phi)^2\right], \text{ and}$$

$$\Psi_0 = \xi_0 = \xi(T_{amb}).$$

These transformations are formulated using $n_1 = n_2 = n_3 = 10$ in Appendix C. The choice of n_1, n_2, n_3 is discussed in the next section. In the equations and relations listed above, the spatial subscripts have been omitted; i.e., ξ, η, ϑ, ρ, Ψ, θ, ϕ, and χ are all functions of space and Dav_x, Del_x, Dav_y, Del_y, Dav_z, Del_z denote special spatial operators. The terms F_a, F_b, F_c, F_d, Υ, Υ_D, λ_T, and λ_r are all dimensionless constants.

4.2. Selection of the Grid Structure

In the last section, it was pointed out that the round-off error could be minimized by a suitable choice of algorithm and by normalizing the variables to dimensionless quantities of the order of unity. But this has little or no effect on the discretization error.

The discretization error depends largely on the nature of the grid structure chosen. For computer applications, it is preferable to use as uniform and regular a grid structure as possible, since this reduces the memory storage requirements and the number of operations on the computer. Thus, this entails not only a saving in terms of computer time and money, it also minimizes the round-off error, which, as was pointed out earlier, depends on the number of operations performed. Hence, a cubic or a rectangular grid are the obvious choices. Recall that a rectangular parallelepiped with a square cross section had been chosen for the semiconducting sample.* To minimize round-off error, an equal number of points are chosen along each axis. Obviously, the mesh spacing in the three directions is not the same; in fact, it is proportional to the dimensions of the sample in the three directions. In other words, if L_x, L_y, L_z are the sample dimensions and n_1, n_2, n_3 are the number of points along the x, y, z directions respectively, then the grid spacings Δx, Δy, Δz are given by

$$\Delta x = \frac{L_x}{n_1}; \ \Delta y = \frac{L_y}{n_2}; \ \Delta z = \frac{L_z}{n_3} \qquad (4.2.1)$$

Since

$$L_y = L_z$$

and

$$n_1 = n_2 = n_3 = n$$

$$x = \frac{L_x}{n}; \quad y = \frac{L_y}{n}; \quad z = \frac{L_z}{n} \qquad (4.2.2)$$

The number n is selected from the following considerations. First, it is desirable to minimize the discretization error. Since all the differential equations are of second order, consider the discretization error involved in obtaining $\frac{\partial^2 f}{\partial x^2}$. From Appendix B, for an interior point (x_0, y_0, z_0)

---

*Another logical choice, from symmetry considerations, would have been a cylindrical sample. However, this choice leads to programming complications because of the singularity of the Laplaciar operator at $r = 0$.

$$\frac{\partial^2 f}{\partial x^2} = \frac{f(x_0 + 2\Delta x, y_0, z_0) - 2f(x_0 + \Delta x, y_0, z_0) + f(x_0, y_0, z_0)}{\Delta x^2}$$

$$+ \frac{x^2}{2!} \frac{\partial^3 f}{\partial x^3} + \ldots$$

The discretization error e is hence given by

$$e \approx \frac{x^2}{2!} \frac{\frac{\partial^3 f}{\partial x^3}}{\frac{\partial^2 f}{\partial x^2}}$$

Thus, e is minimum when $\Delta x \to 0$, and hence when $n \to \infty$.

However, there is a lower limit of Δx determined by the nature of the problem. While discussing the boundary conditions for the charge distribution, it was required that the spacing be much larger than the Debye length λ_D to be able to neglect surface charge effects. Thus

$$x \gg \lambda_D.$$

Hence

$$n = \frac{L_x}{\Delta x} \ll \frac{L_x}{D}.$$

Since

$L_x = 1 \times 10^{-4}$m and $_D = 3.34 \times 10^{-6}$m, $n \ll 30$.

However, practical considerations limit the choice of n even further. Since a number of arrays (at least one for each dependent variable) of size n x n x n have to be simulataneously stored in the computer memory, the core memory requirements and costs increase very rapidly with n. A compromise choice of n was 10, which required an operating computer core memory of 100 k.** In Appendix C, the normalizations are performed with $n = n_1 = n_2 = 10$.

**At the time, the maximum allowable core memory on the CDS 6500 computer used was 120 k.

4.3. The Equation in ϕ

For the equation in ϕ, χ is assumed to have been already evaluated, and so it is a second order elliptic partial differential equation, in three space dimensions with χ as a forcing function. Typically, elliptic PDE's are solved by some kind of relaxation method; in this case the Successive Over Relaxation (SOR)[44] method is used to speed up the converging process. Briefly, this method consists of initializing each element of the matrix to some convenient value. In this specific simulation, the value obtained at the previous time step is used. A new approximation to the value of an element is obtained using the governing Eq. (b) and the relaxation parameter w, and the current value immediately replaces the previous value of the element in the matrix.

For instance, for an interior point, the equation for ϕ is:

$$\mathrm{Dav}_x\phi + \mathrm{Dav}_y\phi + \mathrm{Dav}_z\phi - \gamma_D\phi + \chi = 0 \qquad (4.3.1)$$

Expanding the above by using the definitions of Dav_x, Dav_y, and Dav_z

$$\begin{aligned}&\phi(x+\Delta x, y, z) + \phi(x-\Delta x, y, z) + \phi(x, y+\Delta y, z)\\ &+ \phi(x, y-\Delta y, z) + \phi(x, y, z+\Delta z) + \phi(x, y, z-\Delta z)\\ &- \gamma_D\phi(x, y, z) + \chi(x, y, z) = 0 \qquad (4.3.2)\end{aligned}$$

Rearranging terms:

$$\begin{aligned}\phi(x, y, z) = \frac{1}{\gamma_D}\ &\phi(x+\Delta x, y, z) + \phi(x-\Delta x, y, z) + \phi(x, y+\Delta y, z)\\ &+ \phi(x, y-\Delta y, z) + \phi(x, y, z+\Delta z) + \phi(x, y, z-\Delta z)\\ &+ \chi(x, y, z) \qquad (4.3.3)\end{aligned}$$

In the SOR method, a new value $\phi^+(x, y, z)$ is obtained by

$$\begin{aligned}\phi^+(x, y, z) = \phi(x, y, z) + w * \big[&\phi'(x, y, z)\\ &- \phi(x, y, z)\big] \qquad (4.3.4)\end{aligned}$$

where $\phi'(x, y, z)$ denotes the right hand side of Eq. (4.3.3). Similar expressions for $\phi'(x, y, z)$ can be obtained for points lying on the edge as shown in Appendix E.

The relaxation parameter w determines, to a large extent, the rate of convergence. If chosen too small, the solution tends to converge slowly; if too large, the successive inerations may not converge at all. Forsythe and Wasow[45] recommends an optimal choice of w of 1.5.

Convergence is determined by the relative deviation R_D:

$$R_D = \frac{\sum\limits_{\substack{\text{over}\\\text{all}\\\text{elements}}} \left| \phi^{+}(x, y, z) - \phi(x, y, z) \right|}{\sum \left| \phi(x, y, z) \right|} \tag{4.3.5}$$

when R_D drops below a specified value ϵ_{ps}, convergence is attained, and the solution is acceptable. As before ϕ and ϕ^{+} stand for the older and newer approximations to the solution respectively. For the complete program listing, refer to Appendix F.

4.4. The Equation is θ

The normalized equation for θ is:

$$\frac{\partial\theta}{\partial t} - \frac{1}{\lambda T}\left[Dav_{\hat{x}}\theta + Dav_{\hat{y}}\theta + Dav_{\hat{z}}\theta - \gamma_D\theta\right] = PF_d$$

This is a parabolic partial differential equation in three spacial dimensions. However, the equation is non-linear, the non-linearity arising from the nature of the forcing function $P\,F_D$. From a knowledge of the conductivity and the electric field $\overline{E}$, the forcing function P is first evaluated for each time interval; the differential equation is then solved assuming the forcing function to be invariant during the evaluation process.

The boundary conditions on the six boundaries, as ennumerated earlier, are of the von Neumann type[45]. In normalized form, these are

$\theta = \theta_0$ at $x = 0$ and at $x = L_x$

$\frac{\partial\theta}{\partial y} = 0$ at $y = 0$ and at $x = L_y$

$\frac{\partial\theta}{\partial z} = 0$ at $z = 0$ and at $z = L_z$

Two standard methods exist for solving this kind of equation; i.e., explicit methods and implicit methods. In explicit methods, to obtain a solution at time t_{n+1}, all space derivatives are evaluated at the instant t_n. Though this implies that the calculation procedures are inherently simpler, it requires that very small time steps be taken relative to the space grid size; i.e.

$$0 < t/ x^2 \leq \frac{1}{2}$$

This is undesirable particularly because thermal time constants are usually large and hence would place severe restrictions on the size of the sample and the space grid structure.

Implicit methods overcome this difficulty at the expense of a somewhat more complicated algorithm. It consists of representing the spatial derivatives δ_x^2, δ_y^2, etc. by a finite difference form evaluated at the advanced point of time t_{n+1}, instead of t_n as in the explicit method.

There are, however, two serious drawbacks to the standard implicit method in three dimensions. For the one dimensional case, the scheme is stable and is independent of λ, where

$$\lambda = \Delta t/\Delta x^2$$

But, in three space dimensions, the method is unstable for $\lambda > 3/2$[45]. Furthermore, it requires an inversion of a fairly complex matrix, which takes considerable computation time.

The implicit alternating direction method, developed by Peaceman and Rachford[44] and Douglas[44,45,49] avoids these disadvantages and manages to use a system of equations with a tridiagonal coefficient matrix which can be solved by fairly straightforward methods (see Appendix D). Essentially, the principle is to employ three difference equations for each time step, the solution of the first two being intermediate values denoted by u* and u** as follows:

$$\frac{\Delta x^2}{\Delta t}(u^* - u_n) = \frac{1}{2}\delta_x^2(u^* + u_n) + \gamma\delta_y^2 u_n + \gamma\delta_z^2 u_n + F_D P \quad (4.4.1)$$

$$\frac{\Delta x^2}{\Delta t}(u^{**} - u_n) = \frac{1}{2}\delta_x^2(u^* - u_n) + \frac{\gamma}{2}\delta_y^2(u_n + u^{**}) + \delta_z^2 u_n$$

$$+ F_D P \quad (4.4.2)$$

$$\frac{\Delta x^2}{\Delta t}(u_{n+1} - u_n) = \frac{1}{2}\delta_x^2(u^* + u_n) + \frac{\gamma}{2}\delta_y^2(u^{**} + u_n)$$

$$+\gamma\delta_z^2(u_{n+1} + u_n) + F_D P \quad (4.4.3)$$

In the above difference equations, the time subscripts are n and n + 1. The space-subscripts have been omitted for clarity. Leaving Eq. (4.4.1) as it is, subtracting Eq. (4.4.2) from Eq. (4.4.1) and Eq. (4.4.3) from Eq. (4.4.2) and rearranging terms, we obtain

$$\lambda u^* - \frac{1}{2}\delta_x^2 u^* = \lambda u_n + \frac{x^2}{2} u_n + \gamma\delta_y^2 u_n + \gamma\delta_z^2 u_n + F_D P$$

$$\lambda u^{**} - \frac{\gamma}{2}\delta_y^2 u^{**} = \lambda u^* - \frac{\gamma}{2}\delta_y^2 u_n$$

$$\lambda u_{n+1} - \frac{\gamma}{2}\delta_y^2 u_{n+1} = \lambda u^{**} - \frac{\gamma}{2}\ {}_z^2 u_n$$

In the above set, the right side is a known column matrix, whereas the left side is a tridiagonal matrix. The algorithm for solving such a system is shown in Appendix D. The actual implementation is done in subroutines TEMPEQN and TRIDAG (see listings in Appendix F).

4.5. The Equation in ρ

The equation for ρ in normalized form has been written out in Section 4.2. This also is a parabolic partial differential equation in three space dimensions, but with Dirichlet boundary conditions at the boundaries. However, this equation is considerably more non-linear than the temperature equation, and so, though the alternating-direction scheme developed there could be applied, considerable computational time is involved in merely evaluating the tridiagonal coefficients.

Instead, an iteration scheme based on the SOR method discussed earlier is used. This method is particularly advantageous because of the numerical values of the constants F'_a, F'_b, F'_c, and F'_d. Typical values of these constants are illustrated in Table 4.1 for a VO_2 sample.

Table 4.1

Normalization Constants F'_a, F'_b, F'_c, F'_d

F'_a	$7.96 \times 10^7\ m^2/s$
F'_b	$1.63 \times 10^5\ m^2/s$
F'_c	$6.58 \times 10^{-2} m^2/s$
F'_d	$1.29 \times 10^{-2} m^2/s$

Since F'_a and F'_b are so much larger than either F'_c or F'_d, and all quantities χ, θ, ϕ, etc. have been normalized, the terms containing the coefficients F'_d and F'_c can be neglected to a first approximation. Thus, the equation in ς reduces to

$$\lambda_T \frac{\chi_n - \chi_{n-1}}{\Delta t} \quad F'_a \nabla\cdot (\eta\xi\nabla\phi) - F'_b \nabla\cdot (\eta\nabla(\xi\theta)) \qquad (4.5.1)$$

and hence

$$x_n \cong x_{n-1} + \frac{\Delta t}{\lambda_t} \left[F'_a \nabla\cdot (\eta\xi\nabla\phi) - F'_b \nabla\cdot (\eta\nabla(\xi\theta))\right] \qquad (4.5.2)$$

The right side of the equation is known, and so the first approximation to x_n to start the iterative process is obtained from Eq. (4.5.2). Because of the dominance of this term, the iterative process converges very rapidly. As in the Poisson equation, a relaxation parameter w of 1.5 is used.

4.6. Gestalt of the Logic Flow

In the preceding sections, we have developed schemes to solve each of the three differential equation--in θ, ϕ, and ς --with the appropriate boundary conditions. But, the three equations are mutually

coupled to each other; therefore, solving each of the variables θ, ϕ, and ρ in turn assuming the other two known does not imply simultaneous solution.

To correct for this error, a predictor-corrector loop is employed, its logical flow chart being illustrated in Fig. 4.1. The method utilizes the feature that the thermal time constant is long; in other words, of the three dependent variables θ, ϕ, and ρ, the temperature would vary least within a time step. As the flowchart indicates, an estimate of the terminal voltage $\phi^*_n\ t_{n+1}$ is first made by solving the circuit equation using the values obtained at t_n. This is then used as a boundary condition to solve for the matrix ϕ for all elements of the space grid. Using this value ϕ^* and the temperature at t_n, the continuity equation is solved to obtain *. The electron density n is then computed, and, applying Simpson's Rule, the new estimate of terminal current $i^*_n(t)$ is obtained. The circuit equation is used again to obtain a new estimate of the terminal voltage ϕ^{**}_n. The new estimate is tested against the older estimates; the looping is terminated if

$$\frac{\left| \phi^{****} - \phi^{**}_n \right|}{\phi^*_n} < \epsilon_L$$

where ϵ_L is a preset positive real number. When the above convergence test is satisfied, the current estimates of ρ and ϕ are taken to be the true values at time t_{n+1}. These are then used to solve the temperature equation for time t_{n+1}. The time is then stepped up and the process is repeated for the next time interval.

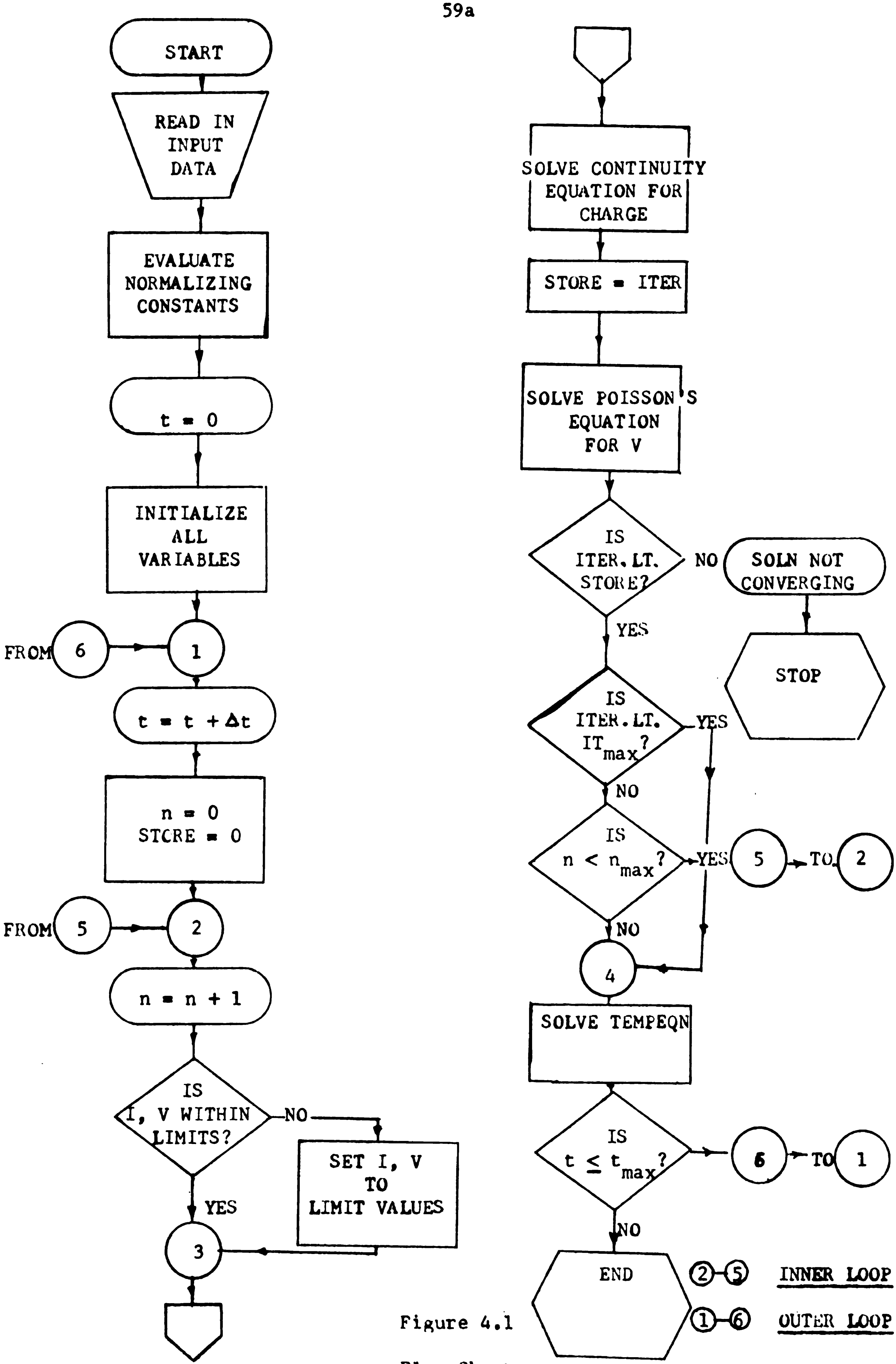

Figure 4.1

Flow Chart

CHAPTER V

RESULTS OF THE SIMULATIONS

Now that the model has been translated into a computer program, it is possible to demonstrate its utility. This is best achieved by simulating the behavior of the ETD's under various biasing and other external conditions to verify its "goodness" and then making some predictions regarding the device based on the outcomes of the simulations. Of course, the "goodness" of a model is relative. It has meaning only in relation to the objectives of the model. In other words, while there are various aspects and facets to an experiment, a model seeks to explain and make understood those aspects which are of primary interest to the investigator. Thus, the model has to fit the objectives and goals set by the investigator, and the "goodness" criteria of the model is determined by how well it is able to attain these objectives. Therefore, in order to be able to judge and criticize the efficiency of the model, it is necessary to delineate clearly the purpose of this study.

From a panoramic viewpoint, the goal of this thesis is to understand the physical nature of the switching process in electrothermal devices. Experimental evidence to date[40,41,42] indicates that the electrical switching process must involve a complex combination of physical phenomena. For instance, the thermal nature of the device has been clearly established, yet, obviously, its extremely fast switching time cannot be accounted for by thermal processes alone. So, a primary objective is to study and develop a better understanding of the physical processes related to the initiation of this fast switching process.

A change in band gap and mobility gap has been presumed to be involved in the switching process. For simplicity, in this model, both of these were assumed to be abrupt step functions of temperature, the step occurring at the critical temperature, T_{cr}. It is proposed to show that such a change does indeed initiate a fast switching mechanism coupled with a change of state. The "goodness" of the model will be judged on the basis of comparisons of the switching times from actual experimental data.

The terminal I-V characteristics of the device also form a focal point of interest, since it forms the interface between the device physicist and the applications engineer. A typical I-V curve for a current negative resistance, shown in Fig. 1.4, is reproduced here in Fig. 5.1. For convenience, this curve is split up into four regions.

The first or low current region extends from the origin to the switching or threshold voltage V_{thr}. The associated terminal current at this point is called the threshold current I_{thr}. As shown in Fig. 5.1, this is a stable region with a positive resistance coefficient. When operated here, the semiconductor will act as a non-linear resistor. The dynamic properties of a device operating in this region are studied in the next section. Since all points in the region are stable, all bulk dynamic characterists should tend to approach a steady state value with time.

The next region is termed the transition region for obvious reasons; it is a highly unstable switching region with a non-linear negative resistance coefficient. Being unstable, this region cannot be obtained as solutions to a static model. Adler and Kaplan's solution[36] of the static equations for energy flow and continuity of charge closely resembles Fig. 5.2a which was obtained as a solution of this more dynamic model.

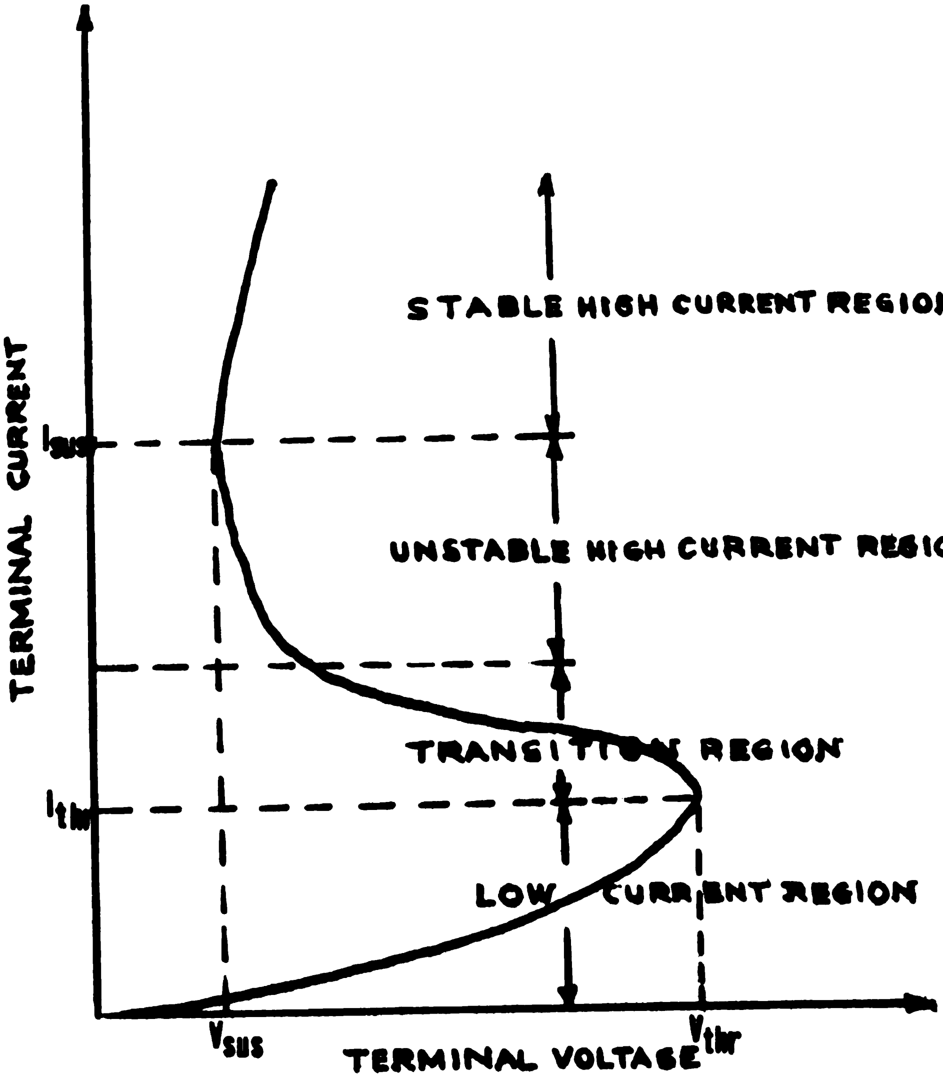

Figure 5.1

Typical I-V Curve of ETD Showing Various Regions

The third important region of the curve, the post-switching region shown in Fig. 5.1, is called the unstable high-current region. It exhibits a slight negative slope; i.e., a negative resistance coefficient implying that the region is still unstable. In fact, as other subsequent experiments show, the device is in a "thermal runaway" condition. Many of the earlier experimental failures with the ETD resulted from a failure to control this post-switching phenomenon.

Though the temperature and hence the conductivity increases very rapidly in this region, the power dissipation, given by $\sigma\overline{E}\overline{E}$, reduces, due to the decrease in the electric field $\overline{E}$. This reduces the rate of temperature rise and effectively increases the terminal dynamic resistance of the device, until finally the resistance coefficient becomes positive. This fourth region is called the "high-current" region. Controlling the length of the third region such that this roll-over takes place before the temperature attained is too high and the device burns out is a current problem in device design.

This dissertation, however, concentrates on the preswitching region; it is of interest here to observe the onset of the switching process rather than the postswitching stabilization process. Hence, it is the first two regions, namely the low-current and transition regions, that are of interest here.

Another subject of interest are the methods of inducing switching in the ETD. Four distinct types of simulated experiments are performed. In the first class of experiments, the external battery voltage V_{app} is small; so that in the final steady-state condition, the ETD remains in the low-current zone. Therefore, in this class, no switching is expected to occur. This type of simulation is useful both in the construction of the low-current zone of the I-V characteristics as well as in the study of the development of steady-state conditions within the sample.

The other three methods are attempts to induce switching by various mechanisms. The first obvious method is to apply a "large" applied voltage such that at least some points within the sample reach or exceed the critical temperature. In the other two methods, switching is attempted by locally applying a power pulse and an optical ionization pulse. The switching characteristics observed, if any, sometimes provide a basis for correlating with existing experimental data, providing further vindications for the goodness of the model.

Other characteristics provide a basis for making useful predictions regarding the behavior of the ETD as a switching device. After all, the model's validity and usefulness is dictated not only by its ability to explain observed phenomena, but also in its ability to predict and foresee phenomena not yet observed. It then becomes a useful tool with which to guide future experimental research.

In this set of simulations, the experiments are performed using the data of VO_2 as a prototype material. The selection is so partly because, in the past decade, VO_2 has been widely experimented with by various investigators. Thus, the documentation on them is fairly good. Correlative work is also much easier, since the switching characteristics of VO_2 have already been observed. Predictions regarding this material is also likely to be more than merely academically useful, since optical effects in VO_2 is a matter of current research. In this chapter, the first few sections concentrate on establishing the goodness of the model, while the later sections deal with the predictive aspects of the model.

5.1. Terminal I-V Curves

The I-V curve obtained by this simulation (Fig. 5.2a) is in agreement with published experimental results in the following sense. Although the magnitudes of currents obtained by the simulation is very much higher than experimental data would indicate, the current density normalized to a unit volume sample is of the same order of magnitude. An experimental curve obtained by Duchene et. al.[40] is reproduced in Fig. 5.2b for comparison. The discrepancy is therefore due to the large sample size chosen. Recall that the choice of a large sample size was dictated by the Debye length for the material; in order to neglect the surface effects at the metal-semiconductor interface, the grid size, and hence the sample size must be chosen much larger than the Debye length. The current densities at the threshold voltage V_{thr} and sustaining voltage V_{sus} are compared with experimentally-obtained figures in Table 5.1.

The sustaining voltage obtained from the simulation is 0.85V which is in excellent agreement with the experimental data; the breakdown or threshold voltage V_{thr} is, however, about an order of magnitude smaller. This is attributed to the oversimplification involved in computing the volume charge densities at the boundaries. In actuality, the diffusion current component due to thermal and concentration diffusions result in much larger charge densities near the ends. One would therefore expect large electric fields to be set up near the electrodes, and, therefore, considerable voltage drops would occur near the ends. Recall, however, that the sustaining voltage obtained compares very well with the experimental data (see Table 5.1). As borne out by the other experiments discussed later, the switching observed is indeed with filament formation. Once the filament extends from one end of the material to the other, the large electric fields at the ends can no longer exist;

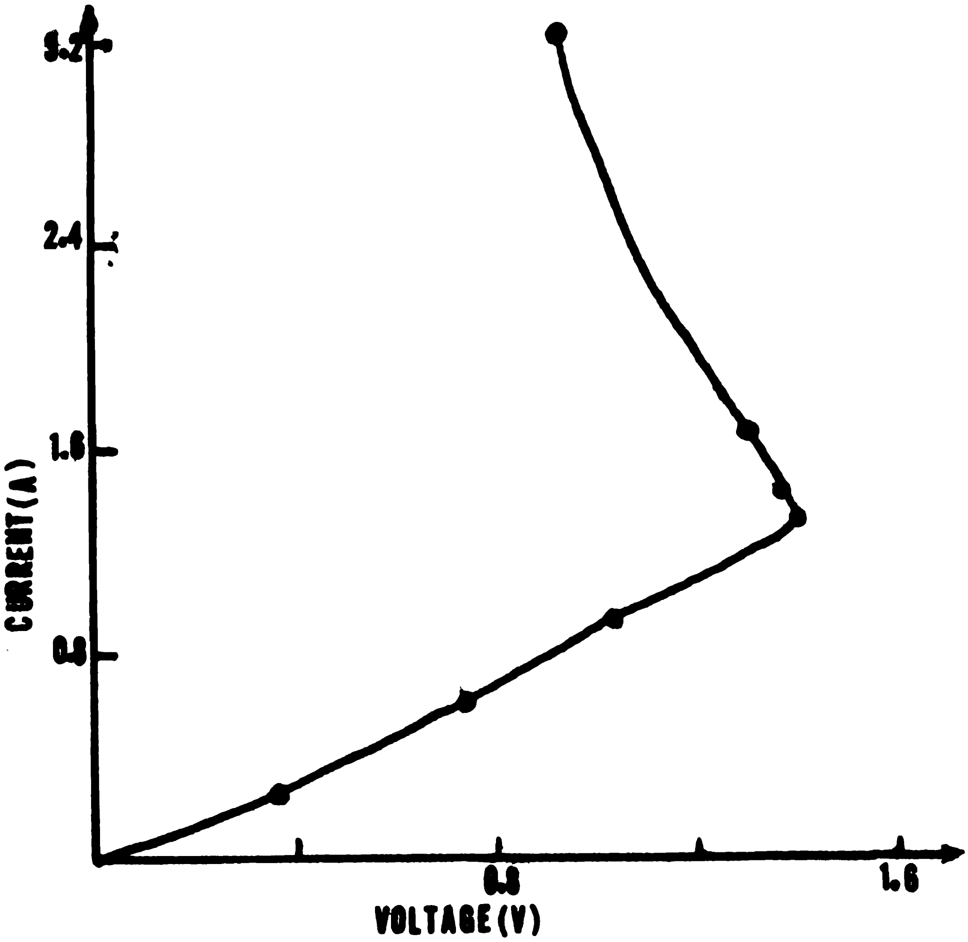

Figure 5.2a

I-V Curve of ETD from Simulation

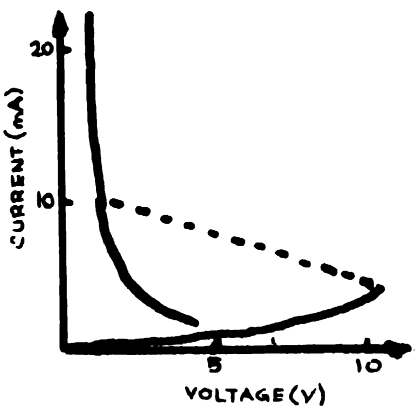

Figure 5.2b

Experimental Current-Voltage Characteristic of a VO_2 Device thus, the error involved in the boundary conditions of the volume charge density does not have a significant contribution.

Table 5.1

Constants of the I-V Curve Depicted in Figs. 5.2a and 5.2b

	Experimental	Simulated
I_{sus}/cross-sectional area	$3.1 \times 10^4 A/m^2$	$3.20 \times 10^4 A/m^2$
V_{sus}	0.8V	0.85V
I_{thr}/cross-sectional area	$3.1 \times 10^4 A/m^2$	$1.27 A/m^2$
V_{thr}	13 V	1.39V

5.2. Steady-State Conditions in the Preswitching Region

In this simulation, the voltage of the battery shown in the circuit diagram of Fig. 3.5 is small. The power dissipation at any point as described by the temperature is given by $\sigma \bar{E} \cdot \bar{E}$; hence, the larger the battery voltage applied, the larger is the expected power dissipated at any point, so the final temperature attained would be expected to be larger. By a small battery voltage it is meant that the voltage is sufficiently small so that no point within the material attains, in the steady-state, the critical temperature T_{cr} beyond which switching is expected to occur.

As evidenced by the I-V characteristics discussed in the preceding section, the preswitching region of the ETD is stable. So, for small voltages, the ETD should reach a steady state in a time t large compared to the thermal time constant of the system; all variables of the system--V, ρ, n, T, etc.--should tend to a final steady state value. That this is indeed the case is evidenced by the curves (Fig. 5.3) obtained from a simulation of the model.

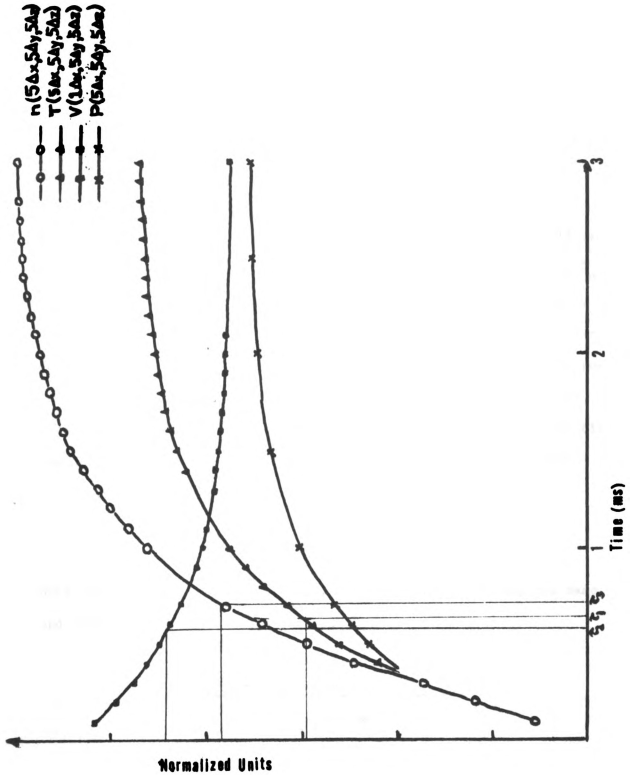

Figure 5.3

Behavior of Bulk Variables
With Time in Low Current Region

In Fig. 5.3, the potential V, dissipated power density P, temperature T, and free election density n are plotted with respect to time for a representative point in the sample. As expected, all of the above variables tend to approach their respective steady-state values. The temperature T starts from the initial ambient value T_{amb} to the final value T_{cr}; the rise can be approximated by an exponential law:

$$T = T_{amb} + (T_f - T_{amb})(e^{-t/\tau_1})$$

The time constant can be computed from the plot. The value of this time constant τ_1 is compared in Table 5.2 with the thermal time constant τ_A.

It is also interesting to note that the other variables V, n, etc. exhibit the same exponential nature. Whereas the potential V reduces with time, decaying to the final steady-state voltage V_f, the power density P and electron concentration n for representative points increase with time. But, in each case, the approximate law is exponential; typically, for voltage V and the electron density n for a representative point, respectively, the relations are:

$$V = V_f + (V_{app} - V_f)e^{-t/\tau_2}$$

$$n = n_f + (n_f - n_0)e^{-t/\tau_3}$$

Note that the time constants τ_1, τ_2, and τ_3 are approximately the same and close to the thermal time constant τ_A.

Table 5.2

Time Constants Computed from Fig. 5.3

τ_1	630 μs
τ_2	580 μs
τ_3	720 μs
τ_A	550 μs

Therefore, in the preswitching region I, the thermal properties are primarily responsible for the transport phenomena in the ETD. This is why the sample Berglund model[34], which utilizes only the equation of energy balance as discussed in the introductory chapter, works so well in the preswitching region.

Consider also the temperature-current curve shown in Fig. 5.4b. This curve is obtained by varying the input current in the simulation runs. More precisely, referring to Fig. 3.5, this is the curve obtained by keeping the battery voltage constant and varying the external resistance R_s to alter the current through the device. The curve (Fig. 5.4a) shows that the time required to reach the switching temperature T_{cr} depends on the input current. This is reasonable since the power dissipated in a volume element of the sample depends on the square of the current density. It was also observed that the time required t_r to attain 95% of the final steady state value depended on the input current; the larger the input current, the larger the final temperature and also the shorter it took to reach the final steady state value, the latter relationship being approximately linear:

$$i = c_1 t_r + c_2$$

The values of t_r for various input terminal currents are tabulated in Table 5.3. A simplistic consideration of the energy balance equation lends substance to this observation. Neglecting the diffusion term, the energy balance equation can be written as:

$$c \frac{\partial T}{\partial t} = \sigma \bar{E} \cdot \bar{E} \tag{5.2.1}$$

Since the electrical conductivity σ can be written as

$$\sigma = ne\mu$$

and n, the free electron density can be approximated by the ionized charge density, it can be written as an explicit function of temperature:

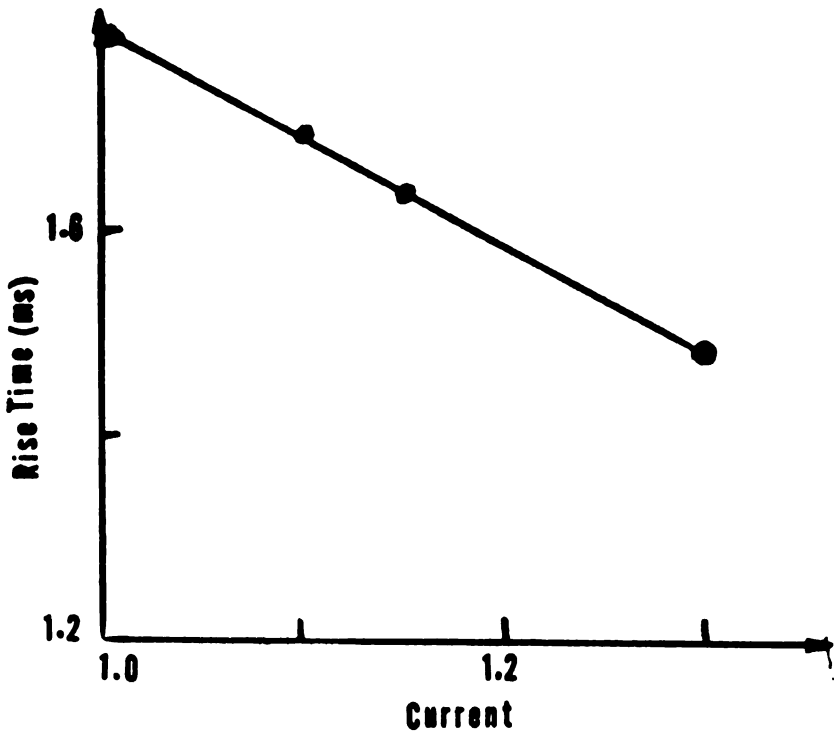

Figure 5.4a

t_r, vs, i in the Absence
of Band Gap Switching

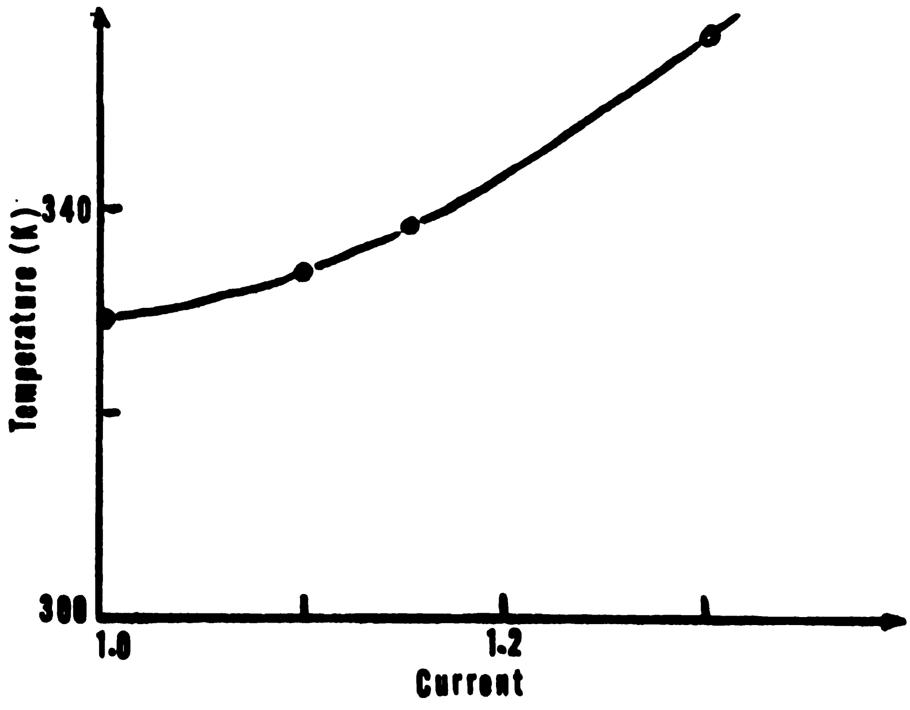

Figure 5.4b

Final Steady State Temperatures in the Absence
of Band Gap Switching-vs-Terminal Current

$$\approx N_d e \mu \exp(-E_g/2kT)$$

The above relation uses the donor ionization equation developed earlier.

Table 5.3

Data Plotted in Figs. 5.4a and 5.4b

i Terminal Current (mA)	Final Temperature (K)	V_{app} Battery Voltage (V)	t_r Rise Time (mS)
1000	328.3	1.875	1.80
1100	333.7	1.875	1.70
1150	338.1	1.875	1.64
1300*	356.5	1.875	1.50

*No band gap switching was simulated in this case.

The approximation $n \sim n_d^+$ is particularly good in the preswitching region because of the absence of temperature and free electron concentration gradients in the y and z directions (see Fig. 5.6). Returning to Eq. (5.2.1), and substituting for the electrical conductivity

$$\frac{dT}{dt} = \frac{N_d e \mu}{c} \exp(-E_g/2kT)\bar{E} \cdot \bar{E}$$

Since both E_g and μ are step functions of temperature (refer Figs. 2.1b and 2.3), and assuming the electric field $\bar{E}$ to be a constant also in this preswitching region, the Eq. (5.2.3) can be integrated. Note that, although no physical justification is given, the assumption that the electric field $\bar{E}$ is constant in the preswitching region has been used extensively by many experimenters[10,31] with considerable success. To simplify the integration involved, consider conductivity to be a linear function of temperature given by

$$\sigma = \sigma_0(1 + \alpha T) = n_e e \mu(1 + \alpha T)$$

Extensive examples of this kind of linear approximation to σ can be found in the literature[31,34].

Rearranging terms:

$$\int_{T_{amb}}^{T} \frac{dT}{1 + dT} = \int_0^t \frac{n_0 e\mu}{c} E^2 dt$$

Integrating:

$$\frac{1}{\alpha} \ln\left(\frac{1 + \alpha T}{1 + \alpha T_{amb}}\right) = \frac{\sigma_0 E^2}{c} t_r$$

Hence for constant V

$$i = c_1 t_r + c_2$$

Since the voltage applied is kept constant, the time t_r is proportional to the terminal current i. Thus, by adjusting the external circuit parameters, it is possible to exceed any known switching temperature T_{cr} for a specified material. Thus, by using high enough applied voltages, switching to the high-conducting state can be induced. Experimental data on this kind of simulation is discussed in a later section.

5.3. Spatial Distribution of Temperatures in the Preswitching Region

For a small applied battery voltage, the ETD reaches a final stable steady state in the preswitching region T. The temperature distribution along the axial line joining the midpoint of the two electrodes is plotted in Fig. 5.5 for various instants in time. Starting from an initially flat distribution (when the sample is uniformly at the ambient temperature T_{amb}), the temperature profile becomes parabolic in shape with the peak occurring at the geometrical center of the device. The plots along the y and z axes remain flat throughout. This is consistent with the thermal boundary conditions for the ETD. At the electrode semiconductor interfaces, the metal electrodes act as heat sinks and so the temperature at these ends remain at the ambient temperature. Since power is being dissipated due to the external circuit, the temperature is bound to increase.

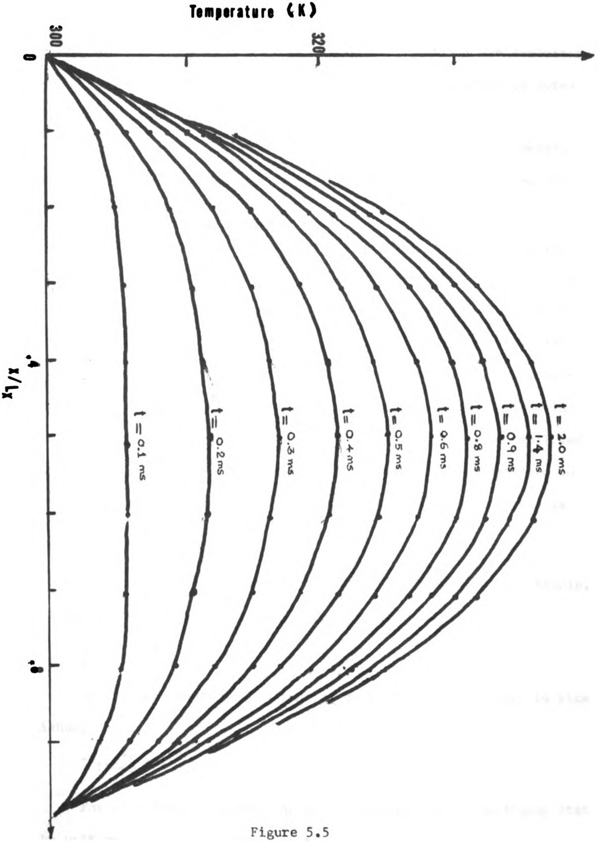

Figure 5.5

Temperature Profile in x-Direction
at Various Times in Low Current Region

Thus, because it is constrained at the ambient temperature at the two ends, a parabolic profile is only to be expected. Furthermore, the thermally insulating boundaries on the other sides of the semiconductor prevent any thermal currents in the lateral directions, which is borne out by experimental data.

The spatial distribution of the power density is of interest. (See Fig. 5.12a.) As discussed in a later section, the power density curve is also approximately parabolic with a minima at the center. This contributes to the stabilizing process in the semiconductor; while the boundary conditions tend to force the temperatures to be higher at the middle than at the ends, the power density curve seeks to balance this by dissipating more power at the ends than near the moddle. In the y and z directions, the temperature distribution is flat and, consistently, so is the power distribution. The steady state profile in the x-direction is readily understandable from the following simplified analysis. The energy balance equation of the system (also referred to in preceeding chapters as the temperature equation) can be written as

$$\frac{\partial T}{\partial t} - \frac{k_{th}}{c} \nabla^2 T = \frac{P}{c}$$

where P is the power dissipation in a unit volume element of the sample. Considering only a one-dimensional variation in the x-direction,

$$\frac{\partial T}{\partial t} - \frac{k_{th}}{c} \frac{\partial^2 T}{\partial x^2} = \frac{P}{c}$$

In the steady state, the partial derivative with respect to time vanishes, and so,

$$-k_{th}\frac{d^2T}{dx^2} = P$$

For simplicity consider the power dissipation in the steady state to be uniform; i.e., independent of x. Hence,

$$\frac{d^2T}{dx^2} = - \frac{P}{k_{th}} \tag{5.3.1}$$

The boundary conditions for the above equation are

$$T = T_{amb} \text{ at } x = 0 \text{ and} \tag{5.3.2}$$

$$T = T_{amb} \text{ at } x = L_x \tag{5.3.3}$$

Solving the above,

$$\frac{dT}{dx} = - \frac{P}{k_{th}} x + c_1$$

and so,

$$T = - \frac{P}{2k_{th}} x^2 + c_1x + c_2 \tag{5.3.4}$$

Here, the constants c_2 and c_1 represent the temperature at the origin and the temperature gradient at the origin respectively. Applying the boundary condition (5.3.2),

$$c_2 = T_{amb} \tag{5.3.5}$$

Applying the remaining boundary condition (5.3.3) to evaluate c_1

$$T_{amb} = - \frac{P}{2k_{th}} L_x^{\ 2} + c_1L_x + T_{amb}$$

and consequently,

$$c_1 = \frac{PL_x}{2k_{th}}$$

The temperature profile T(x) at the final steady state is therefore,

$$T(x) = T_{amb} - \frac{Px(x - L_x)}{2k_{th}}$$

which is parabolic in form. The maxima for the above occurs at the midpoint $x = \frac{L_x}{2}$ which agrees with the curves drawn in Fig. 5.5. Furthermore, the final steady-state temperature at the midpoint $x = \frac{L_x}{2}$ can be estimated from the Eq. (5.3.7) as

$$T_{max} = T_{amb} + \frac{PL_x^{\ 2}}{8k_{th}}$$

Using the data from the simulation run,

$P = 1.7345\ w/m^3$

$L_x = 1.0 \times 10^{-4}\ m$

$k_{th} = 6.0\ J/(m - K)$

$T_{amb} = 300\ K$

the computed value of the maximum temperature is

$T_{max} = 336.14\ K$

This is in good agreement with the value of 337.2 K obtained from the curve of Fig. 5.5.

A noteworthy feature of this analysis is that the maximum steady state temperature attained at any point is independent of the specific heat c; this is reasonable since the specific heat merely determines the rate at which the temperature rises and not the final steady state condition.

The experimentally obtained steady state temperature distribution was fitted to a parabolic curve, the results obtained being shown below in Table 5.4.

Table 5.4

Comparison of Simulated Experimental Data with Analytic Data

	A Coeff of x^2	B Coeff of x	C Const Term	D T_{max}
Math formula	$\frac{Pk_{th}}{2}$	$\frac{PL_x}{2k_{th}}$	T_{amb}	$T_{amb} + \frac{PL_x^2}{8k_{th}}$
Best fit parameters	$.1445 \times 10^{11}$	$.1445 \times 10^{7}$	300 K	336.1 K
Experimental values	$.146 \times 10^{11}$	$.145 \times 10^{7}$	300 K	337.2 K

As can be seen from the above data, the curve fit is excellent. The constant term T_{amb} is determined by the electrode temperature. Here the correlation is exact. The coeff of x and x^2 are related to the slope at the ends;

$$\frac{dT}{dx} = Ax + B \tag{5.3.8}$$

$$\text{At } x = 0 \ \frac{dT}{dx} = B$$

Here the correlation, though good, is not exact. Thus, we can conclude that the final shape of the temperature profile is parabolic with the end points exactly as constrained; both the maxima and the slopes at the ends are, however, slightly lower than that predicted from the one dimensional analysis. This is due in large part in assuming the power density to be a constant instead of the concave shape observed.

5.4. Switching Times

In these simulations, two distinct methods are utilized to initiate switching in the ETD. In the first method, a large battery voltage is applied such that the temperature at a point within the material exceeds the critical temperature T_{cr}, whereas in the second method, a small battery voltage is applied such that the temperature reaches a steady state value just below the critical temperature. A "power pulse" is then applied to switch the device to the "on" state. Here, a "power pulse" means that excessive power is being dissipated at some randomly chosen local point in the ETD. In physical reality, local power dissipation may be caused by the presence of local inhomogeneities in the ETD, e.g., dislocations, crystal disorder, etc. because of its added resistance to the current. In effect, this simulates the effect of a random defect in the material. The results are in agreement with observed fact; a local defect can induce switching in these devices. In each case, there are two distinct switching times associated with the ETD. The first time is a storage time and is related to the heat capacity of the semiconductor and the external circuit parameters. It is the time taken for any one point in the sample to reach the critical temperature. Obviously, from Table 5.3, this time is much smaller in the first method since a larger current is being applied. In either case, the time is of $\sim 100\mu s$. Though this time is large, it can be controlled and empirically determined. The storage time can be considerably reduced by operating at ambient temperatures closer to the critical temperature T_{cr}. For example, in the power-pulse switching method, a storage time of the order of only $50\mu s$ is required if the pulse is applied after steady-state conditions have been reached at a temperature of 33.9 K.

After at least one point in the sample has crossed the critical temperature, the switching occurs with great speed in both cases; this actual switching time is only 2ns as shown in Fig. 5.6. This is slightly faster than the switching times reported in such devices. This small discrepancy is easily explained. First, the experimental devices are not homogeneous and, as such, are liable to contain a number of defects and inhomogeneities in the material. This could cause the band gap reduction at slightly different temperatures creating an overall effect of a smoother transition than the step function variation for E_g assumed in the model. Second, the model neglects inductive effects, which may exist due to two reasons. In the first place, the model neglects magnetic field effects which could be large during switching when the current is varying so rapidly. Also, the effect of stray capacitances and lead inductances due to the external circuit configuration have not been considered. Last, but not least, there is a distinct possibility of experimental error; at such fast switching times, the response time of the measuring circuit may well effect the measurement.

t_0 = 2.772776ms after S is turned on
= 0.2772776ms after application of power pulse

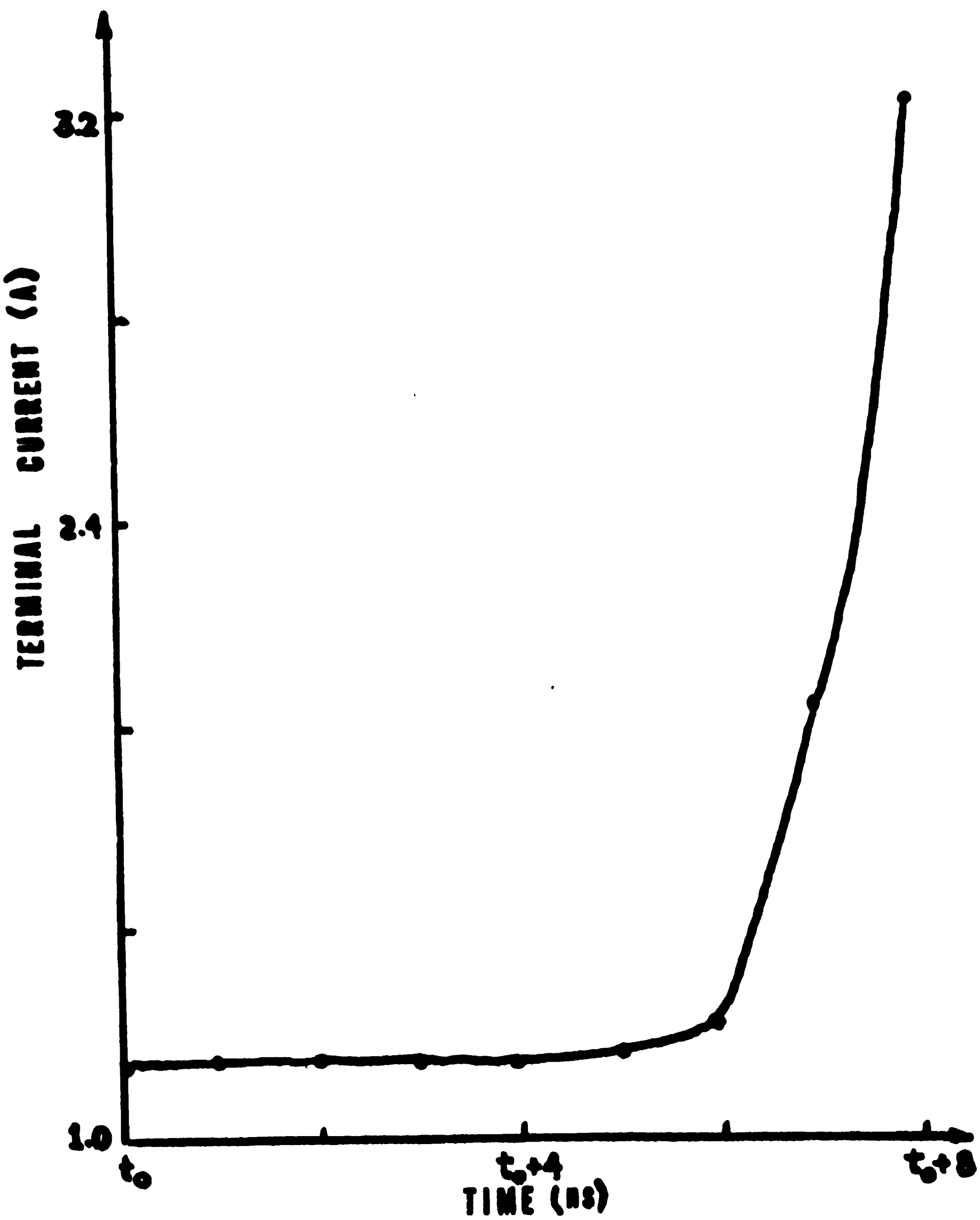

Figure 5.6

Terminal Current-vs-Time in Switching Region

5.5. Filament Formation in the Switching Process

Figures 5.7, 5.8, and 5.9 are sets of plots showing the temperature variation along the various directions x, y, and z at different times. The filament formation is very easily observed in the lateral plots; i.e., the plots along the y and z directions. In the preswitching region, these curves are absolutely flat; no gradients exist in the y and z directions, and there are no diffusion currents due to either thermal or concentration gradients in these directions. Observe that this is true even 2ns before the switching actually occurs. However, once the temperature crosses the critical temperature threshold, the temperature at that point rises very fast to produce a localized hot region--the filament. The phenomenon can best be observed in Fig. 5.8b, which is the plot of $T(2\Delta x, y, 4\Delta z)$ at various times. Once the filament formation has started, the temperature in the region seems to rise without limit. Though this post-switching instability due to thermal runaway lies outside the scope of this present dissertation, it is interesting to recall Ridley's[30] discussion in this context. He pointed out that this can be controlled by limiting the power dissipation through the device. In the circuit configuration used, this can best be done by increasing the external circuit resistance R_s. When switching occurred, the current through the device would be limited by this resistance; the power dissipation in the device would reduce, thereby reducing the rate of temperature until a final steady state is reached. The axial temperature profiles (Figs. 5.7a, b, and c) demonstrate the propagation of the switching phenomenon. Once the first point has switched, the neighbor points in the axial direction also switch; within two nanoseconds, this phenomenon propagates, and the entire axial line reaches a temperature above the critical value. (See Fig. 5.7b.) Points not lying in

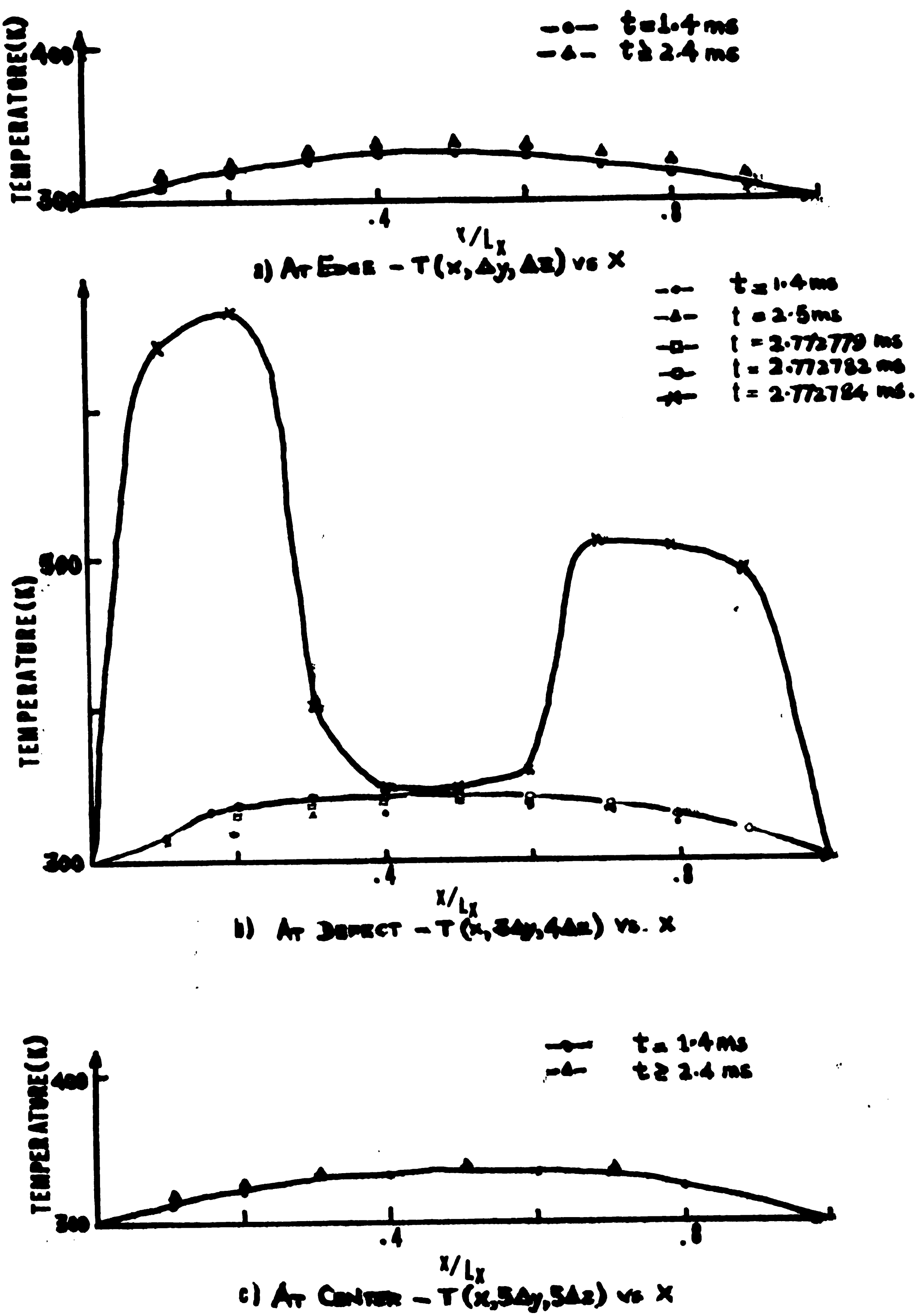

Figure 5.7

Temperature Profiles Along x at Different Times
and Different Planes Showing Initiation of Switching

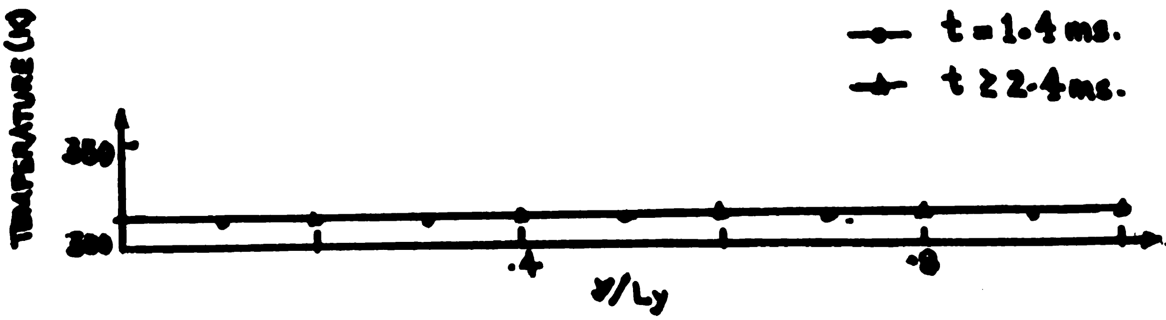

a) At Edge – T(Δx, y, Δz) vs y

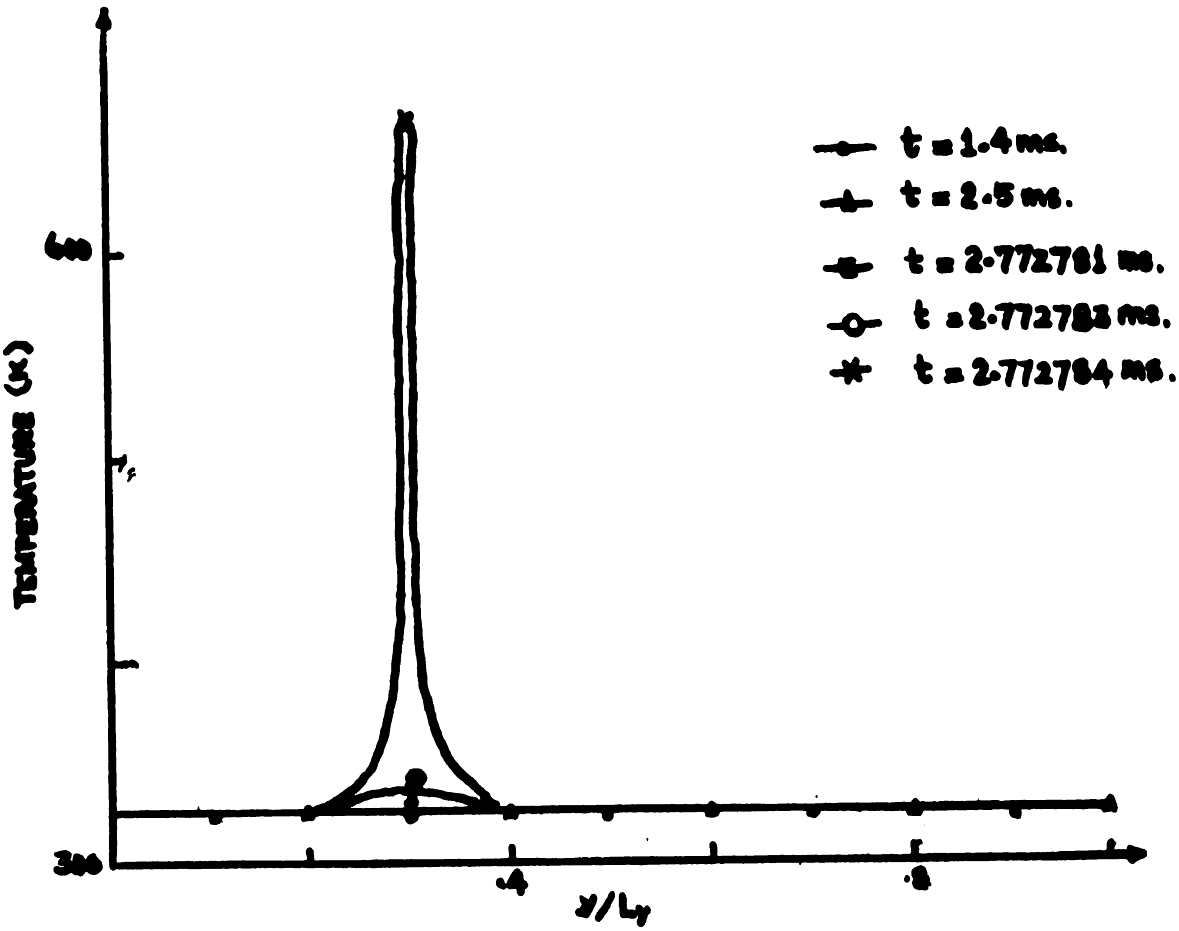

b) At Defect – T(2Δx, y, 4Δz) vs y

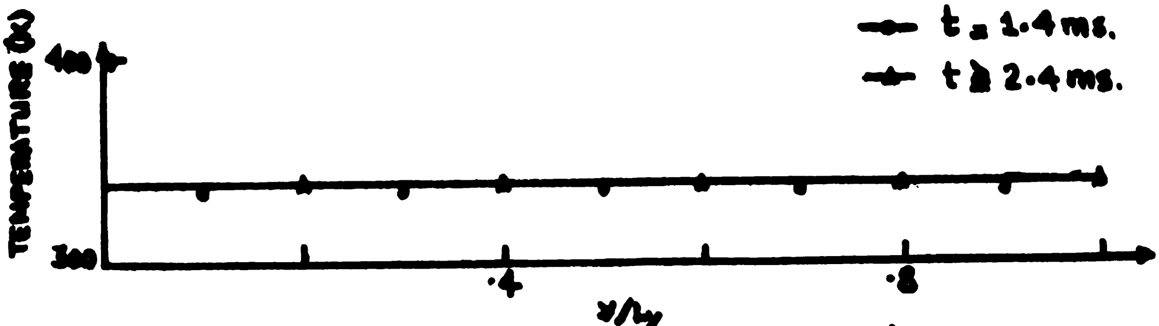

c) At Centre – T(5Δx, y, 3Δz) vs y

Figure 5.8

Temperature Profiles Along y at Different Times and Different Planes Showing Initiation of Switching

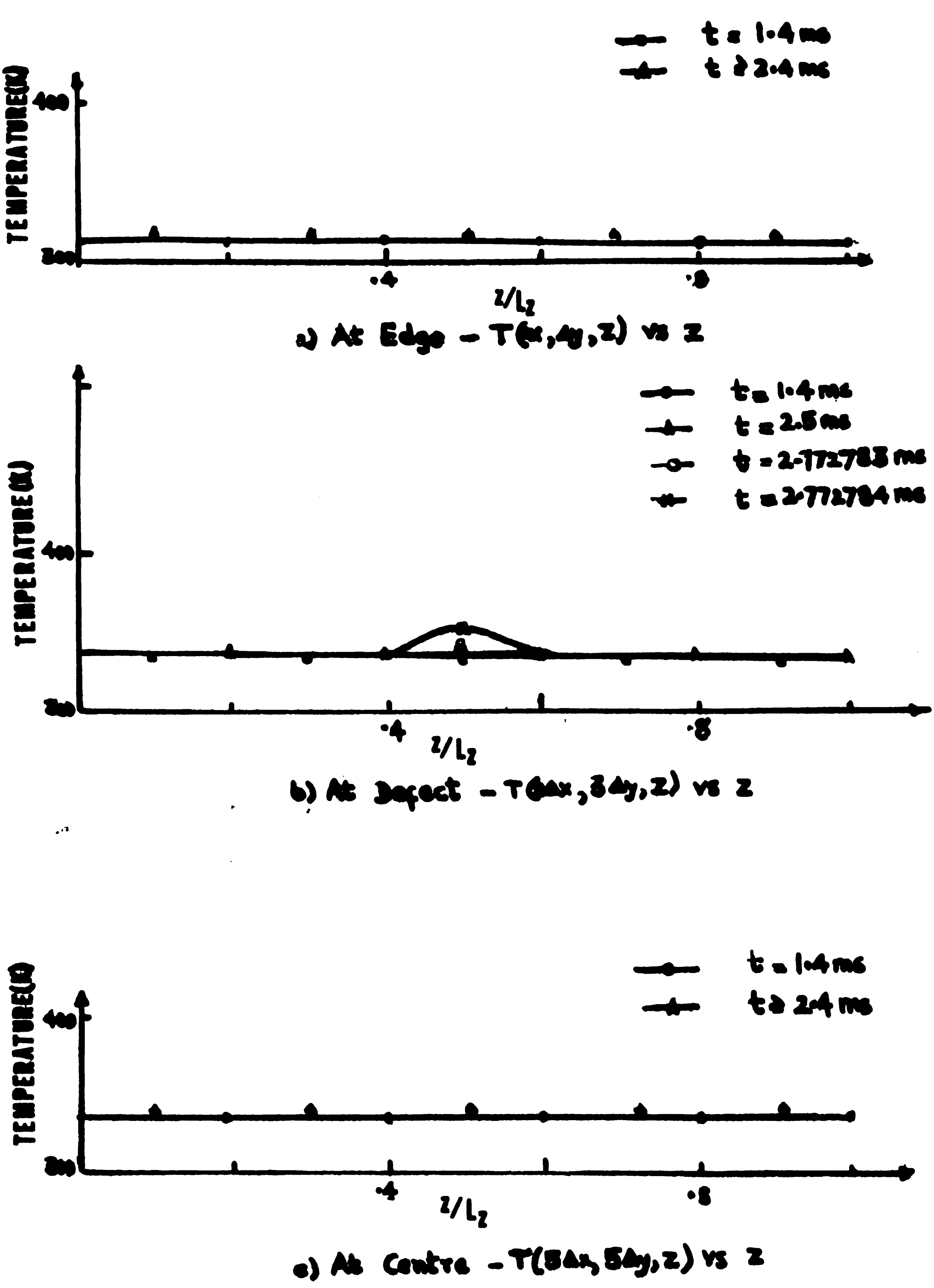

Figure 5.9

Temperature Profiles Along z at Different Times
and Different Planes Showing Initiation of Switching

this axial line (e.g. Fig. 5.7a) are not affected, and the temperature profile remains as if no filament existed within the sample.

An interesting feature is the point of initiation of the switching process. When the switching is induced by the power dissipated due to the electrical current through the device, the switching occurs, as may be expected, in the geometrical center of the device. If, however, a power-pulse is applied to an eccentric point, e.g., ($2\Delta x$, $3\Delta y$, $4\Delta z$), the switching does not originate either at the "power point" which simulates a local defect or at the geometrical center; in fact, it occurs at ($4\Delta x$, $3\Delta y$, $4\Delta z$) (see Fig. 5.9b), a point located between these two points. A moment's consideration will, however, show that this is entirely reasonable and logical.

At first glance, it might seem that the temperature distribution should have a double-humped characteristic with peaks at ($5\Delta x$, $5\Delta y$, $5\Delta z$), the geometrical midpoint and at ($2\Delta x$, $3\Delta y$, $4\Delta z$), the latter peak possibly being larger depending on the power input there. However, such a situation is physically impossible unless there are two heat sources within the device. For, if such was the characteristic, it would imply the existence of a valley between the peaks with a minima somewhere in between the two. The temperature gradients are now such that heat should flow from the peaks into the valley, causing the temperature to rise. For every other point outside this region, there are two thermal forces balancing each other. There is heat imput to each point due to the electrical power dissipation, and there is an established temperature gradient tending to conduct heat away to the nearest electrode. But, for points in the hypothetical valley, both forces tend to add to the heat content, and there are no forces tending to conduct heat away from this region. Consequently, the temperature in this region may be expected to rise more rapidly until the direction of the temperature gradients is reversed. Thus, it is logical to expect that the hottest point would lie here, between the supposed peaks at the midpoint and the defect point and so will be the first to reach the critical switching temperature T_{cr} and initiate switching.

Consider a simple steady-state one-dimensional analysis similar to the preceeding ones. Let x_0 be a point lying between 0 and $L_x/2$ where such a defect is localized. Representing the power pulse by a Dirac delta function, the relevant heat equation becomes

$$k_{th}\frac{d^2T}{dx^2} = -(P_1 + P_2\delta(x - x_0)) \tag{5.5.1}$$

where P_1 is, as before, a constant power dissipated in the material and P_2 is the "power pulse". Solving this yields

$$T = -\left(\frac{P_1x^2}{2k_{th}} + \frac{P_2(x - x_0)u(x - x_0)}{k_{th}}\right) + c_1x + c_2 \tag{5.5.2}$$

Using the boundary conditions that $T = T_{amb}$ at $x = 0$ and at $x = L_x$, the constants c_1 and c_2 can be evaluated

$$c_2 = T_{amb} \text{ and} \tag{5.5.3}$$

$$c_1 = \frac{P_1L_x}{2k_{th}} + \frac{P_2(L_x - x_0)}{k_{th}L_x} \tag{5.5.4}$$

Notice that c_1, which represents the slope of the temperature distribution at the origin, has increased. And so the temperature profile is given by

$$T = -\left[\frac{x^2P_1}{2k_{th}} - \frac{(x - x_0)u(x - x_0)P_2}{k_{th}} - \frac{P_1L_x^2}{2k_{th}} - \frac{P_2(L_x - x_0)x}{L_x2k_{th}}\right] + T_{amb} \tag{5.5.5}$$

The maxima can be localized by differentiating the above and is given by the simple expression

$$x_{max} = \frac{L_x}{2} - \frac{P_2x_0}{2P_1L_x} \tag{5.5.6}$$

As discussed earlier, x_{max} occurs neither at x_0 nor $\frac{L}{2}x$, but displaced from the center $\frac{L}{2}x$ towards x_0. However, since the steady state is preceeded by switching, no numerical correlation is possible.

Once switching has taken place, thermal runaway occurs. As seen from Fig. 5.8b, the temperature rise is now much greater near each end than at the middle. This is due to the speed of switching. The temperature rise is now so rapid that the thermal diffusion forces that tended to inhibit valley formation in the interior of the device can no longer keep pace. Since the spatial distribution of the power dissipation (Figs. 5.12 and 5.13) tends to be higher at the ends than at the center, the temperature rise will now be much faster at the ends and cause hot spots to be visible near each electrode. This situation is, however, unstable; a post-switching mechanism should re-establish the thermal diffusion effect, and the temperature of the valley in between the hot spots should rise. This is consistent with visual observations wherein during filament formation, hot spots have been observed near each end before forming the hot line or filament extending along the length of the sample, which is the final stable state.

In Fig. 5.10, the carrier current densities are plotted versus x and y at various instants of time in similar fashion to the temperature profiles plotted earlier. The filament formation is best observed in the lateral plot of $J_x(2\Delta x, y, 4\Delta z)$ vs y; note the peak occurring at $(2\Delta x, 3\Delta y, 4\Delta z)$. In the axial plots, combinations of diffusion effects blur the picture. However, the phenomena of thermal runaway near the two electrodes can easily be seen.

Another method of observing the mechanism of the switching process is by observations on the local electric field and the carrier current densities along the axes at various times.

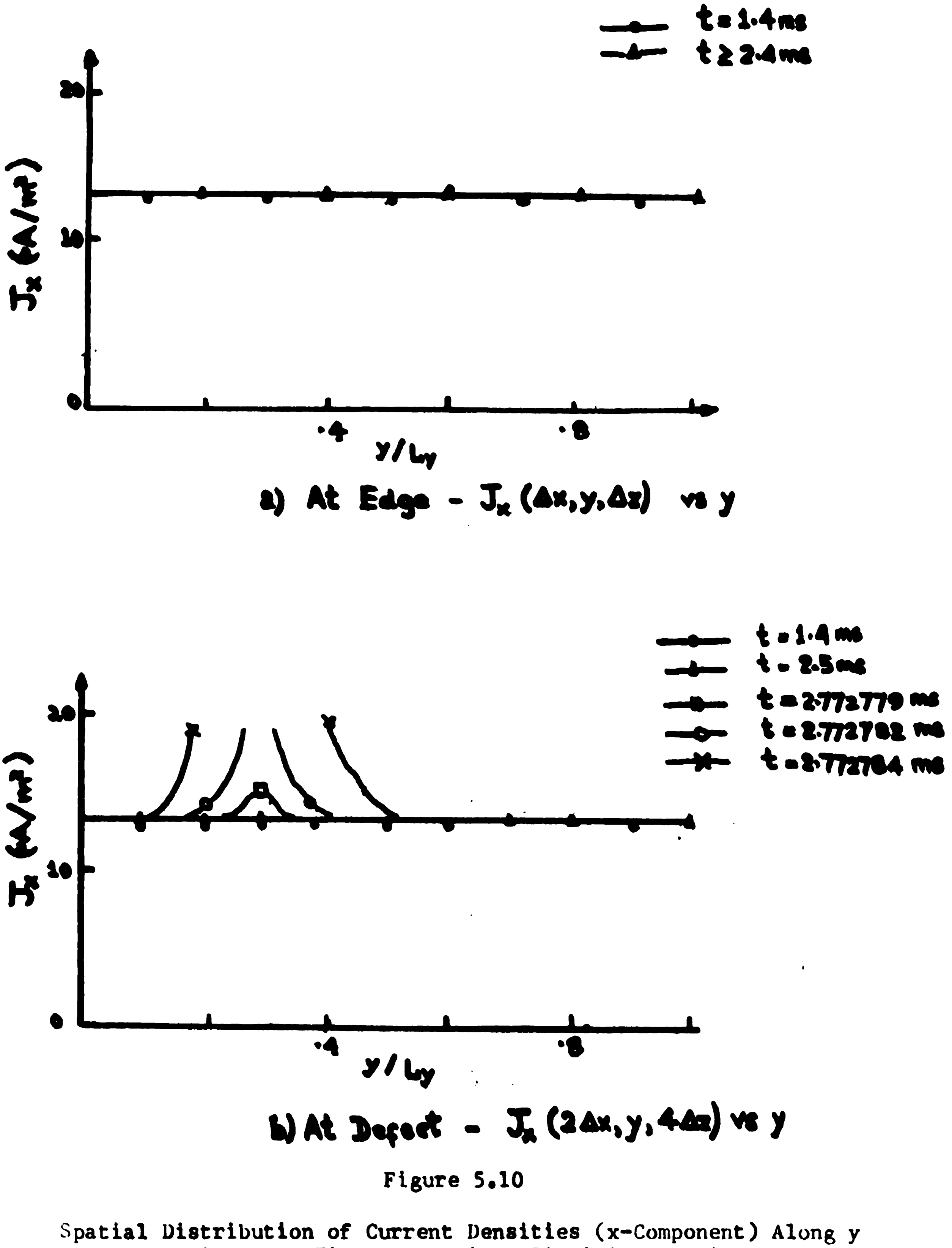

Figure 5.10

Spatial Distribution of Current Densities (x-Component) Along y at Different Times at Various Significant Points

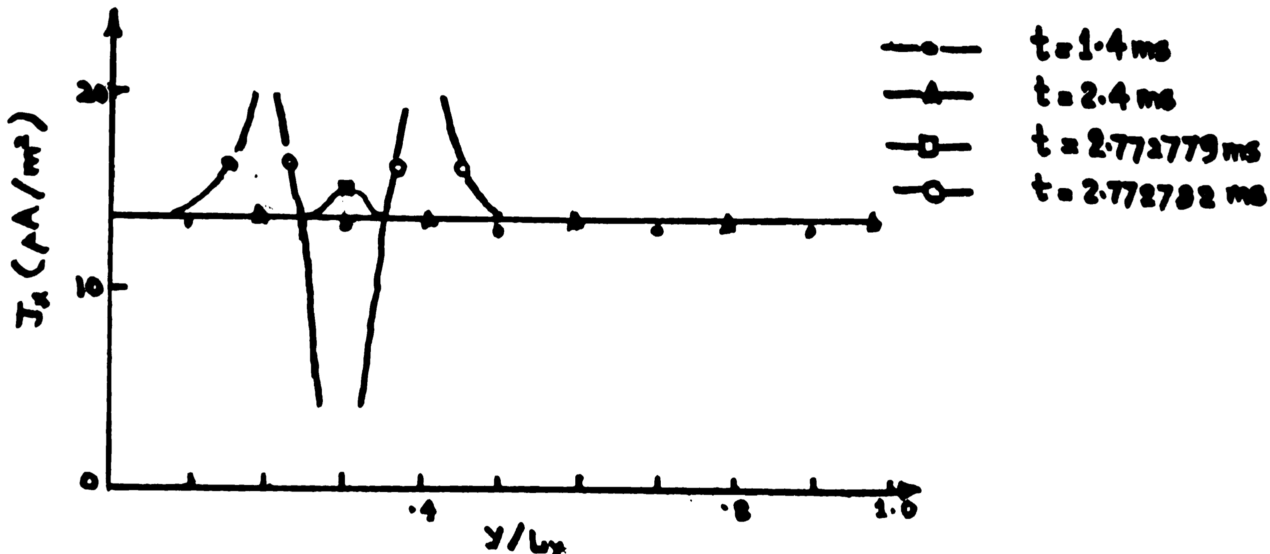

c) At Hot Point – $J_x(4\Delta x, y, 4\Delta z)$ vs y

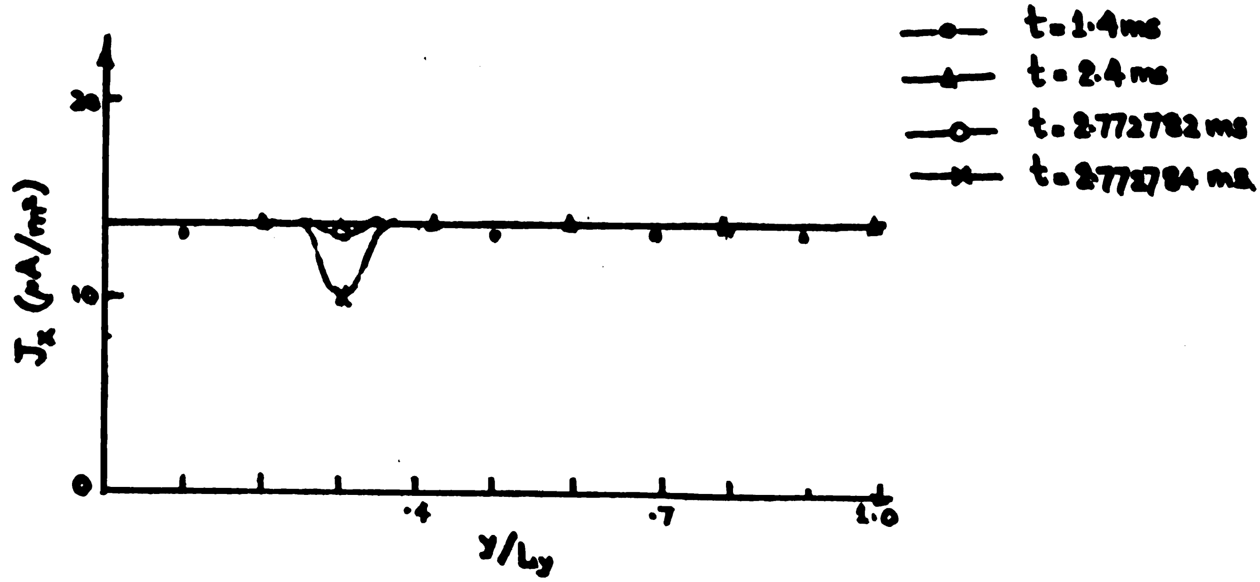

d) At Centre – $J_x(5\Delta x, y, 5\Delta z)$ vs y

Figure 5.10 cont.
from 78a

Figure 5.11 depicts the variation of the magnitude of the electric field $|\bar{E}|$, where

$$|\bar{E}| = \sqrt{Ex^2 + Ey^2 + Ez^2}$$

along the x-direction in the $z = 5\Delta z$ plane.

This coded representation consists of two codes; E_a represents a relatively low field which exists almost uniformly in the preswitching region, E_b represents a field an order of magnitude lower; this is the field once the switching process has commenced. Note how in the first of the three time intervals, it is E_a everywhere except at one point, where switching is originating. In the second, E_b has spread axially to its neighbor points but not laterally. In the third, it has spread axially through the length of the sample.

5.6. Power Dissipation and Energy Flux Density

It has already been established that the switching phenomenon in the ETD has a pronounced thermal character, and the nature of energy balance (as embodied in the temperature equation) plays an important role. But important energy variables, like power dissipation density and the energy flux density in the interior of the sample, are difficult to observe experimentally. On a computer model, however, such observations are relatively simple and of tremendous value to the device and applications engineer.

Figure 5.12b is a set of plots showing the variation of dissipated power density with time. In the preswitching region, for any point within the sample, the dissipated power density increases until a steady state is reached. The plot is similiar to the temperature plots discussed in Sec. 5.2. The rise is exponential, and the rise time is the same as the corresponding temperature profile. However, if

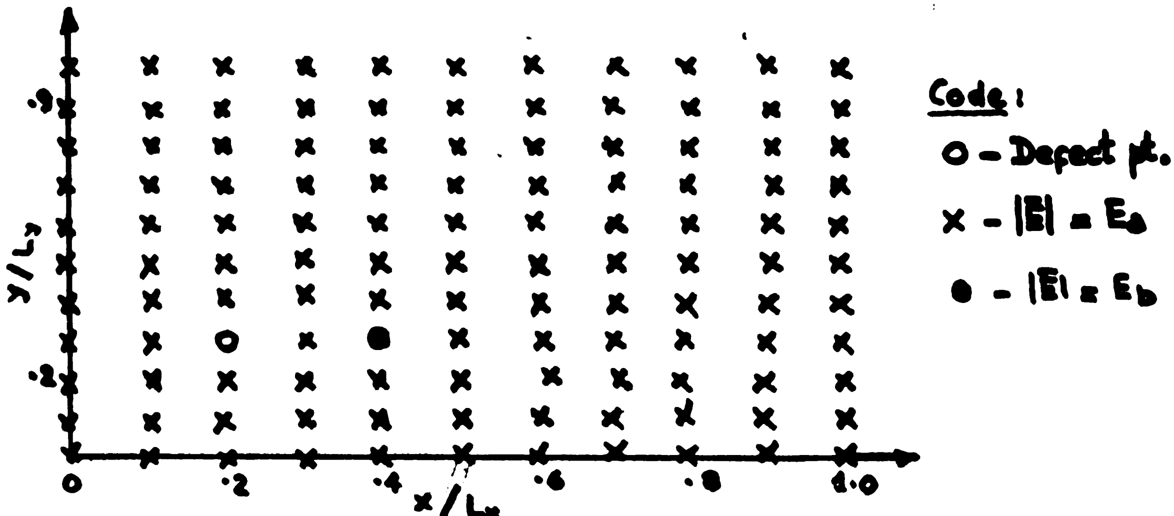

Figure 5.11a
Coded Representation of E-Field Distribution Showing Initiation of Switching at t = 2.5ms

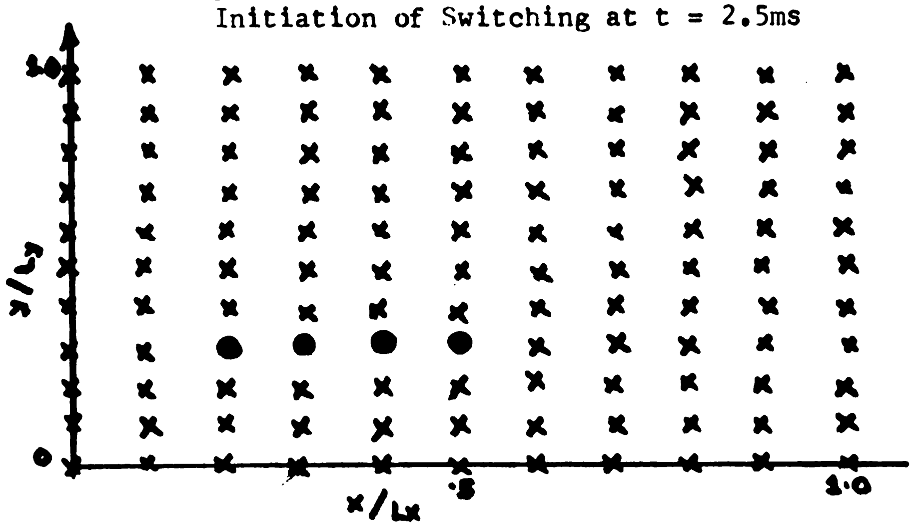

Figure 5.11b
Coded E-Field Representation at t = 2.772781ms

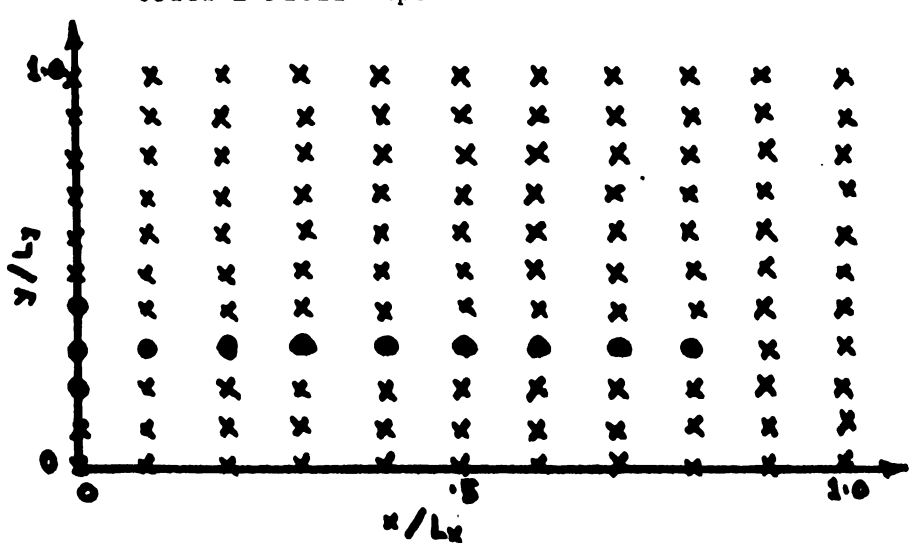

Figure 5.11c
Coded E-Field Representation at t = 2.772783ms

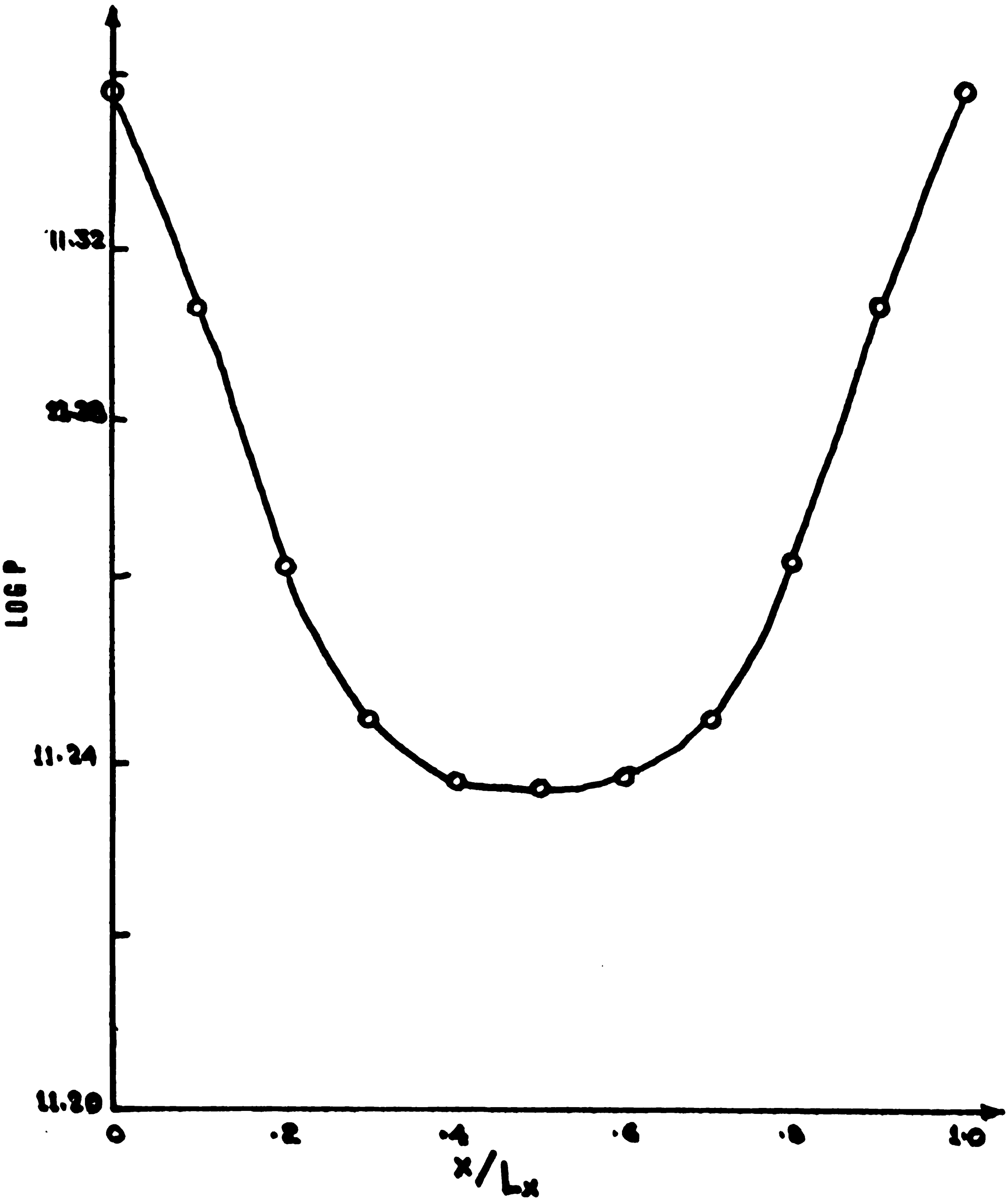

Figure 5.12a

Steady State Spatial Distribution of Power Dissipation Density - Log P(x, 3Δy, 4Δz) - vs - x

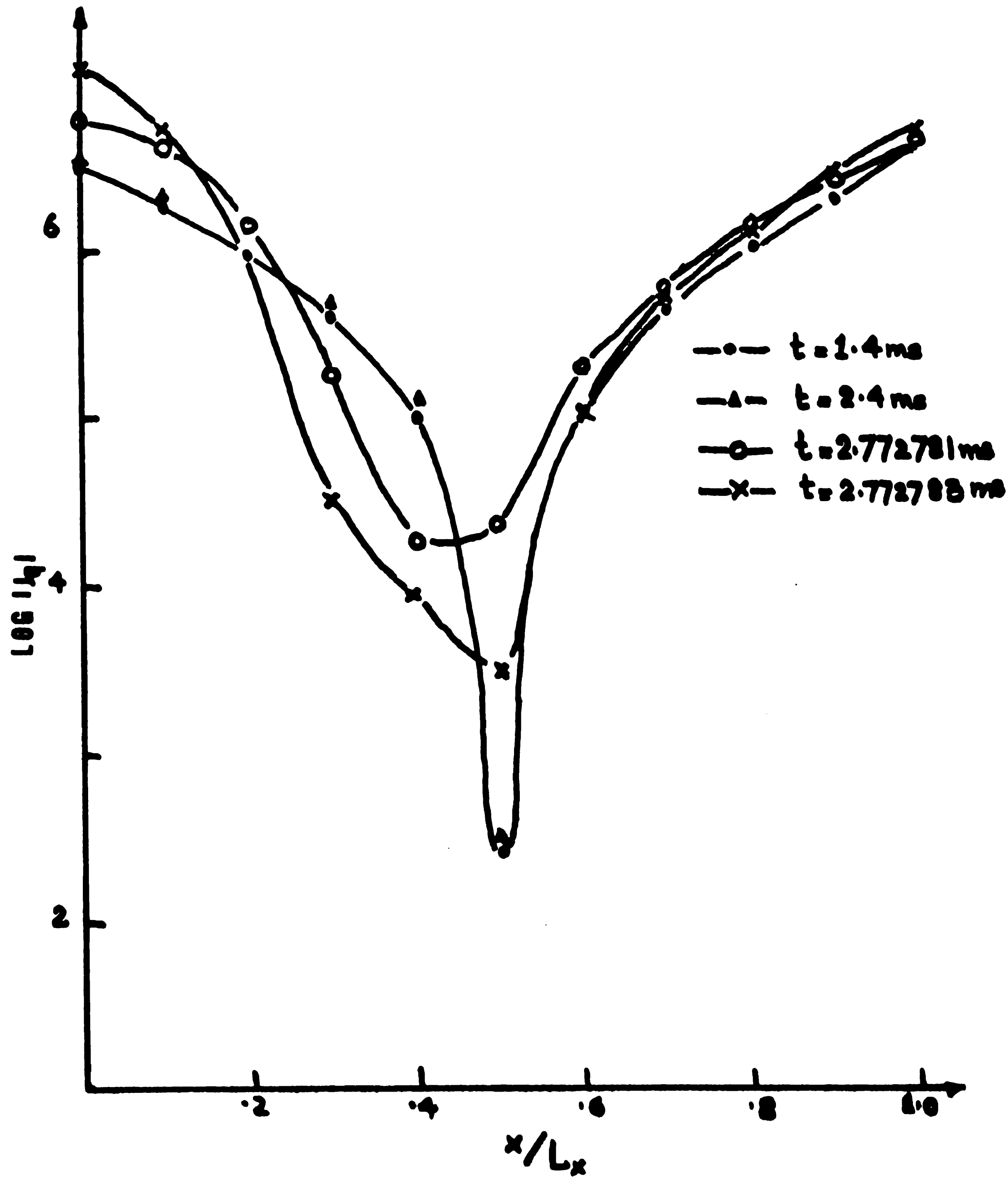

Figure 5.12b

Power Dissipation Density-vs-x During Initiation of Density - Log P(x, 3Δy, 4Δz) - vs - x switching occurs, the power dissipation increases tremendously; this follows logically, too, since the dissipated power is proportional to the square of the electric field which is also increasing rapidly as noted earlier. This, in fact, is the cause of the thermal runaway phenomenon; the rate of power dissipation increases so rapidly that it more than offsets any reduction in the rate of increase of the electric field. Outside the filament region, the power dissipation reduces slightly during this time. Along the x-direction, the profile is roughly the opposite of the temperature profile. Starting from an initially flat profile, the power density tends to show a minima at the center and the highest power dissipations at the two ends. When a power pulse is superposed, the power density profile tends to shift showing a maxima at both the point of impressed power ($2\Delta x$, $3\Delta y$, $4\Delta z$) and the displaced "hot" point ($4\Delta x$, $3\Delta y$, $4\Delta z$), which is consistent with the observations made in Sec. 5.5.

The heat flux resembles the power dissipation profile. (See Fig. 5.13.) The maximum heat energy flows out at either end via the conducting electrodes; the minimum occurs at the center. Once switching occurs due to the occurrence of a "power pulse", the heat flux density is low both at the defect point ($2\Delta x$, $3\Delta y$, $4\Delta z$) and the displaced hot point ($4\Delta x$, $3\Delta y$, $4\Delta z$).

5.7. Optical Switching of the ETD

In this experiment, a random interior point--chosen again to be the point ($2\Delta x$, $3\Delta y$, $4\Delta z$)--is locally excited by a continuous external light source such that the point is totally ionized. In the computer model, this is simulated by setting the ionized donor density n_d^+ at the point equal to the total donor density N_d. The effect is almost

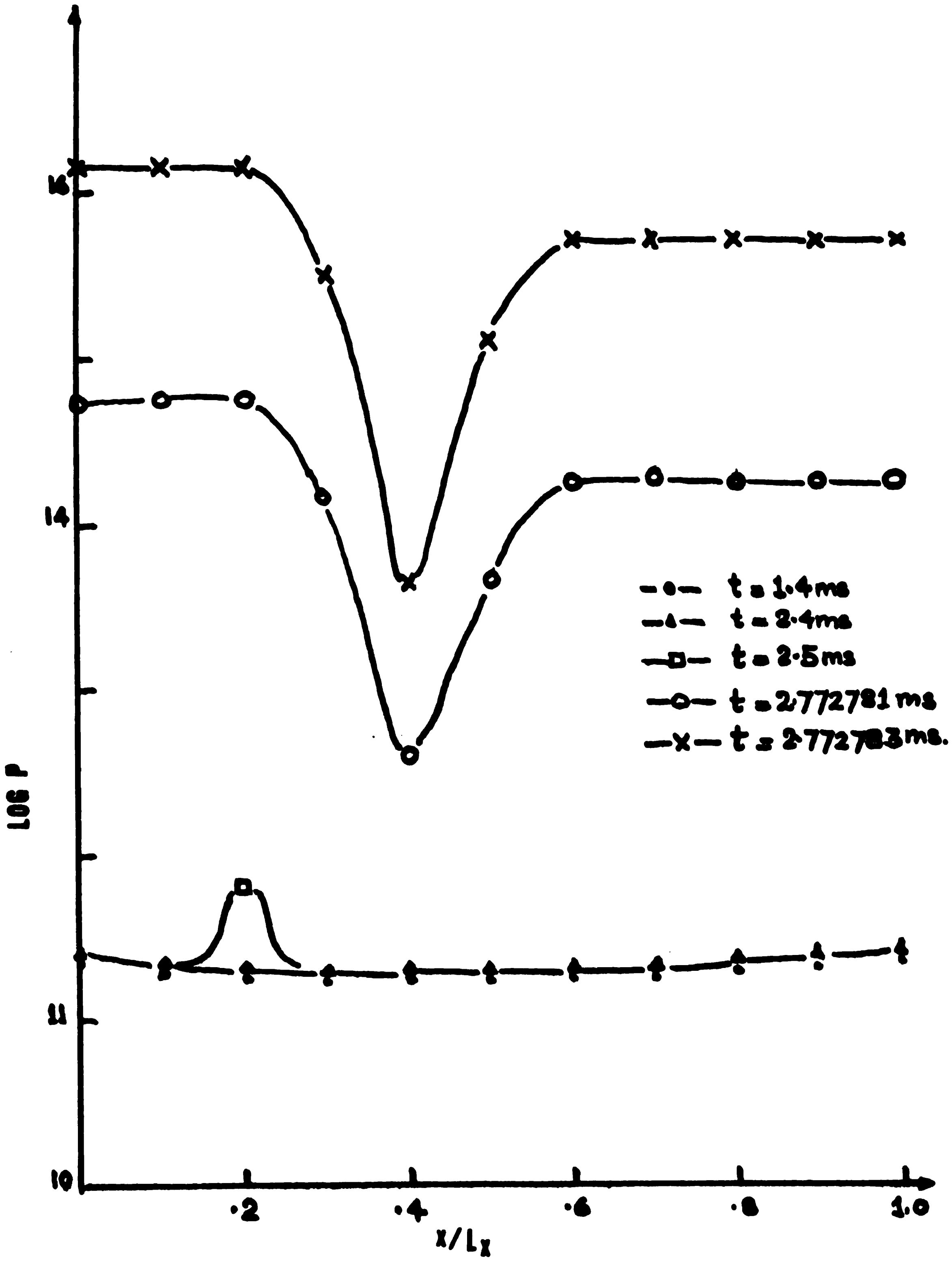

Figure 5.13

Spatial Distribution of Heat Flux Density Showing Initiation of Switching - Log/Jq/(x, 3Δy, 4Δz) - vs - x immediate; the device switches to the unstable high-current region and proceeds, as in the previous switching methods, to experience thermal runaway.

Some interesting observations can be made with regard to this experiment. In this experiment, the external bias voltage V_{app} is low such that the ETD reaches a steady state just below the critical temperature. The light pulse is now applied, and switching is almost immediately observed. Note that in the case of a defect forming in the device, there is still a fairly large ($50\mu s$) storage time associated. In this case, however, it is much, much less than $10\mu s$, and hence opens up very interesting lines of application for the device. For one, since the thermal runaway is controlled by device design and external circuitry, there is a very fast photoswitching device available. Furthermore, the switching can be originated at will anywhere within the sample; this can be developed into a fast read/write unit which would have increasing applications in interfacing with computers and other high-speed equipment.

CHAPTER VI

CONCLUSION

The objective of this research effort was primarily to gain an understanding of the physical principles underlying the initiation of the switching phenomenon in the ETD. Experimental evidence[6,8] and literature surveys[5] indicate that this is a complex phenomenon, and a number of interdependent variables--like V, ρ, n, T--play important roles in determining the switching characteristics of this device. To understand the mechanisms involved in its switching behavior, it is necessary to understand the interrelationships between these variables and be able to analyze the significance of the contribution of each.

The means chosen to assist in achieving this objective was to construct a computer-based model of the ETD. The model embodies all the available physical information known or held to be true regarding the ETD, and is based on well-known physical laws. It is used to simulate the behavior of the ETD in order to study the mechanisms involved in the switching process within the bounds of the model; in other words, the scope of the model is limited to the study of the initiation of the switching process so as to be able to develop a more comprehensive understanding of the physical principles associated with it.

Some of the results obtained from those simulations were compared with available experimental data in order to verify the goodness of the model. The model is useful in understanding the distributed bulk properties of the ETD. This information is not available experimentally, but is important in understanding the overall behavior of a given device under various electrical and thermal boundary conditions. In addition, the model possesses the capacity to simulate conditions which have not, as yet, been experimentally investigated, thus giving it a predictive aspect. This feature enables the model to be used to design optimal devices and understand the practical limitations of existing ETD's.

6.1. Accomplishments of this Research

The major accomplishment of this research project lay in the physical principles that were uncovered and the generalizations that were made regarding the behavior of the ETD. This project has focused on the preswitching region and the processes involved in the initiation of switching. In relation to the I-V characteristics of the device, the stable low-current region and the unstable transition region described in Fig. 5.1 form the primary areas of interest.

The thermal character of the preswitching region was firmly established by the model. In the stable low-current region, the thermal parameters like the thermal conductivity k_{th} and the specific heat c, and the thermal boundary conditions almost completely determine the temperature profile as was shown by the excellent co-relation with the solution of the one-dimensional steady state equation:

$$\frac{d^2T}{dx^2} = \frac{-P}{c}$$

where P, the dissipated power density of the sample is assumed constant. Also, the time constant associated with reaching a steady state was in close accord with the theoretical thermal time constant τ_a as compared in Table 5.2. Therefore, both the final steady-state temperature profile and the time constant involved in reaching this steady state were associated with thermal parameters. Also, the other dependent variables of the device show an exponential time dependence, the time constant involved being again close to the same theoretical time constant τ_a. This agrees with the expectations of numerous theoretical workers in the area like Boer[10], Dohler[31], Ovshinsky[12], and others.

The thermal time constant is also associated with the large storage time observed in the device. However, the switching time in the device is very fast--of the order of nanoseconds--and cannot be attributed to thermal diffusion effects. In this transition region, the model succeeds in describing the simulated behavior of the ETD in close parallelism to actual experimental observations made on these devices. The model describes the switching mechanism as the propagation of a band gap reduction through the length of the material. Such a reduction caused a change in the local electric field which propagated along the length as the switching progressed, as illustrated in the electric field snapshots at succeeding time steps depicted in Fig. 5.11.

The model is also able to simulate the switching behavior of the ETD induced by different methods. Consider, for example, the phenomenon of switching induced by the introduction of a defect in the material. In the first place, the results agreed with the experimentally observed fact that the switching first occurred along an axial line containing the defect. But, that is not all. It also localizes the point of origin of the switching process at a point away from the defect. From hindsight, this is readily understandable and reasonable since thermal diffusion prevents the formation of a double-humped characteristic with humps at the defect point and at the midpoint. Hence, the competing forces result in a maximum forming in between the two points.

The combination of these two regions, the low-current and the transition region form part of the static and dynamic I-V curves together with the unstable and stable high current regions which lie outside the scope of this present model. The overall agreement of this curve to the experimentally observed I-V characteristics of the ETD is further testimony to the validity of the model. Thus, the model is not only capable of providing an understanding of the interactions in the interior of the device; it is also able to relate to the easily observable static and dynamic terminal I-V characteristics. Since the I-V characteristics form a crucial interface between the device engineer and the circuit designer, the ability of the model to depict these characteristics give it considerable value.

6.2. Predictive Aspects of the Model

The predictive aspects of the model are useful guides to further material and device development. This is largely due to the capability of the model to present experimentally inaccessible data regarding the nature of the variables in the interior of the semiconductor material, and so contribute significantly to understanding the physical processes in the ETD. Thus, using the model, one can predict the nature of the electrical potential and charge distribution in the interior of the material; one can also predict the temperature profile, the power dissipation density and the magnitude of heat flux density at various points in the interior in both the low-current and transition regions. It is thus possible to study the interrelationships that exist between the various electrical and thermal variables.

For instance, the power dissipation curve predicted by the model provides a vital link between apparently unrelated experimental observations. The switching times observed in the ETD's are of the order of nanoseconds[34]. This is in agreement with the simulated results of the model; in fact, the switching mechanism can actually be observed progressing through the device by studying the electric field and temperature profile snapshots of the interior. Also, it has been experimentally observed that, prior to filament formation, thermal hot spots appear near each electrode. The ETD simulation also projects similar results as shown by the temperature profile of Fig. 5.8b. The simulation predicts that the power dissipation curve (see Fig. 5.12) is approximately an inverted parabola. Since the thermal time constant is so much larger than the switching time, thermal diffusion is practically nonexistent once the switching process has been initiated. Hence, the power dissipation accounts for the excessive temperature rise near the electrodes resulting in the experimentally observed hot spots.

Simulations were also made to study various methods of initiating switching within the device. Switching was initiated

a) if the external circuit parameters were such that the temperature at a point within the sample exceeded the critical temperature,

b) by simulating a defect wherein excessive power was dissipated resulting in local temperatures greater than the critical temperature, and

c) by simulating a light pulse focused at a point on the ETD operating under suitable bias conditions.

These first two methods agree with experimental observations; the third method has considerable predictive value. In this case, the temperatures at all points within the device were below the critical temperature T_{cr}. The incidence of the simulated light beam creates local donor ionization, and this is sufficient to initiate switching in the device. The simulation results therefore predict that under suitable bias conditions, any energy source capable of causing local ionization is suitable to switch the ETD. Thus, radiant energy of various frequencies and even acoustical waves may be used to initiate switching in ETD's under suitable bias conditions.

6.3. Limitations and Deficiencies of the Model

By virtue of the stated objectives of the model, its scope is limited to simulating the ETD behavior in only the low-current and transition regions of the terminal I-V curves. The third region, namely the unstable high-current region is portrayed to some extent. Thereafter, thermal runaway occurs, and excessive temperatures are generated in the device. The fourth region, the stable high-current region, is thus never reached.

Ridley[(30)] has pointed out that the stability of the ETD depended heavily on the external resistance R_s. This would limit the current through the device and hence the power dissipation. In the model, the iteration scheme* is such that, for large R_s, the scheme is divergent. The iteration scheme referred to is the Inner Loop* elucidated in Chapter 4. Here, the terminal current is computed by integration near the edge of the device, and the terminal voltage is computed therefrom by applying Kirchhoff's voltage law. In such a scheme, the limiting effect is not obtained since a negative voltage would still satisfy the voltage law, and the current continues to increase. Obviously, for simulation of this region, a revision in the iteration scheme is required.

Although such a revision would limit the power dissipation, it still may not limit the temperature to realistic values. The crux lies

---

*See Fig. 4.1.

in the assumptions that the thermal variables k_{th}, the thermal conductivity, and c, the specific heat, remain constant beyond T_{cr}. For stability to be achieved within a reasonable temperature, both c and k_{th} should increase; i.e., the material should require more heat input to raise its temperature and should also conduct heat away faster.

In addition to this, there are other deficiencies in the model. For one, there is a discrepancy between the experimentally observed threshold voltage and the V_{thr} observed in the simulation runs. As pointed out earlier, this is because the assumption that the net charge density remains constant is not strictly valid due to the external circuit configuration. One way of correcting for this would be to reconstruct the circuit so that a charge source instead of a voltage source supplies energy to the semiconductor. An alternative method would be to reevaluate the charge density at the ends at each time step and use this variable charge density as a boundary condition. Another source of numerical disagreement is in the magnitudes of currents; however, this can be adjusted by using sample dimensions closer to the sample sizes used in experiments. There is also a quantitative error between the switching times observed in the simulations and experimental data. Though several reasons for this have been discussed earlier, one possible explanation is that it is due to a breakdown in an assumption of the model. In the model, all magnetic field effects were neglected. However, in the transition region of the I-V curve, the current in the filament region changes very rapidly. By neglecting the magnetic field, the inductive effects of this change is neglected, too, which may affect the switching time, though the extent is difficult to determine. Incorporating the magnetic field in the equations is difficult, as a wave equation is to be solved instead of the Poisson's equation. The wave equation is a vector equation and thus is comprised of three scalar equations, and both computer time and memory requirements is increased tremendously. Obviously, when modifying this model, a balance or compromise has to be readhed; there is a definite tradeoff here between the accuracy and numerical predictability on the one hand and simplicity, ease of interpretation, computer memory requirements, and costs on the other.

6.4. A Possible Simplification of the Model

Because of the existence of this tradeoff, it is worthwhile to consider schemes to simplify the model and reduce the computer costs of simulation. One such example is outlined here.

In the preceding chapter, the temperature equation,

$$\frac{c}{k_{th}}\frac{\partial T}{\partial t} - \nabla^2 T = \frac{P}{k_{th}}$$

was reduced to a simple one-dimensional steady state equation

$$\frac{d^2T}{dx^2} = \frac{-P}{c}.$$

The analytic solution of the above indicated that the temperature distribution should be parabolic in shape. Then the axial temperature distribution obtained by simulating the low-current steady state condition was fitted to a parabolic curve, and the best-fit parameters obtained were very close to the analytic solution. This indicates that reasonable accuracy of simulated results (say within 5%) can be obtained by considering only the temperature equation in this region of operation where the temperatures lie well below the critical temperature.

Let the starting ambient temperature be T_{amb}, T_{cr} the critical temperature, and T_D the temperature difference defined by

$$T_D = T_{cr} - T_{amb}$$

If T is the highest temperature tested at any time, then as long as

$$T \leq T_{amb} + f(T_{cr} - T_{amb}),$$

where f is a preset positive real number less than unity, only this simplified model needs to be solved. At higher temperatures, however, the other parameters will begin to play a more significant role, and the more complete set of equations will have to be solved.

The preset factor f is a function of the material parameters of the ETD, and a good estimate can be obtained by preliminary runs with the present model. For example, for VO_2, a good value for f is 0.9. Using the simplified model, the temperature at the maximum is identical to that obtained from the one-dimensional analysis, as P would be assumed constant. Thus, for $f = 0.9$, the expected error in the maxima estimated from Table 5.5 is less than 5%.

6.5. Suggestions for Future Research

From the results obtained in the simulation runs thus far, some suggestions for future areas of research can be seen and are presented below:

1) An extension and broadening of the objectives of the model to include the final stable steady state of operation is a prime area for research. This would probably necessitate a revision of the computing scheme as discussed. Such a revised model would be able to simulate the behavior of an ETD in all four regions of the I-V curve.
2) Some of the assumptions of the model need to be relaxed to incorporate more of the characteristics of the real device and thus obtain closer numerical agreement. In this regard, the two suggested targets are the assumption of constant

charge density at the electrode interfaces and of neglecting the effects of magnetic field. For the former, an iterative scheme to compute the charge density at the interface at each time step is suggested. For the latter, the Poisson equation $\nabla^2 V = -\rho/\epsilon$ which uses the relation $\overline{E} = -\nabla V$ should be replaced by an appropriate wave equation. Since such modifications would represent a substantial increase in computer time and memory requirements, simplifying modifications of the type outlines in Sec. 6.4 could also be simultaneously made.

3) A single defect in an otherwise homogeneous material has been simulated on this model. A possible extension would be to observe the switching phenomena when a statistical distribution of defects exist in the material.

4) Individual material parameters of the device, like k_{th}, c, N_d, etc., could be varied in the existing model with a view to isolating and analyzing the effect of each parameter on the device switching characteristics. This could provide considerable impetus to material development and guide experimentation in that area.

5) Environmental parameters like the ambient temperature and boundary conditions could be varied. Such studies would be of importance to both the circuit designer and the device engineer. To the circuit designer, a study of the device characteristics under various electrical circuit bias conditions would also be of interest.

6) The model predicts that local ionization by the impinging of an external energy would cause the device to switch

under suitable bias conditions. Optical, u-v radiation, or other radiations could be tried. Acoustic waves could also be tried.

APPENDICES

APPENDIX A

Derivations Using the Boltzmann's Transport Equation

In Sec. A.1, we shall derive the basic charge carrier transport equation used in Chapter 2 from the Boltzmann's equation. Subsequently, in Sec. A.2, we arrive at expressions for the transport parameters, namely σ, the electrical conductivity, D, the concentration diffusion coefficient, and α, the thermal diffusion coefficient.

A.1. The Transport Equation

Let f_0 be the equilibrium distribution function for the electrons in the semiconducting material for all temperatures T in the operating temperature range. Under the application of forces during operation, the perturbed distribution is f, where f is a function of $\bar{r}$ space and velocity space

$$f = f(\bar{r}, \bar{v})$$

Using a first-order perturbation theory, f can be written in terms of the equilibrium distribution f_0 as

$$f = f_0 + \nabla_r f_0 \cdot \bar{v}c + \nabla_v f_0 \cdot \frac{d\bar{v}}{dt} \tau \tag{A.1}$$

where τ is the net time constant associated with the perturbation. This is known as the Boltzmann transport equation.

Consider a unit volume of the sample. The carrier current density due to the flow of electrons is given by:

$$J_i = ne < v > \tag{A.2}$$

where < v > is the expectation value of the electron velocity. The expectation value < v > is defined, for a given statistical distribution f, as:

$$< v > = \frac{\int_{v'} v f dv}{\int_{v'} f dv} \tag{A.3}$$

where v' is the total velocity space.

Using (A.1),

$$< v > = \frac{\int_{v'} \bar{v}(f_0 + \tau(\bar{v}\nabla_r f_0) + (\dot{\bar{v}} \cdot \nabla_v f_0))d\bar{v}}{\int_{v'} f d\bar{v}}$$

Hence

$$\bar{J} = \frac{-ne(\int_{v'} \bar{v} f_0 dv + \int_{v'} \tau \bar{v}\bar{v} \nabla_r f_0 d\bar{v} + \int_{v'} \dot{v}\, \tau \cdot \nabla_v f_0 \cdot \bar{v}_i)dv)}{\int_{v'} f dv}$$

Defining the root-mean-square velocity by the expression

$$w^2 = |\bar{v}^2|$$

and, in cylindrical co-ordinates,

$$\int_{v'} dv = \int_0^\infty \int_0^\pi \int_0^{2\pi} w^2 \sin\theta d\theta d\phi dw$$

The expression for the carrier current thus reduces to:

$$\bar{J} = \frac{+[ne(fvf_0 dv + \int_0^\infty \int_0^\pi \int_0^{2\pi} \tau w + \nabla_r f_0 \sin\theta d\theta d\phi dw + \int_0^\infty \int_0^\pi \int_0^{2\pi} \tau \dot{v}(\nabla_r f_0 \cdot \bar{v}) w^2 \sin\theta d\theta d\phi dw]}{\int_v f_0 d\bar{v}}$$

For simplicity, it is assumed that, in the model, the equilibrium distribution is Maxwellian.

$$f_0 = n\left(\frac{m}{2\pi kT}\right)^{3/2} e^{\frac{-mw^2}{2kT}}$$

Since there are n free particles per unit volume, the integral of the denominator is obviously n. Also, the first integral in the numerator is zero. Thus,

$$\bar{J} = \Big[\int_0^\infty\int_0^\pi\int_0^{2\pi} -\tau e\, w^4 \nabla_r f_0 \sin\theta d\theta d\phi dw$$

(a)

$$+ \int_0^\infty\int_0^\pi\int_0^{2\pi} e\tau \dot{v}(\nabla_v f_0 \cdot \bar{v}) w^2 \sin\theta d\theta d\phi dw\Big]$$

(b)

Consider the term (b). The term $\dot{\bar{v}}$ simplifies as follows:

$$\dot{\bar{v}} = \frac{d\bar{v}}{dt} = \frac{1}{m}\frac{d\bar{p}}{dt} = \frac{1}{m}\bar{F}$$

where F is the applied force. Since the force in this model is due to the presence of the electric field $\bar{E}$

$$\bar{F} = -e\bar{E}$$

$$\dot{\bar{v}} = -\frac{e}{m}\bar{E}$$

The term (b) thus becomes:

$$(b) = \Big[-e\int_0^\infty\int_0^\pi\int_0^{2\pi}\tau(\nabla_v f_0 \cdot \bar{v}) w \sin\theta d\theta d\phi dw\Big]\bar{E}$$

Obviously, this component of current is the conduction component $\bar{J}_{cond}$, since it is proportional to the field $\bar{E}$. The quantity within parenthesis must therefore be the electrical conductivity σ; the integral is evaluated later in this section.

The other term, (a), is the diffusion term $\bar{J}_{diff}$; it comprises of the concentration diffusion component and the thermal diffusion component. Consider the quantity $\nabla_r f_0$.

$$\nabla_r f_0 = \frac{\partial f_0}{\partial n}\nabla n + \frac{\partial f_0}{\partial T}\nabla T$$

Since

$$f_0 = n\left(\frac{m}{2\pi kT}\right)^{3/2} e^{\frac{-mw^2}{kT}}$$

Hence

$$\frac{\partial f_0}{\partial n} = \left(\frac{m}{2\pi kT}\right)^{3/2} e^{\frac{-mw^2}{kT}} = \frac{f_0}{n}$$

and

$$\frac{\partial f_0}{\partial T} = n\left(\frac{m}{2\pi k}\right)^{3/2}\left[\frac{-3e^{\frac{-mw^2}{2kT}}}{2T^{5/2}} + \frac{mw^2}{2kT^2} \cdot \frac{1}{T^{3/2}} e^{\frac{-mw^2}{2kT}}\right]$$

$$= n\left(\frac{m}{2\ kT}\right)^{3/2} e^{-\frac{mw^2}{2kT}}\left[\frac{mw^2}{2kT^2} - \frac{3}{2T}\right]$$

$$= f_0\left[\frac{mw^2}{2kT^2} - \frac{3}{2T}\right]$$

Substituting the above relations back into term a:

$$(a) = \bar{J}_{diff} = \left[\int_0^\infty\int_0^\pi\int_0^{2\pi}\tau w^4 \frac{f_0}{n} \sin\theta d\theta d\phi dw\right]e\, n$$

(c)

$$+\left[\int_0^\infty\int_0^\pi\int_0^{2\pi}\tau e\, w^4 f_0\left(\frac{mw^2}{2kT^2} - \frac{1}{T}\right)\sin\theta d\theta d\phi dw\right]\nabla T$$

(d)

From the form of the equation, it is apparent that the quantities (c) and (d) enclosed in parenthesis are the proportionality factors D and α, the concentration and thermal diffusion coefficients respectively.

A.2. The Proportionality Constants

(a) The Electrical Conductivity σ

The required integral is

$$\bar{J}_{cond} = \frac{-e^2}{m}\int_0^\infty\int_0^\pi\int_0^{2\pi}(\nabla v f_0 \cdot \bar{v})w^2 \sin\theta d\theta d\phi dw \bar{E}$$

and so

$$\sigma = -\frac{e^2}{m}\int_0^\infty\int_0^\pi\int_0^{2\pi}(\nabla v f_0 \cdot \bar{V})w^2 \sin\theta d\theta d\phi dw$$

Expanding $\nabla v f_0$ in spherical co-ordinates,

$$\nabla v f_0 = \frac{\partial f_0}{\partial w}\hat{v} + \frac{1}{w}\frac{\partial f_0}{\partial \theta}\hat{\theta} + \frac{1}{w\sin\theta}\frac{\partial f_0}{\partial \phi}\hat{\phi}$$

Since a spherically symmetric Maxwellian distribution has been chosen, the partials in θ and ϕ are zero. Hence

$$\bar{v} \cdot \nabla v f_0 = \frac{\partial f_0}{\partial w} \hat{v} \cdot \bar{v}$$

$$= \frac{\partial f_0}{\partial w}$$

Assuming τ to be a constant, the integrations in θ and ϕ can be performed:

$$\int_0^{\pi} \sin\theta d\theta = 2$$

$$\int_0^{2\pi} d\phi = 2\pi$$

Since the other terms are independent of θ and ϕ, the integrations in θ and ϕ yields:

$$\sigma = 4\pi \frac{e^2}{m} \int_0^{\infty} -\tau w^3 \frac{\partial f_0}{\partial w} dw$$

Since

$$f_0 = n\left(\frac{m}{2\pi kT}\right)^{3/2} e^{\frac{-mw^2}{2kT}}$$

$$\frac{\partial f_0}{\partial w} = n\left(\frac{m}{2\pi kT}\right)^{3/2} e^{\frac{-mw^2}{2kT}} - \frac{mw}{kT}$$

Therefore

$$= + \frac{4\pi e^2}{m} \int_0^{\infty} \frac{nm}{kT}\left(\frac{m}{2\pi kT}\right)^{3/2} \tau w^4 e^{\frac{-mw^2}{2kT}} dw$$

Substituting

$$u = \left(\frac{m}{2kT}\right)^{1/2} w$$

$$w^4 = u^4\left(\frac{2kT}{m}\right)^2$$

$$dw = \left(\frac{2kT}{m}\right)^{1/2} du$$

Hence

$$\sigma = + 4\pi e^2 n \int_0^{\infty} \frac{\tau}{kT} \frac{m^{3/2} e^{-u^2}}{\pi^{3/2}(2kT)^{3/2}} \frac{(2kT)^2}{m^2} u^4 \cdot \left(\frac{2kT}{m}\right)^{1/2} du$$

$$= + 4\pi e^2 n \int_0^{\infty} \frac{2\tau}{m\pi^{3/2}} u^4 e^{-u^2} du$$

From Tables

$$\int_0^\infty u^r e^{-u^2} du = 1/2 \ (\underline{r-1}) \cdots \frac{5}{2} \cdot \frac{3}{2} \cdot \frac{1}{2} \cdot \sqrt{\pi}$$
$$\qquad\qquad\qquad\quad 2$$

Assuming τ to be a constant,

$$\sigma = +\ 4\pi e^2 n \times \frac{1}{2} \cdot \frac{3}{2} \cdot \frac{1}{2} \cdot \sqrt{\pi} \cdot \frac{2\tau}{m\,\pi^{3/2}}$$

$$= \frac{3ne^2\tau}{m}$$

Defining the average electron drift mobility by

$$\mu_e = 3\,\frac{e\tau}{m} \qquad \text{(A.4)}$$

the expression for the electrical conductivity becomes:

$$\sigma = ne\mu_e \qquad \text{(2.3.1)}$$

This is the expression arrived at in Sec. 2.3. Thus

$$\bar{J}_{cond} = \sigma\bar{E}$$
$$= ne\mu\bar{E}$$

(b) <u>The Concentration Diffusion Coefficient: D</u>

The current density due to concentration diffusion has been obtained earlier as

$$\bar{J}_{diffc} = \left(\int_0^\infty \int_0^\pi \int_0^{2\pi} -\frac{\tau w^4 f_0}{n} \sin\theta d\theta d\phi\right) e\nabla n$$

and so D, the concentration diffusion constant for the mobile electrons, is given by

$$D = \int_0^\infty \int_0^\pi \int_0^{2\pi} -\frac{\tau w^4 f_0}{n} \sin\theta d\theta d\phi dw$$

Since the Maxwellian distribution is spherically symmetric and τ, the perturbation time constant, is assumed constant, the integration in θ and ϕ can be separately performed. Since

$$\int_0^{2\pi} d\phi = 2\pi$$

and

$$\int_0^{\pi} \sin\theta d\theta = 2$$

Hence

$$D = \int_0^{\infty} \tau 4\pi w^4 \left(\frac{m}{2\pi kT}\right)^{3/2} e^{\frac{-mw^2}{2kT}} dw$$

Substituting

$$\frac{mw^2}{2kT} = u^2$$

$$u = \sqrt{\frac{m}{2kT}}\, w$$

$$du = \sqrt{\frac{m}{2kT}}\, dw$$

Thus

$$D = \int_0^{\infty} 4\pi\tau \left(\frac{2kT}{m}\right)^2 u^4 \left(\frac{m}{2kT}\right)^{3/2} \frac{1}{\pi^{3/2}} e^{-u^2} \left(\frac{2kT}{m}\right)^{1/2} du$$

$$= \frac{4}{\sqrt{\pi}} \left(\frac{2kT}{m}\right) \int_0^{\infty} u^4 e^{-u^2} du$$

Using the Tables as before, this integral reduces to:

$$D = \frac{2kT}{m} \frac{4}{\sqrt{\pi}} \quad \frac{1}{2} \cdot \frac{3}{2} \cdot \frac{1}{2} \cdot \sqrt{\pi}$$

$$= \frac{kT}{m} \cdot 3$$

Recalling that μ_e, the electron mobility, had been defined as:

$$\mu_e = \frac{3e\tau}{m}$$

the diffusion coefficient becomes:

$$D = \frac{kT}{e}$$

which is the well-known Einstein relation.

(c) <u>The Thermal Diffusion Coefficient:</u>

The carrier current density due to thermal diffusion is

$$\bar{J}_{diffd} = \left[\int_0^{\infty}\int_0^{\pi}\int_0^{2\pi} e\tau w^4 f_0 \left(\frac{mw^2}{2kT^2} - \frac{1}{T}\right) \sin\theta d\theta d\phi dw\right] \nabla T$$

and so,

$$\alpha = \int_0^\infty \int_0^\pi \int_0^{2\pi} e\tau w^4 f_0\left(\frac{mw^2}{2kT^2} - \frac{1}{T}\right)\sin\theta\, d\theta\, d\phi\, dw$$

Evaluating the integrals in θ and ϕ as before yields

$$\alpha = 4\pi \int_0^\infty e\tau w^4 f_0\left(\frac{mw^2}{2kT^2} - \frac{3}{2T}\right)dw$$

Recalling that

$$f_0 = n\left(\frac{m}{2\pi kT}\right)^{3/2} e^{\frac{-mw^2}{2kT}}$$

and making the substitution

$$w = \left(\frac{2kT}{m}\right)^{1/2} u$$

the integral becomes

$$\alpha = 4\pi \int_0^\infty e\tau u^4 \left(\frac{2kT}{m}\right)^2 \frac{n}{\pi^{3/2}} \left(\frac{m}{2kT}\right)^{3/2} e^{-u^2}\left(\frac{u^2}{T} - \frac{3}{2T}\right)\sqrt{\frac{2kT}{m}}\, du$$

$$= \frac{8kne}{\sqrt{\pi}\, m}\left(\int_0^\infty u^6 e^{-u^2} du - \frac{3}{2}\int_0^\infty u^4 e^{-u^2} du\right)$$

Using the Tables as before

$$= \frac{8kne}{m\sqrt{\pi}}\left(\frac{1}{2} \cdot \frac{5}{2} \cdot \frac{1}{2}\sqrt{\pi} - \frac{3}{2} \cdot \frac{3}{2} \cdot \frac{1}{2} \cdot \sqrt{\pi} \cdot \frac{1}{2}\right)$$

$$= \frac{8kne}{m\sqrt{\pi}} \cdot \frac{6}{16}\sqrt{\pi}$$

$$= kn \cdot \frac{3e\tau}{m}$$

$$= \underline{\underline{\mu kn}}$$

The net diffusion current density $\bar{J}_{diff}$ is therefore:

$$\bar{J}_{diff} = eD\nabla n + \alpha\nabla T$$

$$= e\frac{\mu kT}{e}\nabla n + \mu kn\nabla T$$

$$= \underline{\underline{\mu k\nabla(nT)}}$$

APPENDIX B

The Finite Difference Equations

Consider a continuously differentiable bounded function f(x, y, z). Using a Taylor's series expansion about a point(x_0, y_0, z_0) an adjacent point $f(x_0 + \Delta x, y_0, z_0)$ can be expressed as:

$$f(x_0 + \Delta x, y_0, z_0) = f(x_0, y_0, z_0) + \Delta x \left.\frac{\partial f}{\partial x}\right|_{\substack{x = x_0 \\ y = y_0 \\ z = z_0}}$$

$$+ \frac{\Delta x^2}{2!} \left.\frac{\partial^2 f}{\partial x^2}\right|_{\substack{x = x_0 \\ y = y_0 \\ z = z_0}} + \frac{\Delta x^3}{3!} \left.\frac{\partial^3 f}{\partial x^3}\right|_{\substack{x = x_0 \\ y = y_0 \\ z = z_0}} + \ldots \qquad (B.1)$$

Consider first the point (x_0, y_0, z_0) to be in the interior of of the material. In such a case, both points $f(x_0 + \Delta x, y_0, z_0)$ and $f(x_0 - \Delta x, y_0, z_0)$ exist. Expanding $f(x_0 - \Delta x, y_0, z_0)$ about (x_0, y_0, z_0) using the Taylor's series as before:

$$f(x_0 - \Delta x, y_0, z_0) = f(x_0, y_0, z_0) - \Delta x \frac{\partial f}{\partial x} + \frac{\Delta x^2}{2!} \frac{\partial^2 f}{\partial x^2}$$

$$- \frac{\Delta x^3}{3!} \frac{\partial^3 f}{\partial x^3} + \ldots \qquad (B.2)$$

all partials being assumed to evaluated at (x_0, y_0, z_0), the subscripts having been omitted for conciseness.

Subtracting (B.2) from (B.1) yields the following:

$$f(x_0 + \Delta x, y_0, z_0) - f(x_0 - \Delta x, y_0, z_0) = 2\Delta x \frac{\partial f}{\partial x} + 2 \frac{\Delta x^3}{3!} \frac{\partial^3 f}{\partial x^3} + \ldots$$

Rearranging terms:

$$\left.\frac{\partial f}{\partial x}\right|_{\substack{x = x_0\\ y = y_0\\ z = z_0}} = \frac{f(x_0 + \Delta x,\ y_0,\ z_0) - f(x_0 - \Delta x,\ y_0,\ z_0)}{2\Delta x}$$

$$- \frac{\Delta x^2}{3!} \frac{\partial^3 f}{\partial x^3} \tag{B.3}$$

As discussed in Sec. 4.1, a discretization error of $0(\Delta x^2)$ is tolerated.

So, the truncated expression for $\frac{\partial f}{\partial x}$ is obtained. For an interior point,

$$\left.\frac{\partial f}{\partial x}\right|_{\substack{x = x_0\\ y = y_0\\ z = z_0}} = \frac{f(x_0 + \Delta x,\ y_0,\ z_0) - f(x_0 - \Delta x,\ y_0,\ z_0)}{2\Delta x}$$

$\frac{\partial f}{\partial y}$ can be similarly obtained as:

$$\left.\frac{\partial f}{\partial y}\right|_{\substack{x = x_0\\ y = y_0\\ z = z_0}} = \frac{f(x_0,\ y_0 + \Delta y,\ z_0) - f(x_0,\ y_0 - \Delta y,\ z_0)}{2\Delta y}$$

To obtain the second derivation $\frac{\partial^2 f}{\partial x^2}$, add equations (B.1) and (B.2) to obtain:

$$f(x_0 + \Delta x,\ y_0,\ z_0) + f(x_0 - \Delta x,\ y_0,\ z_0) = 2f(x_0,\ y_0,\ z_0)$$
$$+\ x^2 \frac{\partial^2 f}{\partial x^2} + 2\,\frac{\Delta x^4}{4!} \frac{\partial^4 f}{\partial x^4} + \ldots$$

Rearranging terms and dividing throughout by x^2,

$$\left.\frac{{}^2 f}{x^2}\right|_{\substack{x = x_0\\ y = y_0\\ z = z_0}} = \frac{f(x_0 + \Delta x,\ y_0,\ z_0) + f(x_0 - \Delta x,\ y_0,\ z_0) - 2f(x_0,\ y_0,\ z_0)}{\Delta x^2}$$

$$+\ 2\,\frac{\Delta x^4}{4!} \frac{\partial^4 f}{\partial x^4} + \ldots \tag{B.5}$$

Discretization error terms of order Δx^2 or higher is neglected as before:

$$\left.\frac{\partial^2 f}{\partial x^2}\right|_{\substack{x = x_0 \\ y = y_0 \\ z = z_0}} = \frac{f(x_0 + \Delta x, y_0, z_0) + f(x_0 - \Delta x, y_0, z_0) - 2f(x_0, y_0, z_0)}{x^2} \quad (B.6)$$

Similarly, the second order derivative in y is:

$$\frac{\partial^2 f}{\partial y^2} = \frac{f(x_0, y_0 + \Delta y_0, z_0) + f(x_0, y_0 - \Delta y_0, z_0) - 2f(x_0, y_0, z_0)}{\Delta y^2} \quad (B.7)$$

Consider now a point on the edge $x = 0$. In this case, the point $(x_0 - \Delta x, y_0, z_0)$ does not lie within the domain of the semiconductor. But, $(x_0 + \Delta x, y_0, z_0)$ does, and $f(x_0 + 2\Delta x, y_0, z_0)$ can be expanded by Taylor's Series about (x_0, y_0, z_0) to yield:

$$f(x_0 + 2\Delta x, y_0, z_0) = f(x_0, y_0, z_0) + 4\Delta x \frac{\partial f}{\partial x} + \frac{(2\Delta x)^2}{2!}\frac{\partial^2 f}{\partial x^2} + \frac{(2\Delta x)^3}{3!}\frac{\partial^3 f}{\partial x^3} + \dots \quad (B.8)$$

Multiplying (B.1) by 4 yields:

$$4f(x_0 + \Delta x, y_0, z_0) = 4f(x_0, y_0, z_0) + 4\Delta x \frac{\partial f}{\partial x} + 4\frac{\Delta x^2}{2!}\frac{\partial^2 f}{\partial x^2} + 4\frac{\Delta x^3}{3!}\frac{\partial^3 f}{\partial x^3} + \dots \quad (B.9)$$

Subtracting (B.8) from (B.9) and rearranging terms:

$$\left.\frac{\partial f}{\partial x}\right|_{\substack{x = 0 \\ y = y_0 \\ z = z_0}} = \frac{-3f(x_0, y_0, z_0) + 4f(x_0 + \Delta x, y_0, z_0) - f(x_0 + 2\Delta x, y_0, z_0)}{2\Delta x} + 4\frac{x^3}{3!}\frac{\partial^3 f}{\partial x^3} + \dots \quad (B.10)$$

Neglecting terms containing Δx^2 or larger power of Δx, the equation becomes:

$$\left.\frac{\partial f}{\partial x}\right|_{\substack{x = 0 \\ y = y_0 \\ z = z_0}} \approx \frac{-3f(x_0, y_0, z_0) + 4f(x_0, y_0 + \Delta y, z_0) - f(x_0 + 2\Delta x, y_0, z_0)}{2\Delta x} \qquad \text{(B.11)}$$

Similarly, the partial derivatives and at y = 0 and z = 0 respectively are:

$$\left.\frac{\partial f}{\partial y}\right|_{\substack{x = x_0 \\ y = 0 \\ z = z_0}} = \frac{-3f(x_0, y_0, z_0) + 4f(x_0, y_0 + \Delta y, z_0) - f(x_0 y_0 + 2\Delta y, z_0)}{2\Delta y} \qquad \text{(B.12)}$$

$$\left.\frac{\partial f}{\partial z}\right|_{\substack{x = x_0 \\ y = y_0 \\ z = 0}} = \frac{-3f(x_0, y_0, z_0) + 4f(x_0, y_0, z_0 + \Delta z) - f(x_0, y_0, z_0 + 2\Delta z)}{2\Delta z} \qquad \text{(B.13)}$$

The second partial derivatives for this family of points is obtained by multiplying (B.1) by 2 and subracting it from (B.12). Performing the above mentioned operation and rearranging terms:

$$\left.\frac{\partial^2 f}{\partial x^2}\right|_{\substack{x = 0 \\ y = y_0 \\ z = z_0}} = \frac{f(x_0 + 2\Delta x, y_0, z_0) - 2f(x_0 + \Delta x, y_0, z_0) + f(x_0, y_0, z_0)}{x^2}$$

$$+ \frac{x^2}{2!} \frac{{}^3 f}{x^3} + \ldots$$

Neglecting second order terms, the second partial derivations are:

$$\frac{{}^2 f}{x^2} = \frac{f(x_0 + 2\Delta x, y_0, z_0) - 2f(x_0 + \Delta x, y_0, z_0) + f(x_0, y_0, z_0)}{\Delta x^2}$$

$$\frac{{}^2 f}{y^2} = \frac{f(x_0, y_0 + 2\Delta y, z_0) - 2f(x_0, y_0 + \Delta y, z_0) + f(x_0, y_0, z_0)}{\Delta y^2}$$

$$\frac{{}^2 f}{z^2} = \frac{f(x_0, y_0, z_0 + 2\Delta z) - 2f(x_0, y_0, z_0 + \Delta z) + f(x_0, y_0, z_0)}{\Delta z^2}$$

The third type of point is one lying on the edge $x = L_x$, wherein the point $(x_0 + \Delta x, y_0, z_0)$ is not defined within the semiconductor, but $(x_0 - 2\Delta x, y_0, z_0)$ is. Similar Taylor's series truncations can be made by utilizing the expansion of $f(x_0 - 2\Delta x, y_0, z_0)$, the method proceeding along similar lines to the previous case. Neglecting second order terms the first and second partial derivatives are written below:

$$\left.\frac{\partial f}{\partial x}\right|_{\substack{x = L_x \\ y = y_0 \\ z = z_0}} = \frac{3f(x_0, y_0, z_0) - 4f(x_0 - \Delta x, y_0, z_0) + f(x_0 - 2\Delta x, y_0, z_0)}{2\Delta x}$$

$$\left.\frac{\partial f}{y}\right|_{\substack{x = x_0 \\ y = L_y \\ z = z_0}} = \frac{3f(x_0, y_0, z_0) - 4f(x_0, y_0 - \Delta y, z_0) + f(x_0, y_0 - 2\Delta y, z_0)}{2\Delta y}$$

$$\left.\frac{\partial f}{\partial z}\right|_{x = x_0} = \frac{3f(x_0, y_0, z_0) - 4f(x_0, y_0, z_0 - \ z) + f(x_0, y_0, z_0 - 2\Delta z)}{2\Delta z}$$

APPENDIX C

NORMALIZATION

In Chapter 1, it was pointed out that round-off error could be minimized by normalizing variables and reducing the equations to dimensionless form. The details of such transformations are worked out in this section.

The normalizing variables are:

$$\Delta x = \frac{L_x}{10}\hat{x};\ \Delta y = \frac{L_y}{10}\hat{y};\ \Delta z = \frac{L_z}{10}\hat{z};\ V = V_{app}\phi;$$

$$\rho = \frac{V_{app}\cdot 100\cdot \epsilon\,\chi}{L_x^{\,2}};\ T = (T_{cr} - T_{amb})\theta + T_{amb};\ n = p_{nb}\Psi;$$

$$n_d^+ = p_{nb};\ T = T_{cr} - T_{amb}$$

where

$$p_{nb} = p_{n0} - p_0$$

$$p_0 = \sigma_0/e\mu_a$$

$$p_{na} = n_d^+ e\mu_a$$

$$\eta = \mu/\mu_a$$

$$\nu = \ln\mu$$

Using the truncations discussed in Sec. 4.1, the relevant equations are transformed as follows:

1) Poisson's Equation:

$$\nabla^2 V = -\rho/\epsilon$$

$$\frac{\partial^2 V}{\partial x^2} + \frac{\partial^2 V}{\partial y^2} + \frac{\partial^2 V}{\partial z^2} + \rho/\epsilon = 0$$

Now

$$\frac{\partial^2 V}{\partial x^2} = \frac{V(x+\Delta x, y, z) + V(x-\Delta x, y, z) - 2V(x, y, z)}{\Delta x^2}$$

$$= \frac{V_{app} \cdot 100}{L_x^2} \cdot \left[\phi(x+\Delta x, y, z) + \phi(x-\Delta x, y, z) - 2\phi(x, y, z)\right]$$

The other derivatives can be similarly obtained. Substituting back into the Poisson Equation and using the relationships Dav_x, Dav_y, Dav_z, and γ_d defined in the text, the final relation is obtained below:

$$Dav_x\phi + Dav_y\phi + Dav_z\phi - \gamma_d\phi + \chi = 0$$

2) The Continuity Equation:

$$\frac{\partial\rho}{\partial t} + \nabla \cdot \bar{J} = 0$$

$$\frac{\partial\rho}{\partial t} + \nabla \cdot (-ne\mu\nabla V + \mu k\nabla(nT)) = 0$$

Using the charge neutrality relationship to express the equation in terms of ρ, yields

$$\frac{\partial\rho}{\partial t} + \nabla \cdot (-en_d^+\nabla V + \rho\mu\nabla V + \mu k\nabla\rho(n_d^+ - \rho/e)T) = 0$$

The above equation is now re-expressed in terms of χ by using the transformations used earlier in the text.

$$\frac{\partial\chi}{\partial t} + \frac{\mu_a e p_{nb} V_{app}}{100 V_{app}\epsilon} L_x^2 \cdot (-\eta\xi\nabla\phi) + \frac{100\mu_a\epsilon V_{app}}{100V_{app}}^2 \nabla \cdot (\eta\chi\nabla\phi)$$

$$+ \frac{kT_d}{100} \frac{\mu_a e p_{nb}}{V_{app}} L_x^2 \nabla\cdot\eta\nabla(\xi\theta) + \mu_a \frac{kT_d 100\epsilon V_{app} L_x}{100\epsilon V_{app} L_x^2 e} \nabla\cdot\eta\nabla(\chi\theta) = 0$$

Defining the following constants for conciseness

$$V_0 = \frac{kT_d}{e}$$

$$F_b' = \frac{V_0\mu_a e p_{nb} L_x^2}{100\epsilon V_{app}}$$

$$F_a' = \frac{e p_{nb} L_x^2}{100\epsilon}$$

$$F_c' = \mu_a V_{app}$$

$$F_d' = \mu_a V_0$$

we obtain

$$\frac{\partial \chi}{\partial t} - F_a' \nabla \cdot (\eta \xi \nabla \phi) + F_c' \nabla \cdot (\eta \xi \nabla \phi) + F_b' \nabla \cdot (\eta \nabla(\xi \theta)) + F_d' \nabla \cdot \eta \nabla(\kappa \theta)$$

$$= 0$$

3) <u>The Temperature Equation:</u>

$$\frac{c \partial T}{\partial t} + k_{th} \nabla^2 T = \sigma \bar{E} \cdot \bar{E}$$

$$\frac{\partial T}{\partial t} - \frac{k_{th}}{c} \nabla^2 T = ne\mu \nabla V \cdot \nabla V$$

Applying the same transformations used earlier in this section and considering the equation term by term, we obtain

$$\frac{\partial T}{\partial t} = T_d \frac{\partial \theta}{\partial t}$$

$$\frac{k_{th}}{c} \nabla^2 T = \frac{k_{th} T_d}{c} \nabla^2 \theta$$

Using the truncation sceme developed in Appendix B, the righthand side of the above equation reduces to

$$\nabla^2 \theta = (Dav_x \theta + Dav_y \theta + Dav_z \theta - \gamma_D \theta) \cdot 100/L_x^2$$

and defining F_d and λ_T as

$$F_d = \frac{P_{nb} e \mu_a V_{app} 100}{L_x^2}$$

$$\lambda_T = \frac{k_{th} T_d 100}{c L_x^2}$$

the Temperature equation becomes

$$\frac{\partial \theta}{\partial t} = (Dav_x \theta + Dav_y \theta + Dav_z \theta - \ _d \theta) / \ _T + PF_d$$

APPENDIX D

ALGORITHM FOR SOLVING A SET OF TRIDIAGONAL EQUATIONS

In Chapter 4, the partial differential equation for temperature was reduced to a set of tridiagonal equations by using finite difference techniques. To solve such a system, consider a linear set of n tridiagonal equations whose subdiagonal, diagonal, and superdiagonal coefficients are a_i, b_i, and c_i respectively, the righthand side is d_i, and u_i is the ith variable. The ith equation, therefore, reads

$$a_i u_{i-1} + b_i u_i + c_i u_{i+1} = d_i \tag{D.1}$$

A recursion solution of the form

$$u_i = \alpha_i - \frac{c_i u_{i+1}}{\beta_i} \tag{D.2}$$

is found to be valid. The coefficients α_i and β_i obey backward recursive relations of the form

$$\alpha_i = \frac{d_i - a_i \alpha_{i-1}}{\beta_i} \tag{D.3}$$

$$\beta_i = b_i - \frac{a_i c_{i-1}}{i - 1} \tag{D.4}$$

Since rewriting the first equation of the tridiagonal set yields

$$u_1 = \frac{d_1}{b_1} - \frac{c_1}{b_1} u_2$$

by comparing coefficients, α_1 and β_1 can be evaluated.

$$\beta_1 = b_1$$

$$\alpha_1 = d_1/\beta_1$$

From the recursion relations (D.3) and (D.4), all coefficients α_i and β_i can be evaluated, and, employing the applicable boundary conditions to obtain u_1 and u_n, all u_i's can be obtained.

APPENDIX E

TREATMENT OF THE EDGE POINTS BY THE SOR METHOD

In Sec. 4.3, a finite difference scheme was outlined for solving the electrical potential distribution in the interior of the semiconductor.

The behavior of the edge points is governed by the boundary conditions as outlined here. Consider first the edges in contact with the metal electrodes. These edges, as discussed in the boundary conditions in Chapter 3, are constrained to have

$$V(L_x, y, z) = 0$$

Normalizing,

$$\phi(L_x, y, z) = 0$$

This takes care of all points on the surface $x = L_x$. For points on the surface $x = 0$, the boundary conditions are obtained from a consideration of the circuit equation

$$V(0, y, z, t) = V_{app} - \int_{z=0}^{L_y}\int_{y=0}^{L_y}\left(-\sigma_0 \frac{\partial V}{\partial x} + \mu_a \frac{k\partial(nT)}{\partial x}\right)dydz$$

Normalizing the above equation and using the truncated grid structure discussed in Chapter 4

$$\phi(0, y, z, t) = 1 + \frac{\sigma_0 V_{app}}{L_x 100} 10L_y{}^2 \sum_{j=1}^{"}\sum_{k=1}^{"}\left(V_0\delta_x(\theta\psi) - \delta_x(\phi)\right)_{j,\,k}$$

where

$$\delta_x f = \Delta x \left.\frac{\partial f}{\partial x}\right|_{x = 0}$$

In the computer, the double summation is performed using the Simpson's integration rule.

Consider next the surface $y = 0$. Here,

$$\frac{\partial V}{\partial y} = 0$$

and so

$$\phi(x,\ 0,\ z) = \phi(x, \Delta y,\ z)$$

where the righthand side is an interior point which is evaluated by the SOR method. The other three surfaces in contact with air can be similarly evaluated.

APPENDIX F

LISTING

This section contains a complete listing of the computer program used in the simulation runs and consists of a main program and thirteen other subroutines. The MAIN program controls the overall logic flow and the Outer Loop referred to in Chapter 4.

The MAIN program calls TEMPEQN which sets up the tridiagonal equations corresponding to the Temperature Equation that is solved by TRIDAG. It also calls CONTROL, which controls the Inner Loop. CONTROL, in turn, calls the subroutines CIRCUIT, PSSN, and LMATRIX which solves the Circuit, Poisson, and Continuity of Charge Equations respectively.

The remaining subroutines perform auxiliary functions. BYPASS sets up the initial conditions, PRINT is concerned with all output prints, and RHP computes the power dissipation density required for the solution of the Temperature Equation. The function subprogram SIMPS performs the integrations required in the Circuit Equation using Simpson's Rule, and DELX evaluates the truncated difference operators. Finally, BUFFIN and BUFFOUT control the flow to and from auxiliary memory locations on tape enabling data at any intermediate times to be stored. The actual listing is given in the following pages.

```
      PROGRAM MAIN(INPUT,OUTPUT,TAPE60=INPUT,TAPE61=OUTPUT,TAPE1,TAPE2,   MAIN         2
     1TAPE3)                                                              MAIN         3
      REAL LX,LY                                                          MAIN         4
      COMMON/A/II,JJ,NI,NJ                                                MAIN         5
      COMMON ZA(11,11,11),ZB(11,11,11),ZC(11,11,11)                       MAIN         6
      COMMON/LOOP/KOUNT,TIME                                              MAIN         7
      COMMON/TWO/PZI(11,11,11),PP(11,11,11)                               MAIN         8
      COMMON/RST/RST(11,11,11)                                            MAIN         9
      COMMON/DEGR/THETA(11,11,11)                                         MAIN        10
      COMMON/VOLTS/PHI(11,11,11)                                          MAIN        11
      COMMON/COLS/DIAG(11),SUB(11),SPR(11)                                MAIN        12
      COMMON/MAT/FG,FH                                                    MAIN        13
      COMMON/PP/PA,INDX,LZ,PB                                             MAIN        14
      COMMON/XTRA/FE,RI,TAUB                                              MAIN        15
      COMMON/SIO/A                                                        MAIN        16
      COMMON/B/CA,GA,EGA,EGB                                              MAIN        17
      COMMON/V/VR,VTH,VO                                                  MAIN        18
      COMMON/GAMS/GAMD                                                    MAIN        19
      COMMON/DON/GAMC,ALAMDA                                              MAIN        20
      COMMON/LIMITS/CMAX,CMIN,DELV,NX                                     MAIN        21
      COMMON/VD/VA                                                        MAIN        22
      COMMON/N/NDATA                                                      MAIN        23
      COMMON/MU/GMU,TODEVSQ,NXX                                           MAIN        24
      COMMON/HEADER/HEAD1,HEAD2,HEAD3                                     MAIN        25
      COMMON/OUT/CG,CDENS,PF,CH                                           SINO         1
      COMMON/DIR/X(3),IA(2),JA(2),KA(2)                                   MAIN        26
      COMMON/VAR/VART,VARC,VARV,VARE,VARP,VARD,VARI,VARF,INTA,INTB,INTC,  MAIN        27
     1INTD                                                                MAIN        28
      COMMON/ITEPS/EPSMAX1,ITMAX1                                         MAIN        29
      COMMON/CON/GAMMA,AMDA,GAM2,GAMMB,GAMM2                              MAIN        30
      COMMON/FACTORS/FA,FB,FC,FD                                          MAIN        31
      COMMON/A4/ITMAX,EPSMAX,W                                            MAIN        32
      COMMON/T/THO,TA,TD                                                  MAIN        33
      COMMON/CONDTY/RATIO                                                 MAIN        34
      COMMON/PULSE/TIMEI,TIMEF                                            JULY4        1
      EQUIVALENCE (DELV,PK)                                               MAIN        36
C**   SET INIYIAL CONDITIONS ***                                          MAIN        37
2     FORMAT(1H0,11(E11.4,1X))                                            MAIN        38
C **  IBUFF=0* NO BUFFER OUT **                                           MAIN        39
C** INDEX DETERMINES INITIALIZING INPUT **                                MAIN        40
C** L IS TAPE NO. ON WHICH INITIAL INPUT IS RECORDED **                   MAIN        41
      READ(60,717) INDEX,IBUFF,L                                          MAIN        42
C   **  COMPUTER TIME CONSTANTS **                                        MAIN        43
      READ(60,747) W,DELT,TIMAX,EPSMAX,CX                                 MAIN        44
747   FORMAT(5E16.7)                                                      MAIN        45
C **  GRID SETS AND UNIVERSAL CONSTANTS **                                MAIN        46
      READ(60,747) LX,LY,DEPS,BLTK,ECH                                    MAIN        47
C   **  VARIABLE PARAMETER SET **                                         MAIN        48
      READ(60,747) EMUA,EMUB,EGH,EGL,Q1                                   MAIN        49
C **  CONSTANT PARA SET **                                                MAIN        50
      READ(60,747) THK,SPHT,TAMB,TCR,SIGO                                 MAIN        51
C **  INTEGER CONSTANTS **                                                MAIN        52
      READ(60,717) II,JJ,NI,NJ,ITMAX,KMAX,NX,ND                           JULY4        2
      READ(60,787) DELV,NXX                                               MAIN        54
      READ(60,747)TIMEI,TIMEF                                             JULY4        3
      READ(60,717)(IA(K),JA(K),KA(K),K=1,ND)                              MAIN        56
      READ(60,777) EPSMAX1,ITMAX1,W1                                      JULY4        4
777   FORMAT(E12.4,I10)                                                   MAIN        58
      PRINT 777,EPSMAX1,ITMAX1                                            MAIN        59
      X(1)=1HX        $X(2)=1HY           $X(3)=1HZ                       MAIN        60
      HEAD1=10HDISTRIBUTI                                                 MAIN        61
      HEAD2=10HON ALONG                                                   MAIN        62
      HEAD3=10HDIRECTION                                                  MAIN        63
787   FORMAT(F10.3,I10)                                                   MAIN        64
```

```
717   FORMAT(8I10)                                                        MAIN    65
      RATIO=EMUB/EMUA                                                     MAIN    66
      PRINT 987                                                           MAIN    67
      PRINT 988,NX,NXX,KINIT,KFIN,ITMAX,KMAX                              MAIN    68
988   FORMAT( 1H0,6(5X,I6))                                               MAIN    69
987   FORMAT(1H ,*THE FOLLOWING VARBLES ARE NX,NXX,KINIT,KFIN,ITMAX,KMAX  MAIN    70
     +*)                                                                  MAIN    71
C  ****  CONSTANTS OF TEMPERATURE  ****                                   MAIN    77
      TD=TCR-TAMB                                                         MAIN    78
      TA=TCR/TD                                                           MAIN    79
      THO=TAMB/TD                                                         MAIN    80
      VO=BLTK*TD/ECH                                                      MAIN    81
C   ***  TIME CONSTANTS   ***                                             MAIN    82
      ALPHA=((II-1)/LX)**2                                                MAIN    83
      BETA =((JJ-1)/LY)**2                                                MAIN    84
      TAUA=(SPHT/THK)/ALPHA                                               MAIN    85
      TAUB=1.0/(ALPHA*EMUA*VO)                                            MAIN    86
      TAUC=DEPS/SIGO                                                      MAIN    87
C  ****  CONSTANTS OF TEMP EQN  *****                                     MAIN    88
      GAMMA=(LX/LY)**2.                                                   MAIN    89
      GAM2=2.0*GAMMA                                                      MAIN    90
      GAMMB=1.0/GAMMA                                                     MAIN    91
      GAMM2=0.5*GAMMB                                                     MAIN    92
      GAMD=2.0+4.0*GAMMA                                                  MAIN    93
      EGA=-EGH/(VO*ECH*2.0)                                               MAIN    94
      EGB=-EGL/(VO*ECH*2.0)                                               MAIN    95
      RI=LX/(SIGO*LY**2)                                                  MAIN    96
      RS=0.2*RI                                                           MAIN    97
      CX=CX*LY**2                                                         MAIN    98
      VAPP=CX*(RS+RI)                                                     MAIN    99
      VTH=VAPP/VO                                                         MAIN   100
      VR=RS*SIGO*(II-1)/(BETA*LX)                                         MAIN   101
      FC=LX/LY                                                            MAIN   102
      FE=FC/2.0                                                           MAIN   103
      FG=-GAMMA/2.0                                                       MAIN   104
      FH=FE/2.                                                            MAIN   105
      PO=SIGO/(EMUA*ECH)                                                  MAIN   106
      PNA=PO*EXP(-EGA/THO)*EXP(EGB/TA)                                    MAIN   107
      PNB=PNA-PO                                                          MAIN   108
      A=PO/PNB                                                            MAIN   109
      SIGB=PNB*ECH*EMUA                                                   MAIN   110
      SIGI=PNA*ECH*EMUB                                                   JULY4    5
      DELV=PNA/PO                                                         JULY4    6
      PRINT 565,SIGI,DELV                                                 JULY4    7
565   FORMAT(1H0,*SIGI= *,E16.8,* DELV= *,E16.8)                          JULY4    8
      GA=A*EXP(-EGA/THO)                                                  MAIN   111
      A=GA*EXP(EGA/THO)                                                   MAIN   112
      FD=SIGB*VAPP**2/(TD*THK)                                            MAIN   113
      CC=-VAPP/RS                                                         MAIN   114
      PF=THK*TD*ALPHA                                                     MAIN   115
       Q2=ALPHA*DEPS*VAPP                                                 MAIN   116
      FA=TAUB/(A*TAUC)                                                    MAIN   117
      FB=FA/VTH                                                           MAIN   118
      FC=GAMD*THO                                                         MAIN   119
      CA=W1/(FA*A-FC)                                                     JULY4    9
      AMDA=DELT/TAUA                                                      MAIN   121
      FC=TAUB/DELT                                                        MAIN   122
      VA=VAPP/2.                                                          MAIN   123
      GAMC=1.0+GAMMB/AMDA                                                 MAIN   124
      ALAMDA=1.+1./AMDA                                                   MAIN   125
      RMU=EGB/EGA                                                         MAIN   126
      PI=3.14159265358979                                                 MAIN   127
      DEV=.01                                                             MAIN   128
      TODEVSQ=2.0*DEV*DEV                                                 MAIN   129
      GMU=(RMU-1.0)/(SQRT(2.0*PI   )*DEV)                                 MAIN   130
      GMU=GMU*EGA                                                         MAIN   131
```

```
C**  **  LIMITING VALUES OF THE CIRCUIT CURRENTS AND VOLTAGES ***          MAIN      132
      CMIN=RI/(RI+RS)                                                    MAIN      133
      B=PO/PNA                                                           MAIN      134
      CMAX=0.2/(B/RATIO+0.2)                                             MAIN      135
      PRINT 556,EGL,EGH,EMUA,EMUB,SPHI,CX,PK                             MAIN      136
C  **  **  PRINT INPUT DATA **  **                                       JULY4      10
556   FORMAT(1H1,20X,* INPUT DATA IN RAT MKS UNITS*,//,                  JULY4      11
     2*EGL = *,G10.3,10X,*EGH = *,G10.3,//,                              MAIN      139
     3* EMUA= *,G10.3,9X,*EMUB = *,G10.3,//,                             MAIN      140
     4*SPHI = *,G10.3,*   CURRENT DENSITY =*,G10.3,*PK= *, G10.3)        MAIN      141
      PRINT 557,LX,LY,DEPS,BLTK,ECH,THK,TAMB,TCK,      TIMAX             JULY4      12
557   FORMAT(1H0,                                                        JULY4      13
     1*LX = *,G10.3,10X,*LY = *,G10.3,//,                                JULY4      14
     2*EPSR = *,G10.3,10X,*BLTK = *,G10.3,10X,*E = *,G10.3,10X,*KTH = *, JULY4      15
     3G10.3,10X,//,                                                      JULY4      16
     4*TAMB = *,G10.3,10X,*TCK = *,G10.3,10X,*TIMAX = *,G10.3)           JULY4      17
      PRINT 559                                                          JULY4      18
559   FORMAT(1H0,* THE FOLLOWING INTEGER VARIABLES ARE *,/,              JULY4      19
     2* STARTK,IBUFF,TAPENO,II,JJ,PSSHITMAX,KMAX,NX(MAX ITER OF INNER LP JULY4      20
     6),*,/,* NXX(CONVGT ITER CRIT),RHOITMAX1*)                          JULY4      21
      PRINT 717,     INDEX,IBUFF,L,II,JJ,      ITMAX,KMAX,NX,NXX,ITMAX1  JULY4      22
      TIME=0.0                                                           MAIN      142
      KOUNT=0                                                            MAIN      143
      PRINT 3,VAPP,TD,SIGB,Q2,PNB                                        MAIN      144
3     FORMAT(1H1,////,24X,* CONVERSION FACTORS*,                         MAIN      145
     1//,* VOLTAGE        --*,1PE13.5,* VOLTS*,                          MAIN      146
     2//,* TEMPERATURE    *,1PE13.5,* DEGK*,                             MAIN      147
     2//,* CONDUCTIVITY  --*,1PE13.5,* MHOS/METER*,                      MAIN      148
     2//,* CHARGE DENSITY      --*,1PE13.5,* COUL PER METER CUBE*,       MAIN      149
     3 //,* CARRIER DENSITY--*,1PE13.5,* PER METER CUBE*)                MAIN      150
      PRINT 1,CC                                                         JULY4      23
1     FORMAT(1H0,*CURRENT          --*,1PE13.5,* AMPS*)                  MAIN      152
      CDENS=  SIGO*(II-1)*VAPP/LX                                        MAIN      153
      CG=A*CDENS                                                         SIND        2
      CH=THK*TD*HI/LX                                                    SIND        3
      PRINT 2,CG,CH                                                      SIND        4
      PRINT 475,CDENS                                                    MAIN      154
475    FORMAT(1H0,* CURRENT DENSITY  --*,1PE13.5,* AMPS PER MTR SQUARE*) MAIN      155
      PRINT 474,PF                                                       MAIN      156
474   FORMAT(1H0,* POWER DENSITY  --*,1PE13.5,* WATTS PER METER CUBE*)   MAIN      157
      PRINT 707,SIGO,PO,EMUA,TAMB                                        MAIN      158
707   FORMAT(1H0,* SCALE ADDERS *,///,* SIGO = *,E12.4,10X,* PO = *,E12, MAIN      159
     1.4,10X,                                                            MAIN      160
     *,///,* MUA= *,E12.4,8X,*TAMB= *,E12.4)                             MAIN      161
      PRINT 272                                                          MAIN      162
272   FORMAT(1H1,35X,* OTHER VARIABLES*)                                 MAIN      163
C**  LIST VARIABLES**                                                    MAIN      164
      PRINT 275,THO,TA,TD,VR,VTH,VO,EGA,EGB,PNA,A,RI,RS,                 MAIN      165
     1GA,CA,FD,AMDA,GAMC,                                                MAIN      166
     1ALAMDA,GAMMA,GAM2,GAMMB,GAMM2,GAMD,FG,FH,FA,FB,FC,TAUA,TAUB,TAU^   MAIN      167
275   FORMAT(1H0,*   THO=*,E12.4,5X,*     TA=*,E12.4,5X,/,1H0,           MAIN      168
     1*     TD=*,E12.4,5X,*VR=*,E12.4,5X,/,1H0,                          MAIN      169
     2*    VTH=*,E12.4,5X,*     VO=*,E12.4,5X,/,  1H0,                   MAIN      170
     3*    EGA=*,E12.4,5X,*    EGB=*,E12.4,5X,/,1H0,                     MAIN      171
     4*    PNA=*,E12.4,5X,*      A=*,E12.4,5X,/,1H0,                     MAIN      172
     **     RI=*,E12.4,5X,*     RS=*,E12.4,5X,/,1H0,                     MAIN      173
     5*     GA=*,E12.4,5X,*     CA=*,E12.4,5X,/,1H0,                     MAIN      174
     6*     FD=*,E12.4,5X,*  AMDA=*,E12.4,5X,/,1H0,                      MAIN      175
     7*   GAMC=*,E12.4,5X,*ALAMDA=*,E12.4,5X,/,1H0,                      MAIN      176
     8*     AMMA=*,E12.4,5X,*  GAM2=*,E12.4,5X,/,1H0,                    MAIN      177
     9* GAMMB=*,E12.4,5X,*GAMM2  =*,E12.4,5X,/,1H0,                      MAIN      178
     1*  GAMD=*,E12.4,5X,*     FG=*,E12.4,5X, /,1H0,                     MAIN      179
     2*     FH=*,E12.4,5X,/,1H0,                                         MAIN      180
     3*     FA=*,E12.4,5X,*     FB=*,E12.4,5X,/,1H0,                     MAIN      181
     4*     FC=*,E12.4,5X,*  TAUA=*,E12.4,5X,/,1H0,                      MAIN      182
     5*  TAUB=*,E12.4,5X,*  TAUC-*,E12.4,5X)                             MAIN      183
```

```
      PRINT 4,KOUNT,TIME                                                MAIN      184
      NDATA=1                                                           MAIN      185
C**   READ IN FROM BUFFER ON OPTION **                                  MAIN      186
      CALL BYPASS                                                       SIND        5
      IF (INDEX) 95,99,97                                               SIND        6
95    CALL SPECIN(INDEX,L)                                              MAIN      188
      GO TO 99                                                          MAIN      189
97    CALL BUFFIN(INDEX,L)                                              MAIN      192
99    CONTINUE                                                          MAIN      193
10    TIME=TIME+DELT                                                    MAIN      194
      KOUNT=KOUNT+1                                                     MAIN      195
      IF(TIME.GE.TIMEI)  NDATA=ND                                       DUMMY       1
      PRINT 4,KOUNT,TIME                                                MAIN      197
4     FORMAT(1H1,///,* KOUNT = *,I3,*  TIME = *,1PE12.5,* SECS*)        MAIN      198
      IF(KOUNT.GT.KMAX) GO TO 12                                        MAIN      199
      CALL CONTROL                                                      JULY4      25
      CALL PRINT(PHI,VARV)                                              JULY4      26
C ** A) RIGHT HAND SIDE -- POWER                                        MAIN      202
C  *** B) LEFT HAND SIDE --- TEMPEQN                                    MAIN      203
      CALL RHO                                                          MAIN      204
      CALL PRINT(ZA,VARE)                                               JULY4      27
      CALL PRINT(ZC,VARP)                                               JULY4      28
      IF(IBUFF)7,9,6                                                    MAIN      205
7     CALL SPECOUT(IBUFF,INDEX)                                         MAIN      206
      GO TO 9                                                           MAIN      207
6     CALL BUFFOUT(IBUFF)                                               MAIN      208
9     CONTINUE                                                          MAIN      209
      CALL TEMPEQN                                                      MAIN      210
      IF(IBUFF)16,19,17                                                 MAIN      211
17    CALL SPECOUT(IBUFF,INDEX)                                         MAIN      212
      GO TO 19                                                          MAIN      213
16    CALL BUFFOUT(IBUFF)                                               JULY4      29
19    CONTINUE                                                          MAIN      215
C***  SET UP MATRICES ***                                              MAIN      216
C**   STORE AND PRINT OUTPUTS ***                                       MAIN      217
      IF(TIME.LT.TIMAX) GO TO 10                                        MAIN      218
12    CONTINUE                                                          MAIN      219
      END                                                               MAIN      220
```

```
      SUBROUTINE TEMPEQN
      DIMENSION USTST(11,11,11)
      COMMON UST(11,11,11),X(11,11,11),Q(11,11,11)
      COMMON/DEGR/     G(11,11,11)
      COMMON/TWO/P/T(11,11,11),P(11,11,11)
      COMMON/VAR/VART,VARC,VARV,VARE,VARP,VARD,VARI,VARF,INTA,INTB,INTC,
     1INTD
      COMMON/WORK/A(11),D(11),C(11),B(11)
      COMMON/COLS/DIAG(11),SUB(11),SPR(11)
      COMMON/DON/GAMC,ALAMDA
      COMMON/TIMES/TAUD,Q1,TAUF,Q2
      COMMON/V/VR,VTH,VU
      COMMON/A/II,JJ,NI,NJ
      COMMON/CON/GAMMA,AMDA,GAM2,GAMMB,GAMMZ
      COMMON/L/LA,LB
      COMMON/T/THO,TA,TD
      EQUIVALENCE(UST,USTST)
      EQUIVALENCE(JJ,KK)
      DO 10 I=1,II
      SUB(I)=-0.5
      SPR(I)=-0.5
10    CONTINUE
      SPR(1)=-1.0
      SUB(II)=-1.0
C  ****  SOLVE IN I-DIRECTION   ****
      DO 50 I=1,II
      DO  50  J=1,JJ
      DO  50  K=1,JJ
      U(I,J,K)=U(I,J,K)-THO
      P(I,J,K)=U(I,J,K)+U(I,J,K)/AMDA
50    CONTINUE
      LA=2    $   LB=NJ
      DO 54  I=1,II
      DIAG(I)=ALAMDA
54    CONTINUE
      DO 5 K=1,JJ
      DO 5 J=1,JJ
      DO 6 I=2,NI
      A(I)=(U(I+1,J,K)+U(I-1,J,K)-2.0*U(I,J,K))*0.5
      IF((J.NE.1).AND.(J.NE.JJ))
     1B(I)=(U(I,J+1,K)+U(I,J-1,K)-2.0*U(I,J,K))*GAMMA
      IF(J.EQ.1)
     +B(I)=(U(I,J+1,K)-U(I,J,K))*GAM2
      IF(J.EQ.JJ)     B(I)=(U(I,J-1,K)-U(I,J,K))*GAM2
      IF((K.NE.1).AND.(K.NE.KK))C(I)=(U(I,J,K+1)+U(I,J,K-1)-2.*U(I,J,K))
     +*GAMMA
      IF(K.EQ.1) C(I)=(U(I,J,K+1)-U(I,J,K))*GAM2
      IF(K.EQ.KK) C(I)=(U(I,J,K-1)-U(I,J,K))*GAM2
C     D(I)=RHS TERMS
C     D(I)=P(I,J,K)+U(I,J,K)/LAMDA
      P(I,J,K)=P(I,J,K)+A(I)+B(I)+C(I)
6     D(I)=P(I,J,K)
C     RHAND IS COMPLETE
C     NO CORRECTION REQUIRED AT BOUNDARIES SINCE BOUNDARY VALUES AREZERO
C     SOLVE BY TRIDAG MATRIX METHOD
      CALL TRIDAG
C     SOLUTION RETURNED IN D(I)
      UST(1,J,K)=0.0
      UST(II,J,K)=0.0
      DO 5  L=2,NI
      UST(L,J,K)=D(L)
 5    CONTINUE
C     PART 2 --- CONSTRUCTING USTST MATRIX
      LA=1     $   LB=NJ+1
```

```
      DO  56  J=1,JJ                                                    TEMPEQN
   56 DIAG(J)=GAMC                                                      TEMPEQN
      DO  15    I=2,NI                                                  TEMPEQN
      DO 15  K=1,JJ                                                     TEMPEQN
      DO 16 J=1,JJ                                                      TEMPEQN
      IF((J.NE.1).AND.(J.NE.JJ))                                        TEMPEQN
     1B(J)=(U(I,J+1,K)+U(I,J-1,K)-2.0*U(I,J,K))*0.5                     TEMPEQN
      IF(J.EQ.1)                                                        TEMPEQN
     2B(J)=U(I,J+1,K)-U(I,J,K)                                          TEMPEQN
      IF(J.EQ.JJ)                                                       TEMPEQN
     3B(J)=U(I,J-1,K)-U(I,J,K)                                          TEMPEQN
      A(J)=(UST(I+1,J,K)+UST(I-1,J,K)-2.0*UST(I,J,K))*GAMM2             TEMPEQN
      P(I,J,K)=GAMMB*P(I,J,K)-B(J)+A(J)                                 TEMPEQN
 16   D(J)=P(I,J,K)                                                     TEMPEQN
C     RHS  IS  COMPLETE                                                 TEMPEQN
C     CORRECT  FOR  BOUNDARIES                                          TEMPEQN
      CALL TRIDAG                                                       TEMPEQN
C     SOLUTION  RETURNED  IN  D(J)                                      TEMPEQN
      DO 15 L=1,JJ                                                      TEMPEQN
 15    USTST(I,L,K)=D(L)                                                TEMPEQN
      DO 25 J=1,JJ                                                      TEMPEQN
      DO 25 I=2,NI                                                      TEMPEQN
      DO 26 K=1,JJ                                                      TEMPEQN
      IF(K.EQ.1)                                                        TEMPEQN
     1C(K)=U(I,J,K+1)-U(I,J,K)                                          TEMPEQN
      IF(K.EQ.JJ)                                                       TEMPEQN
     2C(K)=U(I,J,K-1)-U(I,J,K)                                          TEMPEQN
      IF((K.NE.1).AND.(K.NE.JJ))                                        TEMPEQN
     3C(K)=(U(I,J,K+1)+U(I,J,K-1)-2.0*U(I,J,K))*0.5                     TEMPEQN
      IF(J.EQ.1)                                                        TEMPEQN
     1B(K)=USTST(I,J+1,K)-USTST(I,J,K)                                  TEMPEQN
      IF(J.EQ.JJ)                                                       TEMPEQN
     1B(K)=USTST(I,J-1,K)-USTST(I,J,K)                                  TEMPEQN
      IF((J.NE.1).AND.(J.NE.JJ))                                        TEMPEQN
     1B(K)=0.5*(USTST(I,J+1,K)+USTST(I,J-1,K)-2.0*USTST(I,J,K))         TEMPEQN
      P(I,J,K)=P(I,J,K)-C(K)+B(K)                                       TEMPEQN
 26   D(K)=P(I,J,K)                                                     TEMPEQN
C  ****  RHS IS COMPLETE  ***                                           TEMPEQN
C  ****  CORRECT FOR BOUNDARIRS  ****                                   TEMPEQN
      CALL TRIDAG                                                       TEMPEQN
C     SOLUTION  RETURNED  IN  D(K)                                      TEMPEQN
      DO 25 L=1,JJ                                                      TEMPEQN
 25   UST(I,J,L)=D(L)                                                   TEMPEQN
C**X  BOUNDARIES ***                                                   TEMPEQN
      DO 220 K=1,JJ                                                     TEMPEQN
      DO 220 J=1,JJ                                                     TEMPEQN
      U(1,J,K)=THO                                                      TEMPEQN
      U(II,J,K)=THO                                                     TEMPEQN
 220   CONTINUE                                                         TEMPEQN
C**  ALL INTERIOR PTS  **                                               TEMPEQN
      DO 225 I=2,NI                                                     TEMPEQN
      DO 225 J=2,NJ                                                     TEMPEQN
      DO 225 K=2,NJ                                                     TEMPEQN
 225  U(I,J,K)=UST(I,J,K)+THO                                           TEMPEQN
      MA=2                                                              TEMPEQN
      DO 7 KL=1,JJ,NJ                                                   TEMPEQN
      M=MA                                                              TEMPEQN
      IF(KL.EQ.II)  M=NJ                                                TEMPEQN
C  **  ALL FACES  **                                                    TEMPEQN
      DO 253 I=2,NI                                                     TEMPEQN
      DO 253 J=2,NJ                                                     TEMPEQN
      U(I,J,KL)=U(I,J,M)                                                TEMPEQN
      U(I,KL,J)=U(I,M,J)                                                TEMPEQN
 253   CONTINUE                                                         TEMPEQN
 7     CONTINUE                                                         TEMPEQN
C  **  ALL EDGES  **                                                    TEMPEQN
```

```
      DO 235 J=1,JJ,NJ                                                  TEMPEQN   132
      DO 235 I=2,NI                                                     TEMPEQN   133
      U(I,J,1)=U(I,J,2)                                                 TEMPEQN   134
      U(I,J,JJ)=U(I,J,NJ)                                               TEMPEQN   135
      U(I,1,J)=U(I,2,J)                                                 TEMPEQN   136
      U(I,JJ,J)=U(I,NJ,J)                                               TEMPEQN   137
235    CONTINUE                                                         TEMPEQN   138
      CALL PRINT(U,VART)                                                TEMPEQN   139
      RETURN                                                            TEMPEQN   140
      END                                                               TEMPEQN   141
```

```
      SUBROUTINE PRINT(V,VAR)
      COMMON/N/NDATA
      COMMON/A/II,JJ,NI,NJ
      COMMON/DIR/X(3),IA(2),JA(2),KA(2)
      COMMON/HEADER/HEAD1,HEAD2,HEAD3
      DIMENSION V(11,11,11)
      DO 5 I=1,3
      PRINT 1,HEAD1,HEAD2,X(I),HEAD3
      DO 5 K=1,NDATA
      IX=IA(K)
      IY=JA(K)
      IZ=KA(K)
      GO TO (8,9,10) I
8     PRINT 3,VAR,X(I),JA(K),KA(K)
      PRINT 2,(V(L,IY,IZ),L=1,II)
      GO TO 6
9     PRINT 4,VAR,IA(K),X(I),KA(K)
      PRINT 2,(V(IX,L,IZ),L=1,JJ)
      GO TO 6
10     PRINT 7,VAR,IA(K),JA(K),X(I)
4     FORMAT(1H0,5X,A10,2X,I1,*,*,A1,*,*,I1)
7     FORMAT(1H0,5X,A10,2X,I1,*,*,I1,*,*,A1)
      PRINT 2,(V(IX,IY,L),L=1,JJ)
6     CONTINUE
5     CONTINUE
1     FORMAT(1H0,40X,2A10,A2,A10)
3     FORMAT( 1H0,5X,A10,2X,A1,*,*,I1,*,*,I1)
2     FORMAT(1H0,11(E11.4,1X))
      RETURN
      END
```

```
      SUBROUTINE CONTROL
      COMMON/LIMITS/CMAX,CMIN,DELV,NX
      COMMON/MU/GMU,TODEVSQ,NXX
      COMMON/A/II,JJ,NI,NJ
      COMMON/RST/RST(11,11,11)
      COMMON ZA(11,11,11),ZB(11,11,11),ZC(11,11,11)
      ITER=1     $L=0      $N=0
      DO 70 I=1,II
      DO 70 J=1,JJ
      DO 70 K=1,JJ
70    RST(I,J,K)=ZB(I,J,K)
C** THUS RST CONTAINS OLD CHI FOR ENTIRE INNER LOOP**
85    N=N+1
      M=ITER
      CALL LMATRIX
      CALL CIRCUIT
      CALL PSSN(ITER)
      IF(ITER-M)  80,80,90
C**   **  TENDENCY TO DIVERGE ** **
90    L=L+1
C**   **  TENDS TO CONVERGE ** **
80    PRINT 4,ITER,M,L,N
      IF(ITER.LE.NXX) GO TO 75
      IF(N.GE.NX)   GO TO 75
      GO TO 85
75    CONTINUE
      DO 76 I=1,II
      DO 76 J=1,JJ
      DO 76 K=1,JJ
76    RST(I,J,K)=ZC(I,J,K)
C**  RST STORES DIFFN CURRENT DENSITY **
      RETURN
100   PRINT 4,ITER,M,L,N
      PRINT 5
      CALL EXIT
4     FORMAT(1H0,* ITER = *,I3,*  M= *,I3,*  L= *,I3,*  N = *,I3)
5     FORMAT(1H0, *THIS IS TENDING TO DIVERGE *)
      END
```

```
      SUBROUTINE BUFFOUT (IBUFF)                                        BUFFOUT
      COMMON ZA(11,11,11),ZB(11,11,11),ZC(11,11,11)                     BUFFOUT
      COMMON/LOOP/KOUNT,TIME                                            BUFFOUT
      COMMON/TWO/PZI(11,11,11),CONDJ(11,11,11)                          BUFFOUT
      COMMON/RST/RST(11,11,11)                                          BUFFOUT
      COMMON/DEGR/THETA(11,11,11)                                       BUFFOUT
      COMMON/VOLTS/PHI(11,11,11)                                        BUFFOUT
      L=1                                                               BUFFOUT
40    IF(IBUFF.LT.0)  GO TO 50                                          BUFFOUT
C  **  IBUFF IS +                                                       BUFFOUT
C  **  BUFFER OUT UNLABELLED BLOCK ** ** **                             BUFFOUT
C  **  **  IN ORDER, SIGMA,RHO,POWER **                                 BUFFOUT
73    CONTINUE                                                          BUFFOUT
      IF (UNIT,L) 73,63,74,75                                           BUFFOUT
63    BUFFER OUT(L,1)(ZA(1,1,1),ZC(11,11,11))                           BUFFOUT
      GO TO 60                                                          BUFFOUT
C  **  IBUFF IS -                                                       BUFFOUT
C  **  **  BEFFER OUT LABELLED BLOCKS)                                  BUFFOUT
C  **  IN ORDER , KOUNT,TIME,NT,JCOND,JDIFF,U,V **                      BUFFOUT
50    CONTINUE                                                          BUFFOUT
      IF (UNIT,L) 50,55,74,75                                           BUFFOUT
55    BUFFER OUT(L,1)(KOUNT,PHI(11,11,11))                              BUFFOUT
60    IBUFF=-IBUFF                                                      BUFFOUT
      PRINT 717,IBUFF,L,KOUNT                                           BUFFOUT
C** THE ABOVE ENSURES THAT LABELLED AND UNLABELLED BLOCKS ARE BUFF,D ALT BUFFOUT
90    CONTINUE                                                          BUFFOUT
      IF(UNIT,L) 90,91,74,75                                            BUFFOUT
91    CONTINUE                                                          BUFFOUT
      RETURN                                                            BUFFOUT
74    PRINT 36                                                          BUFFOUT
36    FORMAT(*  EOF ON LAST OPERATION *,//,* ISKIP,I*)                  BUFFOUT
      PRINT 717,IBUFF,L,KOUNT                                           BUFFOUT
      CALL EXIT                                                         BUFFOUT
75    PRINT 37                                                          BUFFOUT
37    FORMAT(* PARITY ERROR *)                                          BUFFOUT
      CALL EXIT                                                         BUFFOUT
72    FORMAT( *  UNIT NOT READY *)                                      BUFFOUT
717   FORMAT(8I10)                                                      BUFFOUT
      END                                                               BUFFOUT
```

```
      SUBROUTINE BUFFIN(IRECNO,L)                                       BUFFIN
      COMMON ZA(11,11,11),ZB(11,11,11),ZC(11,11,11)                     BUFFIN
      COMMON/LOOP/KOUNT,TIME                                            BUFFIN
      COMMON/TWO/PZI(11,11,11),CONDJ(11,11,11)                          BUFFIN
      COMMON/RST/RST(11,11,11)                                          BUFFIN
      COMMON/DEGK/THETA(11,11,11)                                       BUFFIN
      COMMON/VOLTS/PHI(11,11,11)                                        BUFFIN
C  **  INDEX DETER MINES THE STARTING POINT,L IS THE                    BUFFIN
C  **  REQUIRED  TAPE NO. READ IN MAIN                                  BUFFIN
C  **  ** L IS THE REQUIRED TAPE NO **                                  BUFFIN
      REWIND L                                                          BUFFIN
      ISKIP=IRECNO*2-2                                                  BUFFIN
      ICOUNT =0                                                         BUFFIN
      IF(ISKIP.EQ.0) GO TO 527                                          BUFFIN
C ** ** SKIP TO THE REQUIRED RECORD ** **                               BUFFIN
      DO 50 I=1,ISKIP                                                   BUFFIN
52    ICOUNT=ICOUNT+1                                                   BUFFIN
      IF (UNIT,L) 52,53,74,75                                           BUFFIN
53    BUFFER IN(L,1)(X,X)                                               BUFFIN
50    CONTINUE                                                          BUFFIN
527   PRINT 717,ICOUNT,ISKIP,IRECNO,L                                   BUFFIN
C**   **  BUFFER IN ALL ARRAYS ***                                      BUFFIN
73    CONTINUE                                                          BUFFIN
      IF (UNIT,L) 73,65,74,75                                           BUFFIN
65    CONTINUE                                                          BUFFIN
60    BUFFER IN (L,1) (ZA(1,1,1),ZC(11,11,11))                          BUFFIN
5     CONTINUE                                                          BUFFIN
      IF (UNIT,L)  5,88,74,75                                           BUFFIN
88    BUFFER IN(L,1)(KOUNT,PHI(11,11,11))                               BUFFIN
  6   FORMAT(1H1,* KOUNT = *,I4,* INDEX = *,I4,* TIME =*,E14.7,* VAPP = BUFFIN
     1*,E14.7)                                                          BUFFIN
      READ(60,717)   LL                                                 BUFFIN
70    CONTINUE                                                          BUFFIN
      IF(UNIT,L)70,77,74,75                                             BUFFIN
77    CONTINUE                                                          BUFFIN
      KK=KOUNT-LL                                                       BUFFIN
      PRINT 6,KOUNT,IRECNO,TIME,PHI(1,1,1)                              BUFFIN
      IF(KK   .NE.IRECNO)  CALL EXIT                                    BUFFIN
      RETURN                                                            BUFFIN
74    PRINT 36                                                          BUFFIN
36    FORMAT(*  EOF ON LAST OPERATION *,//,* ISKIP,I*)                  BUFFIN
      PRINT 717,ISKIP,I                                                 BUFFIN
      CALL EXIT                                                         BUFFIN
75    PRINT 37                                                          BUFFIN
37    FORMAT(* PARITY ERROR *)                                          BUFFIN
      CALL EXIT                                                         BUFFIN
72    FORMAT( *  UNIT NOT READY *)                                      BUFFIN
717   FORMAT(8I10)                                                      BUFFIN
      END                                                               BUFFIN
```

```
      SUBROUTINE LMATRIX                                                LMATRIX     2
C**   ** THIS IS CALLED BY LMATRIX TO EVALUATE RHS OF CONTINUITY EQN *** LMATRIX    3
      COMMON/CON/GAMMA,AMDA,GAM2,GAMMB,GAMM2                            LMATRIX     4
      COMMON/DEGK/THETA(11,11,11)                                       LMATRIX     5
      COMMON/VOLTS/PHI(11,11,11)                                        LMATRIX     6
      COMMON/LOOP/KOUNT,TIME                                            LMATRIX     7
      COMMON/PULSE/TIMEI,TIMEF                                          JULY4      30
      COMMON/LIMITS/CMAX,CMIN,DELV,NX                                   JULY4      31
      COMMON/TWO/PZI(11,11,11),TEMP(11,11,11)                           LMATRIX     8
      COMMON/RST/RST(11,11,11)                                          LMATRIX     9
      COMMON PSI(11,11,11),CHI(11,11,11),DZI(11,11,11)                  LMATRIX    10
      COMMON/A/II,JJ,NI,NJ                                              LMATRIX    11
      COMMON/VAR/VART,VARC,VARV,VARE,VARP,VARD,VARI,VARF,INTA,INTB,INTC, LMATRIX   12
     1INTD                                                              LMATRIX    13
      COMMON/FACTORS/FA,FB,FC,FD                                        LMATRIX    14
      COMMON/SIO/A                                                      LMATRIX    15
      COMMON/B/CA,GA,EGA,EGB                                            LMATRIX    16
      COMMON/V/VR,VTH,VO                                                LMATRIX    17
      COMMON/GAMS/GAMD                                                  LMATRIX    18
      COMMON/CONDTY/RATIO                                               LMATRIX    19
      COMMON/T/THO,TA,TD                                                LMATRIX    20
      COMMON/ITEPS/EPSMAX,ITMAX                                         LMATRIX    21
      COMMON/VD/VA                                                      LMATRIX    22
      COMMON/XTRA/FE,RI,TAUB                                            LMATRIX    23
      FB=2.0*FE                                                         LMATRIX    24
366    CONTINUE                                                         LMATRIX    25
      DO 1 I=1,II                                                       LMATRIX    26
      DO 1 J=1,JJ                                                       LMATRIX    27
      DO 1 K=1,JJ                                                       LMATRIX    28
      IF(THETA(I,J,K).LT.TA)  GO TO 120                                 LMATRIX    29
      DZI(I,J,K)=ALOG(RATIO)                                            LMATRIX    30
      EG=EGB                                                            LMATRIX    31
      PSI(I,J,K)=-FC/RATIO                                              LMATRIX    32
      GO TO 130                                                         LMATRIX    33
120   EG=EGA                                                            LMATRIX    34
      PSI(I,J,K)=-FC                                                    LMATRIX    35
      DZI(I,J,K)=0.                                                     LMATRIX    36
130   TEMP(I,J,K)=PSI(I,J,K)*RST(I,J,K)                                 LMATRIX    37
      PZI(I,J,K)=GA*EXP(EG/THETA(I,J,K))                                LMATRIX    38
      IF((TIME.GT.TIMEI).AND.(TIME.LE.TIMEF))  PZI(3,4,5)=PZI(3,4,5)+   JULY4      32
     1DELV                                                              JULY4      33
      CHI(I,J,K)=PZI(I,J,K)*THETA(I,J,K)                                LMATRIX    39
1     CONTINUE                                                          LMATRIX    40
      DO 3 I=1,II                                                       LMATRIX    41
      DO 3 J=1,JJ                                                       LMATRIX    42
      DO 3 K=1,JJ                                                       LMATRIX    43
      TEMP(I,J,K)=TEMP(I,J,K)+FB*(DAVX(CHI,I,J,K)+DAVY(CHI,I,J,K)       LMATRIX    44
     *+DAVZ(CHI,I,J,K)-GAMD*CHI(I,J,K) )                                LMATRIX    45
      TEMP(I,J,K)=TEMP(I,J,K)+FB*(DELX(DZI,I,J,K)*DELX(CHI,I,J,K)       LMATRIX    46
     *+DELY(CHI,I,J,K)*DELY(DZI,I,J,K)+DELZ(CHI,I,J,K)*DELZ(DZI,I,J,K)) LMATRIX    47
      TEMP(I,J,K)=TEMP(I,J,K)-FA*PZI(I,J,K)*( DELX(DZI,I,J,K)*DELX(PHI,I LMATRIX   48
     *,J,K)+DELY(DZI,I,J,K)*DELY(PHI,I,J,K)+DELZ(PHI,I,J,K)*DELZ(DZI,I,J LMATRIX   49
     *,K))                                                              LMATRIX    50
      TEMP(I,J,K)=TEMP(I,J,K)-FA*(DELX(PZI,I,J,K)*DELX(PHI,I,J,K)       LMATRIX    51
     1+DELY(PZI,I,J,K)*DELY(PHI,I,J,K)+DELZ(PZI,I,J,K)*DELZ(PHI,I,J,K)) LMATRIX    52
C** PSI IS THE COEFF OF -CHI **                                         LMATRIX    53
      PSI(I,J,K)=DAVX(THETA,I,J,K)+DAVY(THETA,I,J,K)                    LMATRIX    54
     1+DAVZ(THETA,I,J,K)-GAMD*THETA(I,J,K)                              LMATRIX    55
     1*2+VTH*RST(I,J,K)+PSI(I,J,K)                                      LMATRIX    56
     2-FA*PZI(I,J,K)                                                    LMATRIX    57
      PSI(I,J,K)=PSI(I,J,K)-(DELX(DZI,I,J,K)*(DELX(PHI,I,J,K)*VTH       LMATRIX    58
     *-DELX(THETA,I,J,K))+DELY(DZI,I,J,K)*(DELY(PHI,I,J,K)*VTH-         LMATRIX    59
     *DELY(THETA,I,J,K))+DELZ(DZI,I,J,K)*(DELZ(PHI,I,J,K)*VTH-DELZ(THETA LMATRIX   60
     *,I,J,K)))                                                         JULY4      34
```

```
3     CONTINUE                                                           LMATRIX
C**   ** INITIALIZATION OF VARIABLES **                                  LMATRIX
      DO 33 I=1,II                                                       LMATRIX
      DO 33 J=1,JJ                                                       LMATRIX
      DO 33 K=1,JJ                                                       LMATRIX
      IF((I.EQ.1).OR.(J.EQ.1).OR.(K.EQ.1))  GO TO 373                    LMATRIX
      IF((I.EQ.II).OR.(J.EQ.JJ).OR.(K.EQ.JJ)) GO TO 373                  LMATRIX
      CHI(I,J,K)=TEMP(I,J,K)/PSI(I,J,K)                                  LMATRIX
      GO TO 33                                                           LMATRIX
373   CHI(I,J,K)=0.0                                                     LMATRIX
      GO TO 33                                                           LMATRIX
33    CONTINUE                                                           LMATRIX
C  ***START  OVERRELAXATION.  ***                                        LMATRIX
C   *** FC=200*DR*DJ.  ***                                               LMATRIX
C   **  WR=W/FC=CA                                                       LMATRIX
      PRINT 777,EPSMAX,ITMAX                                             LMATRIX
777   FORMAT(1H0,* LMATRIX*,E16.7,I10)                                   LMATRIX
      ITER=0                                                             LMATRIX
 4    EPS=0.0                                                            LMATRIX
      ITER=ITER+1                                                        JULY4
      SUM=0.0                                                            LMATRIX
      DO  6  I=2,NI                                                      LMATRIX
      DO  6  J=2,NJ                                                      LMATRIX
      DO  6  K=2,NJ                                                      LMATRIX
      STORE= CHI(I,J,K)                                                  LMATRIX
      CHI(I,J,K)=CHI(I,J,K)-CA*(                                         LMATRIX
     1CHI(I+1,J,K)*(VA*DELX(PHI,I,J,K)-DELX(THETA,I,J,K)-THETA(I,J,K)*   LMATRIX
     2(1.0+0.5*DELX(DZI,I,J,K)))                                         LMATRIX
     3+CHI(I-1,J,K)*(DELX(THETA,I,J,K)-VA     *DELX(PHI,I,J,K)           LMATRIX
     4-THETA(I,J,K)*(1.-0.5*DELX(DZI,I,J,K)))                            LMATRIX
     5+CHI(I,J+1,K)*(FX*(VA*DELY(PHI,I,J,K)-DELY(THETA,I,J,K))           LMATRIX
     6-THETA(I,J,K)*(GAMMA+FE*DELY(DZI,I,J,K)))                          LMATRIX
     7+CHI(I,J-1,K)*(FX*(DELY(THETA,I,J,K)-VA* DELY(PHI,I,J,K))          LMATRIX
     8-THETA(I,J,K)*(GAMMA-FE*DELY(DZI,I,J,K)))                          LMATRIX
     9+CHI(I,J,K+1)*(FX*(VA*DELZ(PHI,I,J,K)-DELZ(THETA,I,J,K))           LMATRIX
     A-THETA(I,J,K)*(GAMMA+FE*DELZ(DZI,I,J,K)))                          LMATRIX
     B+CHI(I,J,K-1)*(FX*(DELZ(THETA,I,J,K)-VA* DELZ(PHI,I,J,K))          LMATRIX
     C-THETA(I,J,K)*(GAMMA-FE*DELZ(DZI,I,J,K)))                          LMATRIX
     D-CHI(I,J,K)*PSI(I,J,K)+                                            LMATRIX
     8TEMP(I,J,K))                                                       LMATRIX
       EPS=EPS+ABS(CHI(I,J,K)-STORE)                                     LMATRIX
       SUM=SUM+ABS(CHI(I,J,K))                                           LMATRIX
 6    CONTINUE                                                           LMATRIX
      IF(SUM.EQ.0.0)  SUM=1.0E-10                                        LMATRIX
      EPS=EPS/SUM                                                        LMATRIX
      PRINT 2,EPS,SUM                                                    LMATRIX
      IF(EPS.LE.EPSMAX)  GO  TO  9                                       LMATRIX
      IF(ITER-ITMAX)   4,4,8                                             LMATRIX
 8    PRINT  202,ITER,EPS,SUM                                            LMATRIX
 202  FORMAT(1H0,*NO  CONVERGANCE  AFTER *,I4,*ITERATIONS WITH EPS=*,    LMATRIX
     1E8.1,*AND  SUM=*,G11.4)                                            LMATRIX
      GO  TO  155                                                        LMATRIX
 9    PRINT  201,ITER,EPS,SUM                                            LMATRIX
201   FORMAT(1H0,*CONVERGENCE  HAS  REACHED AFTER *,I4,*ITERATIONS WITH  LMATRIX
     1EPS =*,E8.1, * AND  SUM = *,G11.4)                                 LMATRIX
155   CONTINUE                                                           LMATRIX
C  ***OBTAIN  CONDUCTIVITY.**                                            LMATRIX
      DO  11  I=1,II                                                     LMATRIX
      DO  11  J=1,JJ                                                     LMATRIX
      DO  11  K=1,JJ                                                     LMATRIX
      R=1.                                                               LMATRIX
      IF(THETA(I,J,K).GE.TA)  R=RATIO                                    LMATRIX
      PSI(I,J,K)=PZI(I,J,K)-CHI(I,J,K)/FB                                LMATRIX
      PZI(I,J,K)=THETA(I,J,K)*PSI(I,J,K)                                 LMATRIX
       PSI(I,J,K)=R*PSI(I,J,K)                                           LMATRIX
 11   CONTINUE                                                           LMATRIX
```

```
C     **PSI  CONTAINS SIGMA ,THETA CONTAINS NORMALIZED  TEMP.**
C     ***COMPUTE  CURRENT IN ,CURRENT OUT FOR LOOPING**
C     ***DZI=DIFF  CURRENT  DENSITY ,PZI-COND.  CURRENT DENSITY.**
C     ***DZI=DIFF  CURRENT  DENSITY ,PZI-COND.  CURRENT DENSITY IN X DIR-.*
      DO  12  I=1,II
      DO  12  J=1,JJ
      DO  12  K=1,JJ
      TEMP(I,J,K)=-PSI(I,J,K)*DELX(PHI,I,J,K)/A
      DZI(I,J,K)=DELX(PZI,I,J,K)/(A*VTH)
 12   CONTINUE
2     FORMAT(1H0,11(E11.4,1X))
      RETURN
      END
```

```
      SUBROUTINE RHO
      COMMON/CON/GAMMA,AMDA,GAM2,GAMMB,GAMM2
      COMMON/A/II,JJ,NI,NJ
      COMMON ZA(11,11,11),ZB(11,11,11), P(11,11,11)
      COMMON/VOLTS/PHI(11,11,11)
      COMMON/SIO/A
      COMMON/T/THO,TA,TD
      COMMON/V/VR,VTH,VO
      COMMON/FACTORS/FA,FB,FC,FD
      COMMON/TIMES/TAUO,QI,TAUF,Q2
      COMMON/LOOP/KOUNT,TIME
9     FORMAT(1H0,4I10,F10.3)
C**  **  P CONTAINS  SIGMA-E-SQUARED
      DO 5 I=1,II
      DO 5 J=1,JJ
      DO 5 K=1,JJ
      P(I,J,K)=FD*(DELX(PHI,I,J,K)**2
     1+DELY(PHI,I,J,K)**2 +DELZ(PHI,I,J,K)**2)
     2*ZA(I,J,K)
5     CONTINUE
      RETURN
      END
```

```
      SUBROUTINE BYPASS
      COMMON/B/CA,GA,EGA,EGB
      COMMON/X/RS
      COMMON/CON/GAMMA,AMDA,GAM2,GAMMB,GAMM2
      COMMON/A/II,JJ,NI,NJ
      COMMON/TWO/PZI(11,11,11),TEMP(11,11,11)
      COMMON/DEGK/THETA(11,11,11)
      COMMON/SIO/A
      COMMON/VAR/VART,VARC,VARV,VARE,VARP,VARD,VARI,VARF,INTA,INTB,INTC,
     1INTD
      COMMON /ZA(11,11,11),ZB(11,11,11),ZC(11,11,11)
      COMMON/VOLTS/PHI(11,11,11)
      COMMON/I/THO,TA,TD
      COMMON/V/VR,VTH,VO
      COMMON/XTRA/FE,RI,TAUB
      EQUIVALENCE(ZA,PSI)
      DIMENSION PSI(11,11,11)
C**  **  CALLED FROM BYPASS
      VART=10HTEMP AT
      VARC=10HCHARGE AT
      VARV=10HVOLTAGE AT
      VARE=10HCONDTY AT
      VARP=10HPOWER AT
      VARD=10HDONORS AT
      VARI=10HCOND J AT
      VARF=10HDIFF J AT
      INTA=10HD2CHI COEF
      INTB=10HDCHI COEFF
      INTC=10HCHI COEFFT
      INTD=10HCONST TERM
      DO 20 I=1,II
      DO 20 J=1,JJ
      DO 20 K=1,JJ
      ZC(I,J,K)=0.0
      THETA(I,J,K)=THO
C** ZB IS NET CHARGE DENSITY,ZA IS IONIZED DONOR DENSITY ** **
      ZB(I,J,K)=0.0
      PZI(I,J,K)=A
      ZA (I,J,K)=A
20    PHI(I,J,K)=(II-I)/12.0
      DO 6 I=1,II
      DO 6 J=1,JJ
      DO 6 K=1,JJ
6     TEMP(I,J,K)=-PSI(I,J,K)*DELX(PHI,I,J,K)/A
      CALL CIRCUIT
      RETURN
      END
```

```
      SUBROUTINE CIRCUIT
      COMMON/CON/GAMMA,AMDA,GAM2,GAMMB,GAMM2
      COMMON/A/II,JJ,NI,NJ
      COMMON/V/VR,VTH,VO
      COMMON/SIO/A
      COMMON/T/THO,TA,TD
      COMMON/VOLTS/PHI(11,11,11)
      COMMON/DEGK/THETA(11,11,11)
      COMMON ZA(11,11,11),ZC(11,11,11),ZA(11,11,11)
      COMMON/LIMITS/CMAX,VMAX,DELV,NX
      COMMON/TWO/PZI(11,11,11),TEMP(11,11,11)
      COMMON/COLS/F(11),FF(11),G(11)
      COMMON/H/CA,GA,EGA,EGB
      KL=0     $NN=NI-2
      DO 6 I=1,II,NI
      KL=KL+1
C  ***   OBTAIN THE  CURRENT AT (I,J,K)                      *****
      DO 21 J=1,JJ
      DO 22 K=1,JJ
22    F(K)=ZA(I,J,K)+TEMP(I,J,K)
C  **  **  ZA IS DIFF CURRENT DENSITY ** **
C  **  **  PZI IS COND CURRENT DENSITY ** **
C**  **  F IS INTEGRATED FROM 1,JJ FOR EACH J ** ** **
21    FF(J)=SIMPS(F)
      FFF=SIMPS(FF)*VR
      IF(KL.EQ.1)    F1=1.0-FFF
      IF(KL.EQ.2)  F2=1.0-FFF
6      CONTINUE
      FA=0.5*(F1+F2)
      PRINT 3,F1,F2
      PRINT 2
      PRINT 3,CMAX,VMAX
      IF(FA.GE.VMAX)   FA=VMAX
      FFF=1.0-FA
       IF(FFF.GE.CHAX) FFF=CHAX
      FA=1.0-FFF
2     FORMAT(1H0,* MAX LIMITS ARE *)
      PRINT 3, FFF,FA
5     CONTINUE
3     FORMAT(1H0,10X,*I= *,E12.5,10X,*V= *,E12.5)
      DO 51 J=1,JJ
      DO 51 K=1,JJ
51    PHI(I,J,K)=FA
      RETURN
      END
```

```
      FUNCTION SIMPS(F)
C  **  **P 86 CARNAHAN
C**  **  H=1 TWOH=2 B=11 A=1
C**  **  COMMON IN WORK ARRAY
      DIMENSION F(11)
      COMMON/A/II,JJ,NI,NJ
C  **     INITIALIZE PARAMETERS  **  **
      SUMEND=0.0   $  SUMMID=0.0
C**  **  EVALUATE SUMEND AND SUMMID  ***
      DO 1 M=1,5
      K=2*M-1
      SUMEND=SUMEND+F(K)
      SUMMID=SUMMID+F(K+1)
1     CONTINUE
C  **  ** RETURN ESTIMATED VALUE OF INTEGRAL ***
      SIMPS=(2.0*SUMEND+4.0*SUMMID-F(1)+F(11))/3.0
      RETURN
      END
```

```
      SUBROUTINE PSSN(ITER)
      COMMON ZA(11,11,11),AR7(11,11,11),ZC(11,11,11)
      COMMON/VOLTS/AR6(11,11,11)
      COMMON/CON/GAMMA,AMDA,GAM2,GAMMB,GAMM2
      COMMON/VAR/VART,VARC,VARV,VARE,VARP,VARD,VARI,VARF,INTA,INTB,INTC,
     1INTD
      COMMON/A/II,JJ,NI,N1
      COMMON/GAMS/GAMD
      COMMON/V/VR,VTH,VO
      COMMON/LOOP/KOUNT,TIME
      COMMON/A4/ITMAX,EPSMAX,W1
      COMMON/T/THO,TA,TD
      COMMON/SIO/A
      EQUIVALENCE(NI,NJ)
823   FORMAT(1H0,* EPS=  *,G11.5,* EPSMAX= *,G11.5,* TA= *,G11.5)
      ITER=0
4     EPS=0.00
      SUM=0.0
      ITER=ITER+1
      DO 5 J=1,JJ
      L1=J-1
      L2=J+1
      DO 5 K=1,JJ
      M1=K-1
      M2=K+1
      IF(J.EQ.1)  GO TO 12
      IF(J.EQ.JJ)   GO TO 13
16    IF(K.EQ.1)   GO TO 14
      IF(K.EQ.JJ) GO TO 15
      GO TO 17
12    L1=2
      GO TO 16
13    L2=N1
      GO TO 16
14    M1=2
      GO TO 17
15    M2=N1
17    CONTINUE
      DO 5 I=2,NI
      TEMP=AR6(I,J,K)
      AR6(I,J,K)=AR6(I,J,K)*(1.0-W1)+W1*
     *(AR6(I+1,J,K)+AR6(I-1,J,K)+GAMMA*
     *(AR6(I,L1,K)+AR6(I,L2,K)+
     *AR6(I,J,M1)+AR6(I,J,M2))+
     *AR7(I,J,K))/GAMD
      SUM=SUM+ABS(AR6(I,J,K))
5     EPS=EPS+ABS(AR6(I,J,K)-TEMP)
      EPS=EPS/SUM
      IF (EPS.LE.EPSMAX) GO TO 6
C     STOP ITER IF CONVERGENT OR EXESSIVE ITER
      IF(ITER-ITMAX) 4,4,8
8     WRITE(61,202)ITER,EPS,TIME
202   FORMAT(1H0,*NO CONVERGENCE AFTER*,I4,* ITERATIONS WITH EPS=*,
     1E8.1,* AT TIME =*,G11.4)
      GO TO 155
6     WRITE(61,201) ITER,EPS,TIME
201   FORMAT(1H0,*CONVERGENCE HAS BEEN REACHED AFTER*,I4,*ITERATIONS
     1WITH EPS=*,
     1E8.1,* AT TIME =*,G11.4)
155   CONTINUE
      MA=2
      DO 7 [illegible]
      [illegible]
```

```
      DO 170 I=2,NI
      DO 170 J=2,NJ
C**   ALL RIGHT HAND PTS ARE CORRI DEFINED **
      ARG(I,J,KL)=ARG(I,J,M)
      ARG(I,KL,J)=ARG(I,M,J)
170   CONTINUE
C **  4 EDGES OF THE CUBE REMAIN **
      DO 171 I=2,NI
      ARG(I,1,KL)=ARG(I,1,M)
      ARG(I,JJ,KL)=ARG(I,JJ,M)
      ARG(I,KL,1)=ARG(I,M,1)
      ARG(I,KL,JJ)=ARG(I,M,NJ)
171     CONTINUE
7     CONTINUE
      PRINT 823,EPS,EPSMAX,SUM
      RETURN
      END
```

```
      SUBROUTINE TRIDAG
      COMMON/A/II,JJ,NI,NJ
      COMMON/L/LA,N
      COMMON/COLS/BB(11),AA(11),GG(11)
      COMMON/WORK/AR1(11),AR3(11),AR5(11),AR8(11)
C     SUBROUTINE TRDG FOR SOLVING LINEAR SIMULTANEOUS EQNS.
C*** APP. NUM. METHODS --PP446
      IF=LA+1
      AR1(LA)=BB(LA)
      AR5(LA)=AR3(LA)/AR1(LA)
      DO 101 I=IF,N
      AR1(I)=BB(I)-AA(I)*GG(I-1)/AR1(I-1)
      IF(ABS(AR1(I)).LE.1.0E-23)   AR1(I)=1.0E-23
101   AR5(I)=(AR3(I)-AA(I)*AR5(I-1))/AR1(I)
      AR3(N)=AR5(N)
      LAST=N-LA
      DO 102 K=1,LAST
C     TRIDAG FOR SOLVING SIMULTANEOUS E
      I=N-K
102   AR3(I)=AR5(I)-GG(I)*AR3(I+1)/AR1(I)
      RETURN
      END
```

```
      FUNCTION DELX(U,I,J,K)
      DIMENSION U(11,11,11)
      COMMON/A/II,JJ,NI,NJ
      COMMON/CON/GAMMA,AMDA,GAM2,GAMMB,GAMM2
      COMMON/SIO/A
      COMMON/V/VR,VTH,VO
      COMMON/XTRA/FE,RI,TAUH
      IF(I.EQ.1)   GO TO 111
      IF (I.EQ.II)  GO TO 222
      DELX=(U(I+1,J,K)-U(I-1,J,K))/2.0
      GO TO 333
  111 DELX=-0.5*(3.0*U(I,J,K)-4.0*U(I+1,J,K)+U(I+2,J,K))
      GO TO 333
  222 DELX= 0.5*(3.0*U(I,J,K)-4.0*U(I-1,J,K)+U(I-2,J,K))
  333 CONTINUE
      RETURN
      ENTRY DELY
      IF(J.EQ.1)  GO TO 55
      IF(J.EQ.JJ) GO TO 55
      DELX=FE*(U(I,J+1,K)-U(I,J-1,K))
      GO TO 53
   55 DELX=0.0
   53 CONTINUE
      RETURN
      ENTRY DELZ
      IF(K.EQ.1)          GO TO 55
      IF(K.EQ.JJ)  GO TO 55
      DELX=FE*(U(I,J,K+1)-U(I,J,K-1))
      RETURN
      ENTRY DAVX
      IF(I.EQ.1)  GO TO 43
      IF(I.EQ.II)  GO TO 45
      DELX=U(I+1,J,K)+U(I-1,J,K)
      RETURN
      ENTRY DAVY
      IF(J.EQ.1)  GO TO 33
      IF(J.EQ.JJ) GO TO 35
      DELX=GAMMA*(U(I,J+1,K)+U(I,J-1,K))
      GO TO 37
   33 DELX=GAMMA*(U(I,J+1,K)+U(I,J,K))
      GO TO 37
   35 DELX=GAMMA*(U(I,J-1,K)+U(I,J,K))
   37 CONTINUE
      RETURN
      ENTRY DAVZ
      IF(K.FQ.1) GO TO 12
      IF(K.EQ.JJ)  GO TO 14
      DELX=GAMMA*(U(I,J,K+1)+U(I,J,K-1))
      RETURN
   12 DELX=GAMMA*(U(I,J,K+1)+U(I,J,K))
      RETURN
   14 DELX=GAMMA*(U(I,J,K-1)+U(I,J,K))
      RETURN
   43 DELX=3.0*U(I,J,K)-2.0*U(I+1,J,K)+U(I+2,J,K)
      RETURN
   45 DELX=3.0*U(I,J,K)-2.0*U(I-1,J,K)+U(I-2,J,K)
      RETURN
      END
*EOR
*EOR
```

APPENDIX G

THE DONOR IONIZATION EQUATION

The n type semiconductor modelled in Chapter 2 is assumed to be only partially ionized at any temperature T in the operating temperature range. In this section, an expression for the ionized donor density at any specified temperature is derived using Fermi statistics and the sample band model of the semiconductor outlined in Chapter 2.

The n type semiconductor chosen has been assumed to have negligible acceptor attoms, i.e.,

$$N_a \ll N_d$$

Further, the semiconductor has been assumed to be a nondegenerate semiconductor. Those donors are incompletely ionized in the temperature range of operation. Thus, at T = 0K, the valence band is full, and the conduction band is empty. In the operating temperature range, some of the electrons from the donor states are thermally excited into the conduction band, leaving behind ionized donors. Since, as shown in Fig. 2.1a, the valence level lies much further away below the conduction band than the donor level, only a negligible number of electrons acquire sufficient energy to be excited from the valence band to the conduction band.

Thus, if $p(E_c)$ be the probability of finding an electron in the conduction band, then, applying Fermi statistics

$$p(E_c) = (1 + \exp(E_c - E_f)/kT)^{-1} \qquad (G.1)$$

Also, if n be defined as the number of ionized donors per unit volume and p(E) be the probability of occupation of a donor state, then,

$$n_d^+ = N_d(1 - p(E_d)) \tag{G.2}$$

But, $p(E_d)$, the probability of occupation of a donor state can be obtained by applying Fermi statistics:

$$p(E_d) = (1 + \exp(E_d - E_f)/kT)^{-1} \tag{G.3}$$

From Fig. 2.1, E_f is greater than E_d, measured from the valence band edge. Also, it has been assumed that the operating temperature range is low enough such that only partial ionization takes place and so kT E_d, E_f. The quantity $(E_d - E_f)/kT$ is thus negligible compared to unity. Under equilibrium conditions, charge neutrality is maintained everywhere within the sample. Since both acceptor density and hole concentrations have been neglected in the model, then, in equilibrium,

$$n = n_d^+$$

$$N_d\exp((E_f - E_c)/kT) = N_d\exp((E_d - E_f)/kT) \tag{G.4}$$

Hence,

$$E_f = (E_c + E_d)/2$$

Note that this is true only under equilibrium conditions. Under operating conditions, it is only approximately true. Eq. (G.2), therefore, reduces to the simple expression

$$n_d^+ = N_d\exp((E_d - E_f)/kT \tag{G.5}$$

Similarly, using Eq. (g.1), the number of electrons per unit volume under equilibrium conditions is given by

$$n = N_d p(E_c)$$

$$= \frac{N_d}{1 + \exp((E_f - E_c)/kT)} \tag{G.6}$$

Also, in the selected temperature range,

$$kT \ll E_c - E_f$$

Hence,

$$\exp((E_c - E_f)/kT) \gg 1$$

and so,

$$n = N_d \exp((E_f - E_c)/kT) \qquad (G.7)$$

Defining E, the activation energy, by the relation

$$E_a = E_c - E_d \qquad (G.8)$$

and substituting back in the relation Eq. (G.5) for N_d,

$$n_d^+ = N_d \exp(E_a/kT) \qquad (G.9)$$

This is the relation stated in Eq. (2.2.1). There is an approximation involved since equilibrium conditions are utilized in the derivation. Since considerable diffusion effects are expected to be encountered, the equilibrium expression for n cannot be used. However, the ionized donors are stationary, and the equilibrium expressions are here as an approximation.

APPENDIX H

THE GENERALIZED CONTINUITY EQUATION

The various dependent variables, like , the charge density, are functions of space and time and often occur as total differentials. In this section, the total differential is expressed in terms of partial derivatives and the divergence operator, both of which can be directly evaluated by finite difference techniques.

Consider a real function defined in a region R. The function represents any real physical property. It is, therefore, finite, bounded, and continuously differentiable, and a function of space and time. In cartesian co-ordinates,

$$f = f(x, y, z, t)$$

Taking the total derivative of this function with respect to time,

$$\frac{df}{dt} = \frac{\partial f}{\partial t} + \frac{\partial f dx}{\partial x dt} + \frac{\partial f dy}{\partial y dt} + \frac{\partial f dz}{\partial z dt}$$

$\frac{dx}{dt}$, $\frac{dy}{dt}$, and $\frac{dz}{dt}$ represent the velocities with which the property in x, y, and z directions respectively. Writing v_x, v_y, and v_z for the respective velocities,

$$\frac{df}{dt} = \frac{\partial f}{\partial t} + \frac{\partial f}{\partial x} v_x + \frac{\partial f}{\partial y} v_y + \frac{\partial f}{\partial z} v_z$$

v_x, v_y, v_z are the components of the velocity vector $\bar{v}$. Consider the vector function $f\bar{v}$. Since $\bar{v}$ is the velocity associated with the property f, the quantity $f\bar{v}$ represents the current or flux density associated with the property. Performing the divergence operation on th this function,

$$\nabla \cdot (f\bar{v}) = f\,\nabla \cdot \bar{v} + v \cdot \nabla f$$

But $\nabla \cdot \bar{v} = 0$. Also,

$$v \cdot \nabla f = v_x \frac{f}{x} + v_y \frac{f}{y} + v_z \frac{f}{z}$$

Hence,

$$\frac{df}{dt} = \frac{\partial f}{\partial t} + \nabla \cdot (f\bar{v})$$

$$= \frac{\partial f}{\partial t} + \nabla \cdot \bar{J}_f$$

where $\bar{J}_f$ is the current density associated with the property f.

The above equation is utilized in arriving at the continuity equations for charge and energy flow in Chapters 2 and 3 respectively.

BIBLIOGRAPHY

BIBLIOGRAPHY

BIBLIOGRAPHY

1. A. D. Pearson, "Chemical, Physical, and Electrical Properties of Some Unusual Inorganic Glasses: Part 2", Advances in Glass Technology, New York, Plenum Press, (1962) 357.

2. A. D. Pearson, "Characteristics of Semiconducting Glass Switching/Memory Diodes", IBM J Res Develop, 13 (1969) 510.

3. S. R. Ovshinsky, "Amorphous Semiconductors", Sci J, 5A:2 (Aug 1969) 73.

4. K. W. Boer, G. Dohler, S. R. Ovshinsky, "Time Delay for Reversible Electric Switching in Semiconducting Glasses", J Non-Cryst Solids, 4 (1970) 573.

5. E. A. Davis, R. F. Shaw, "Characteristic Phenomena in Amorphous Semiconductors", J Non-Cryst Solids, 2 (1970) 107.

6. P. J. Walsh et al, "Experimental Results in Amorphous Semiconductor Switching Behavior", J Non-Cryst Solids, 2 (1970) 107.

7. Editorial Staff, "Glassy Semiconductors Show Switching and Memory Effects", Phys Today, 22:1 (1969) 62.

8. R. R. Shanks, "Ovonic Threshold Switching Characteristics", J Non-Cryst Solids, 2 (1970) 99.

9. D. F. Weirauch, "Threshold Switching and Thermal Filaments in Amorphous Semiconductors", Appl Phys Letters, 16:5 (1970) 212.

10. K. W. Boer, S. R. Ovshinsky, "Electrothermal Initiation of an Electronic Switching Mechanism in Semiconducting Glasses", J Appl Phys, 41:6 (1970) 2675.

11. M. H. Cohen, H. Fritzsche, S. R. Ovshinsky, "Simple Band Model for Amorphous Semiconducting Alloys", Phys Rev Letters, 22:20 (1969) 1065.

12. H. Fritzsche, S. R. Ovshinsky, "Electronic Conduction in Amorphous Semiconductors and the Physics of the Switching Phenomena", J Non-Cryst Solids, 2 (1970) 393.

13. N. F. Mott, "Conduction in Non-Crystalline Systems; Part I - Localized Electronic States in Disordered Systems", Phil Mag, 17:150 (Jun 1968) 1259.

14. N. F. Mott, "Conduction in Non-Crystalline Materials; Part III - Localized States in a Pseudogap and Near Extremities of Conduction and Valence Bands", Phil Mag, 19:160 (1969) 835.

15. N. F. Mott, "Conduction and Switching in Non-Crystalline Materials", Contemp Phys, 10:2 (1969) 125.

16. A. I. Gubanov, "Quantum Theory of Amorphous Semiconductors", Translated by A. Tybulewicz, New York: Consultants Bureau, 1965.

17. E. Harmik, A. Lapek, "Current Filaments in Acoustically Amplifying CdS", Solid State Commun, 8 (1970) 1287.

18. A. M. Barnett, H. A. Jensen, "Observation of Current Filaments in Semi-Insulating GaAs", Appl Phys Letters, 12:10 (1968) 341.

19. A. P. Ferro, S. K. Ghandi, "Observations of Current Filaments in Chromium-Doped GaAs", Appl Phys Letters, 16:5 (1970) 196.

20. G. Nimtz, K. Seeger, "Current Controlled Negative Differential Resistivity of p - Type Tellurium", Appl Phys Letters, 14:1 (1969) 19.

21. R. A. Smith, "Semiconductors", Cambridge (Eng), Univ Press, 1959.

22. D. Adler, J. Feinleib, H. Brooks, W. Paul, "Semiconductor-to-Metal Transitions in Transition Metal Compounds", Phys Rev, 155 (1967) 851.

23. F. J. Morin, J. P. Maita, Phys Rev, 96 (Oct 1954) 28.

24. G. W. Ludwig, R. L. Walters, Phys Rev, 101 (Mar 1956) 1699.

25. J. Moss, "Photoconductivity in the Elements", Butterworth, 1952.

26. R. A. Smith, Physics, 20 (1954) 910.

27. J. Feinleib, W. Paul, "Semiconductor-to-Metal Transition in V_2O_3", Phys Rev, 155 (1967) 841.

28. H. J. Stocker, "Phenomenology of Switching and Memory Effects in Semiconducting Chalcogenide Glasses", J Non-Cryst Solids, 2 (1970) 558.

29. D. L. Nelson, "Ovonic Device Applications", J Non-Cryst Solids, 2 (1970) 371.

30. B. K. Ridley, "Specific Negative Resistance in Solids", Proc Phys Soc, 82 (1963) 954.

31. K. W. Boer, G. Dohler, "Temperature Distribution and Its Kinetics in a Semiconducting Sandwich", Phys Stat Sol, 36 (1969) 679.

32. D. Adler, H. Brooks, "Theory of Semiconductor-to-Metal Transitions", Phys Rev, 155 (1967) 826.

33. H. Futaki, "A New Type Semiconductor (Critical Temperature Resistor)", Jap J of Appl Phys, 13 (1965) 34.

34. C. N. Berglund, R. H. Walden, "A Thin Film Inductance Using Thermal Filaments", IEEE Trans on Electron Devices, ED-17 (1970) 137.

35. A. C. Warren, "Switching Mechanisms in Chalcogenide Glasses", Electronics Letter, 5 (1969) 461.

36. D. Adler, T. Kaplan, "Electrothermal Switching in Amorphous Semiconductors", 8-10 (1972) 544.

37. C. Kittel, "Introduction to Solid State Physics", John Wiley & Sons, 1968.

38. R. W. P. King, "Fundamental Electromagnetic Theory", New York: Dover Publications (1963).

39. H. S. Carslow, H. C. Jaeger, "Heat Conduction in Solids", Oxford Clarendon Press, (1959).

40. J. C. Duchene, M. M. Terraillon, M. Pailly, G. Adams, "Initiation of Switching in VO Coplanar Devices", IEEE Trans on Electron Devices, ED-71 (1971) 1151.

41. R. J. Yu, "Electrical Switching Effects in Vanadium Oxide Complexes", PhD Thesis, MSU 1972.

42. P. D. Fisher, R. J. Yu, "Inductance Properties of Oxidized Vanadium Foils", IEEE Trans on Electron Devices, ED-16 (1971) 975.

43. C. N. Berglund, "Thermal Filaments in Vanadium Dioxide", IEES Trans on Electron Devices, ED-16 (1967) 432.

44. B. Carnahan, H. A. Luther, J. O. Wilkes, "Applied Numerical Methods", John Wiley & Sons, (1969).

45. G. E. Forsythe, W. R. Wasow, "Finite Difference Methods for Partial Differential Equations", John Wiley & Sons, (1960).

46. A. Nussbaum, "Semiconductor Device Physics", Englewood Cliffs, Prentice Hall, (1962).

47. J. Douglas, "Alternating Direction Methods for Three Space Variables", Numerische Mathematik, 4 (1962) 41.

48. B. S. Tanenbaum, "Plasma Physics", McGraw Hill, (1967).